

# Classification of 2.4–45.2 $\mu\text{m}$ Spectra from the *ISO* Short Wavelength Spectrometer<sup>1</sup>

Kathleen E. Kraemer,<sup>2,3</sup> G. C. Sloan,<sup>4,5</sup> Stephan D. Price,<sup>2</sup>

and

Helen J. Walker<sup>6</sup>

## ABSTRACT

The *Infrared Space Observatory* observed over 900 objects with the Short Wavelength Spectrometer in full-grating-scan mode (2.4–45.2  $\mu\text{m}$ ). We have developed a comprehensive system of spectral classification using these data. Sources are assigned to groups based on the overall shape of the spectral energy distribution (SED). The groups include naked stars, dusty stars, warm dust shells, cool dust shells, very red sources, and sources with emission lines but no detected continuum. These groups are further divided into subgroups based on spectral features that shape the SED such as silicate or carbon-rich dust emission, silicate absorption, ice absorption, and fine-structure or recombination lines. Caveats regarding the data and data reduction, and biases intrinsic to the database, are discussed. We also examine how the subgroups relate to the evolution of sources to and from the main sequence and how this classification scheme relates to previous systems.

*Subject headings:* catalogs — stars: fundamental parameters — infrared: ISM: continuum and lines — infrared: stars — ISM: general

---

<sup>2</sup>Air Force Research Laboratory, Space Vehicles Directorate, 29 Randolph Rd., Hanscom AFB, MA 01731; kathleen.kraemer@hanscom.af.mil, steve.price@hanscom.af.mil

<sup>3</sup>Institute for Astrophysical Research, Boston University, Boston, MA 02215

<sup>4</sup>Institute for Scientific Research, Boston College, Chestnut Hill, MA 02467; sloan@ssa1.arc.nasa.gov

<sup>5</sup>Infrared Spectrograph Science Center, Cornell University, Ithaca, NY 14853-6801

<sup>6</sup>Rutherford Appleton Laboratory, Chilton, Didcot, Oxon, OX11 0QX, UK; H.J.Walker@rl.ac.uk

<sup>1</sup>Based on observations with the *Infrared Space Observatory (ISO)*, an European Space Agency (ESA) project with instruments funded by ESA Member States (especially the Principle Investigator countries: France, Germany, the Netherlands, and the United Kingdom) and with the participation of the Institute of Space and Astronautical Science and the National Aeronautics and Space Administration (NASA).

## 1. Introduction

Spectral classification organizes astronomical sources into groups with similar properties based on the general or detailed morphology of their spectral energy distributions (SEDs). Consequently, the classification criteria depend on the wavelength region and spectral resolution used. Both of these parameters must be uniform in order to create consistent criteria for arranging the sources in a database. The similarities and differences that result from applying a successful classification system to a sufficiently large sample of sources not only improve our knowledge about the sources but provide a basis for understanding the physical parameters of the objects.

The best example of how a classification system can lead to insight into the physical properties of the objects studied is provided by optical spectral classification (cf. Hearnshaw 1986). From the earliest systems based on general color (e.g. Rutherford 1863), several competing systems emerged based on spectral line ratios (e.g. Secchi 1866, 1868; Vogel 1874; Vogel & Wilsing 1899; Pickering 1890). Of these, the Harvard system used originally in the Draper Memorial Catalogue (Pickering 1890) grew to predominate due to the large numbers of sources classified ( $> 10,000$ ), and served as the basis for the Henry Draper Catalogue (beginning with Cannon & Pickering 1918).

The MK spectral classification system evolved from the Harvard system (e.g. Morgan 1938; Morgan, Keenan, & Kellman 1943). This two-dimensional system provided the clues necessary to disentangle the different stages of the life cycle of a star and the relation of intrinsic parameters such as mass and metallicity to directly observable properties. MK spectral classification remains the single most powerful diagnostic tool available to astronomers when applied to naked stars, i.e. stars not embedded in dust.

Unfortunately, the very early and very late stages of stellar evolution rarely involve naked stars. The sources are deeply embedded within interstellar dust clouds or circumstellar dust shells, either of which absorb the optical radiation and re-emit it in the infrared. This dust can absorb so much of the optical radiation from the star that traditional classification based on the photospheric properties of the star in the optical is difficult, if not impossible. Near-infrared observations can often penetrate the obscuring dust, permitting direct measurements of the stellar photosphere. The spectral region between 1 and 9  $\mu\text{m}$  is rich in atomic and molecular lines which trace temperature and luminosity. For example, CO, SiO, and water vapor are sensitive indicators in oxygen-rich stars, even with low spectral resolution; the Phillips and Ballick-Ramsey  $\text{C}_2$  bands as well as CN and CO serve for carbon stars. However, the emission from the dust distorts the photospheric continuum and fills in the absorption features, making analysis difficult. Observations in the thermal infrared trace the emission from the dust itself. The characteristic SED of the dust is distinctive enough to serve as the

basis for classification (Little-Marenin & Price 1986; Little-Marenin et al. 1987; Cheeseman et al. 1989).

The infrared spectra obtained by the Low-Resolution Spectrometer (LRS) on the *Infrared Astronomical Satellite* (*IRAS*) are the best example of a nearly complete, self-consistent database that is ideal for spectral classification. These spectra cover wavelengths from 7.7 to 22.7  $\mu\text{m}$  at a spectral resolution of  $\lambda/\Delta\lambda \sim 20\text{--}60$ . The original LRS atlas contained spectra from 5,425 sources (*IRAS* Science Team 1986). Volk et al. (1991) expanded the database to 6,267 and Kwok et al. (1997) extracted almost 5000 additional spectra from the raw data to create a spectral database of 11,224 sources, making the LRS observations the largest infrared spectral database to date. This database includes most of the 12  $\mu\text{m}$  objects in the sky brighter than 10 Jy at 12  $\mu\text{m}$  (magnitude +1), and several infrared classification systems have been developed from it.

The initial LRS classification scheme (*IRAS* Science Team 1986; *IRAS* Explanatory Supplement 1988) sorted the original database of 5,425 sources into 10 groups, essentially based on the dominant spectral feature in the 10  $\mu\text{m}$  region. These groups were subdivided further, usually by the strength of the dominant feature. The AutoClass algorithm (also known as AI for artificial intelligence) used a Bayesian algorithm to sort the database into self-consistent classes with no a priori input about the nature of the spectra (Cheeseman et al. 1989; Goebel et al. 1989). Kwok et al. (1997) used one-letter codes to identify the character of each spectrum in the expanded database (11,224 sources). These various classification systems have divided the LRS database into distinct sets of spectral classes. However, none of these systems has been applied to a substantial number of spectra from instruments other than the LRS.

Other schemes focused on subsets of the LRS database. For example, Little-Marenin & Little (1988, 1990, hereafter, LML) classified evolved oxygen-rich stars based on their dust emission characteristics. This system, as modified by Sloan & Price (1995, 1998, hereafter SP), has also been applied to ground-based spectral measurements (e.g. Creech-Eakman et al. 1997; Monnier et al. 1998).

Spectra taken by the Short Wavelength Spectrometer (SWS) on the *Infrared Space Observatory* (*ISO* Kessler et al. 1996; de Graauw et al. 1996) are now publically available. In this paper, we focus on the full-range, moderate-resolution spectra obtained in the SWS01 observing mode. These observations are over a greater wavelength range than the LRS database (2.4–45.2  $\mu\text{m}$  compared to 7.7–22.7  $\mu\text{m}$ ), and at a higher spectral resolution ( $>300\text{--}400$  vs.  $20\text{--}60$ ). The SWS01 spectral resolution is sufficient for detailed examination of band structure and atomic fine-structure lines. The extended wavelength range includes both the near-infrared spectral region, which is dominated by molecular bands from stellar

photospheres, and the thermal infrared region, which is dominated by dust emission. The LRS database is compromised by inadequate wavelength coverage on the short-wavelength side of the strong spectral features produced by silicate dust ( $10\ \mu\text{m}$ ) and silicon-carbide grains ( $11.5\ \mu\text{m}$ ), making it difficult unambiguously define the stellar continuum.

*ISO* obtained observatory-style pointed observations whereas *IRAS* obtained spectra as an adjunct to the main survey with the LRS as a secondary instrument. Consequently, the SWS database only contains full-range spectra of  $\sim 910$  specifically targeted sources (1248 total spectra, including duplicates and off-positions). To ensure that *ISO* obtained SWS spectra of as wide a variety of sources as possible, the observing lists of the STARTYPE proposals<sup>7</sup> targeted sources in categories which were under-represented in the infrared classification systems (§2.1). The result is a robust database of infrared spectra which is the basis for our infrared spectral classification system.

We describe the sample of the observed sources and the structure and calibration of the spectral data in Section 2. Section 3 details the criteria for the classification system, which we discuss in Section 4. The actual classifications are presented in Appendix A.

## 2. Observations and Data Analysis

### 2.1. The Sample

#### 2.1.1. Source Selection

The SWS database contains observations obtained for a wide range of individual observing projects. A series of observing proposals, referred to collectively as the STARTYPE proposals, was developed to supplement observations from other dedicated and open-time experiments. The original observing lists included at least one source from each category defined by the MK spectral types, LRS classifications, AutoClass classifications, and the spectral templates in the Galactic Point Source Model (Wainscoat et al. 1992). While the MK classification system is familiar to most readers, the infrared classification systems may be less so. Therefore, we describe below the three infrared classification systems used to create the STARTYPE observation lists.

The LRS classifications presented in the LRS atlas (*IRAS* Science Team 1986) used a two-digit scheme to describe a spectrum. The scheme subjectively divided the spectra into

---

<sup>7</sup>The STARTYPE proposals received *ISO* project names STARTYP1, STARTYP2, and ZZSTARTY.

10 groups (identified by the first digit) based on spectral morphology and, in part, on ideas about the underlying physics producing the spectra. For blue sources (i.e. flux decreasing with wavelength), the first digit represents (1) featureless spectra, (2) silicate emission, (3) silicate absorption, or (4) carbon-rich dust emission features. Red sources were assigned a first digit of 5, 6, or 7 (analogs of 1, 2, or 3). Spectra dominated by emission lines were divided into (8) those with unidentified infrared (UIR) bands and (9) those without UIR bands. Miscellaneous spectra were assigned an initial digit of 0. The second digit was typically based on the strength of the features identified by the first digit. In general, the spectral morphology is clearly different among the groups, but some inconsistencies and misclassifications exist.

The AutoClass scheme (Goebel et al. 1989; Cheeseman et al. 1989) used artificial intelligence to sort the LRS spectra into a series of self-consistent classes. By separating features on the basis of both shape and strength, this method distinguished subtleties not addressed by the LRS atlas characterizations, which separated features based on strength alone. It also found weak features that had been previously undetected.

Selecting sources only from classification systems based on the LRS database excludes information about the wavelength regions not covered by the LRS, that is, shortward of  $7.7\ \mu\text{m}$  and longer than  $22\ \mu\text{m}$ . To address this shortcoming, the STARTYPE experiments also selected sources based on the spectral templates in the Galactic Point Source Model (Wainscoat et al. 1992). Sources in this scheme are divided into classes based either on the MK spectral classifications or location in the  $[12] - [25]$ ,  $[25] - [60]$  color plane. Cohen et al. (1990) grouped sources in the  $[12] - [25]$ ,  $[25] - [60]$  plane and created prototypical spectral templates used in the Wainscoat et al. (1992) Galactic Point Source Model.

An initial list of 1316 sources brighter than 40 Jy at  $12\ \mu\text{m}$  was compiled by randomly selecting  $\sim 10\%$  of the sources that were used to create the classification schemes described above. Because all three infrared schemes use the LRS spectra, roughly 25% of the sources were randomly selected from the LRS atlas, then sorted by LRS class. When a particular LRS sub-class was well-populated after the initial selection, sources associated with objects in other catalogs were preferentially chosen due to the additional information available on them. Because the  $12\ \mu\text{m}$  flux criterion discriminated against red and emission line objects, the flux limit was lowered to 5 Jy at  $12\ \mu\text{m}$  to include 347 red objects (LRS classes  $5n$  through  $9n$ ) and to increase the number of sources in other under-populated LRS classes. The resulting list was tabulated in terms of the number of sources in each LRS and AutoClass sub-classes. If a sub-class had more than ten objects in the list, objects with higher quality LRS spectra were preferentially selected. Noisy counterparts of other, better defined, sub-classes and faint, unique classes (such as 01 or  $\theta 0$ ) were proportionately under-represented

in the observing list. The final 10% observing list was comprised of somewhat less than 800 sources.

Given the time constraints of the *ISO* mission, only a fraction, approximately one tenth, of the 10% list could be observed. The initial STARTYPE observing list sparsely, but uniformly, sampled the LRS and AutoClass subclasses (Table 1) and populated the MK classes. Because astrophysically interesting sources included in our list would likely be observed by other experimenters, we deferred the majority of our observations until we had surveyed the observing lists for the dedicated-time and open-time SWS01 spectra to determine which spectral classes were under-represented. As expected, the SWS01 observing lists of other experimenters sampled the red LRS classes ( $5n$  through  $9n$ ) and the equivalent AI classes well. The other classes were not as well sampled. We then concentrated the STARTYPE observations on the types of objects not observed by other *ISO* investigators, such as those with featureless continua and carbon stars with small circumstellar excesses. Therefore, additional sources within LRS classes  $1n$ ,  $2n$ , and  $4n$  were included in the STARTYPE observing list to provide more spectral representatives, particularly for the important subclasses 29, 43 and 44. Several LRS class  $3n$  sources were also included to correct the slight under-representation across the entire class. In this sample, stars of MK luminosity class V are well represented from B to early G, IIIs from early G to late M, and there is a sprinkling of temperature classes for the Is and IIs. Because M dwarfs are faint, we used the PHT spectrometer PHT-S to obtain spectra of 6 sources in the M dwarf sequence (Price et al. in preparation).

The observing scheme worked well. Of the  $\sim 910$  individual sources with SWS01 spectra, 275 were among the 800 sources in our 10% list. This number is increased to 379 if we had chosen to populate our subclasses to the 10% limit with the sources actually observed, although the coverage is not as uniform (see below). Table 1 shows how the number of sources observed compares to the number proposed, and to the total number of objects in each LRS and AutoClass subclass.

### 2.1.2. Selection Effects

Although the STARTYPE program aimed at producing a uniform sample, other programs did not. Objects in most programs were chosen with a particular research objective in mind, to investigate a particular phenomenon or a specific source. Sources with unusual features, intrinsically more interesting than sources which are more typical, were observed more often than they would have been in a completely uniform sample. For example,  $\eta$  Carina, as a unique object, would likely not have been observed in a randomly selected sample of

the 1248 objects, but was observed twice with SWS. However, the tendency to observe more unusual sources makes it more likely that the grid of subgroups for classification includes most of the possible types of infrared spectra.

Comparing the number of objects in each LRS and AI class with the number actually observed (Table 1) provides some insight into the bias of the SWS database. Although 47% of the STARTYPE 10% list was observed, the coverage of the *IRAS* classes (either LRS or AI) was significantly less uniform than the STARTYPE selections. For example, STARTYPE proposed to observe 34 of the 324 objects (10%) in LRS class 14, but the SWS database includes only 7 (2%). This apparently uninteresting group consists of nominally naked stars with spectral indices of  $\beta \sim 2$  (*IRAS* Explanatory Supplement 1988); in reality, these sources exhibit low-contrast dust emission (see LML and SP). In contrast, a group of truly naked stars with high signal-to-noise defined by AutoClass  $\delta 0$  (Cheeseman et al. 1989; Goebel et al. 1989) had 44 of 256 objects (16%) observed instead of the 27 suggested by STARTYPE, primarily because this group included the chosen calibration stars. Roughly 15% of the LRS and AutoClass classes had significantly fewer sources observed than if the STARTYPE sample had been followed, including several which in the end had no members observed. On the other hand, the SWS database includes more than twice as many PNe and star forming regions, source types which include the brightest objects in the infrared sky, than does the LRS Atlas (*IRAS* Science Team 1986), significantly expanding the available database on these important object types.

## 2.2. Data from the *ISO* Data Archive

The SWS obtained 1248 SWS01 spectra of over 900 different sources. The SWS01 spectra<sup>8</sup> cover wavelengths from 2.4 to 45.2  $\mu\text{m}$  in 12 spectral segments (or bands). The bands vary in length from 0.2  $\mu\text{m}$  (Band 1A: 2.4–2.6  $\mu\text{m}$ ) to over 16  $\mu\text{m}$  (Band 4: 29–45  $\mu\text{m}$ ). Each includes data from 12 individual detectors taken in two scan directions (“up” and “down” scans), giving a total of 24 discrete spectra in each spectral segment. Thus, to produce one full-scan spectrum from the SWS, 288 individual spectra must be calibrated and combined.

The standard “basic science” format for SWS spectra from the *ISO* Data Archive (IDA) is the Auto-Analysis Result (AAR) produced by the Off-Line Processing (OLP) pipeline. To classify the spectra, we typically used the browse product, which was created from OLP version 7.1. The browse product collapses the individual spectral scans to one usable spectrum,

---

<sup>8</sup>Hereafter, the set of 1248 SWS01 spectra are referred to as “the SWS database.”

which usually sufficed for classification. For problematic spectra, we used a preliminary release of OLP version 10.0, combining the data into one spectrum using software written at the Air Force Research Laboratory. Sloan et al. (2002) will present further details of this method, as well as a spectral atlas of the 1248 spectra.

Despite efforts to calibrate the flux of each spectral segment in the standard pipeline, discontinuities often exist at the boundaries between each of the 12 bands (Sloan et al. 2001; Kraemer et al. 2001; Shipman et al. 2001). For compact sources (smaller than the aperture), this problem most likely results from errors in satellite pointing (Shipman et al. 2001). Since the point spread function (PSF) is comparable to the angular size of the aperture, a slight offset from the center of the aperture will truncate the PSF.

A formal solution to the discontinuities does not yet exist, but a work-around has produced satisfactory results. Although the bands have sharply defined edges, adjacent bands include overlap regions of  $\sim 0.15\text{--}2.0\ \mu\text{m}$ . While only data from one band was considered to be “in-band” for a particular overlap region, with a well-calibrated relative spectral response function (RSRF), the “out-of-band” data can often be used to verify spectral features, the shape of the SED in that overlap region, and, most importantly, the flux level. To correct for the band-to-band discontinuities, the flux from a (usually) well-behaved spectral segment was chosen to be the fiducial segment and the other segments normalized to it, usually by a multiplicative factor. An additive factor was used for fainter sources where dark current variations might dominate gain variations. The same band could not be used for all sources due to the lack of flux in that band for certain SEDs. Band 1B ( $2.60\text{--}3.02\ \mu\text{m}$ ) served as the fiducial segment for sources dominated by flux from the stellar photosphere. For red sources peaking beyond  $\sim 15\ \mu\text{m}$ , Band 3C ( $16.5\text{--}19.5\ \mu\text{m}$ ) was the fiducial segment.

The detectors of Bands 2 ( $4.08\text{--}12.0\ \mu\text{m}$ , Si:Ga) and 4 ( $29.0\text{--}45.2\ \mu\text{m}$  Ge:Be) exhibit memory effects which can lead to differences in signal between the up and down scans (cf. Sloan et al. 2001; Kraemer et al. 2001). This problem manifests itself as a variation in dark current during a scan, the magnitude of which depends on the recent flux history of the detector. The SWS Interactive Analysis<sup>9</sup> (IA) routine *dynadark* was developed to model the dark current in Band 2. The algorithm in this routine is based on the Fouks-Schubert formalism (Fouks & Schubert 1995; Fouks 2001; Kester, Fouks, & Lahuis 2001), which accounts for non-linear responses in the flux history of the detectors. In its current form, this routine behaves erratically. It can substantially improves the Band 2 data, but it can

---

<sup>9</sup>The SWS Interactive Analysis system is developed and maintained by the SWS consortium members (Space Research Organization of the Netherlands, Max Planck Institut für Extraterrestrische Physik, Katholieke Universiteit Leuven, and the European Space Agency).



also overcorrect the data, degrading the match between up and down segments in Band 2A or 2B (Sloan et al. 2001; Kraemer et al. 2001). The Pipeline 10 processing automatically includes the *dynadark* routine.

The memory effect in Band 4 affects the shape of the spectrum longward of  $\lambda \sim 38\text{--}40\ \mu\text{m}$ . The degree to which a spectrum is affected depends on the underlying SED of the source and its brightness, as well as when during the mission and at what speed the observation was made. Changes in the calibration strategy involving photometric checks and dark current measurements by revolution 200 helped to some extent. However, the underlying problem with the memory effects remains unsolved.

Discontinuities in the  $26\text{--}30\ \mu\text{m}$  region are caused by a combination of changing aperture size (especially for extended sources), pointing issues, a light leak in Band 3D, and the poor behavior of Band 3E in many spectra. The first two problems require multiplicative corrections (to first order). The light leak appears at the long-wavelength end of Band 3D and results from radiation from Band 3A leaking through the filter for Band 3D. When it occurs, it invalidates data in Band 3D beyond  $\sim 27.3\ \mu\text{m}$ . Band 3E often contains very noisy data, especially at fainter flux levels. While the boundary between Bands 3D and 3E is officially  $27.5\ \mu\text{m}$  (Leech et al. 2001), the former cannot be used beyond  $27.3\ \mu\text{m}$  due to the light leak and the latter is invalid below  $27.7\ \mu\text{m}$ . As a result, normalization of one band to the other requires extrapolation of the data in the gap between them. Fortunately, Band 4 provides relatively reliable data at wavelengths down to  $27.7\ \mu\text{m}$  in OLP 10.0, even though its official cut-off is  $29.0\ \mu\text{m}$ . This extension allows normalization of Band 4 directly to Band 3D by extrapolation, bypassing the unreliable data in Band 3E.

The procedure used to reduce the band discontinuities assumes that the flux levels for Band 1B or 3C are reliable. Any errors in the absolute flux level within those bands will be propagated to the other bands through the normalization process. Furthermore, if the wrong reference band was chosen or an overlap region is unusually noisy, incorrect normalization can degrade the data. This problem is especially acute for weak sources with peak fluxes less than  $\sim 25\ \text{Jy}$ . The impact of these calibration issues on the classification effort is discussed in §4.1.

### 2.3. Classification Method

We created a list of all SWS01 observations, regardless of object type or quality flag, from the IDA, giving a total of 1248 spectra. The browse product spectrum for each of the 1248 observations was examined for quality. If a spectrum had no apparent signal, it

was set aside; this included most observations designated as off or reference positions by the observer. (If a spectrum had a discernible signal, it remained in the sample regardless of designation, such as the observation originally designated M17NOFF.) Roughly 35 objects contained no signal because the observer entered incorrect coordinates. The OLP software flagged an additional 30 or so spectra as having instrumentation, telemetry, pointing, or quality problems, but we classified them anyway.

Two of the authors (KEK and GCS) classified the sources independently, without prior knowledge of the MK spectral type, LRS class, or AutoClass category. The separate classifications were then compared and combined into a single scheme. Sources for which the placement was uncertain or unclear were reprocessed and re-examined. Typically this reprocessing resolved the ambiguity, although often the assigned classification included a “.” or “:.” to indicate uncertainty (see below).

### 3. The Classifications

We established three levels of classification<sup>10</sup>. The Level 1 categories (hereafter “groups”) are sorted based on the general morphology of the SED, which is determined primarily by the temperature of the strongest emitter (be it stellar or dust). Level 2 classification places each spectrum into a self-consistent subgroup based on the presence of prominent spectral features, such as silicate dust emission or absorption, carbon-rich dust emission, or atomic fine-structure lines.<sup>11</sup>

Level 3 classification will be the arrangement of spectra within a given subgroup into a sequence. This is a complex, interactive project left for the future. Some studies have reached Level 3 classification for certain subgroups already well defined by previous spectral databases. For example, Sloan & Price (1995, 1998) have already developed a sequence for oxygen-rich dust spectra produced by optically thin circumstellar shells.

---

<sup>10</sup>Use of existing LRS classifications was considered. However, those classes were based on a limited spectral range and focused too strongly on the strength of a single feature. This scheme was rejected as inadequate to describe the full range of SWS spectra (see §4.2.2).

<sup>11</sup>Acceding to a request by the editor to name our classification scheme, we hereby christen it “the KSPW system.”

### 3.1. Level 1 Classification

The Level 1 classes primarily depend on the temperature of the dominant emitter. Five main categories emerged, ranging from the hottest objects such as naked stars (1) to the coolest objects such as protostellar cores (5). Additional categories include spectra with emission lines but no detected continuum (6) and spectra which either contain no classifiable flux or are flawed for some other reason (7).

1. Naked stars. Photospheric emission with no apparent influence from circumstellar dust dominates these spectra. All sources have optical identifications with known and well-classified stars.
2. Stars with dust. The SEDs are primarily photospheric at shorter wavelengths, but they also show noticeable or significant dust emission at longer wavelengths. Most sources are red supergiants or are associated with the asymptotic giant branch (AGB).
3. Warm, dusty objects. These sources are dominated by emission from warm dust. Any photospheric contribution from an embedded star is either absent or significantly less than the peak emission. The emission typically peaks between  $\sim 5$  and  $\sim 20 \mu\text{m}$ , which implies dust temperatures hotter than  $\sim 150$  K. The majority of these spectra arise from deeply enshrouded AGB sources, transition objects, planetary nebulae (PNe), or other evolved sources.
4. Cool, dusty objects. These objects are dominated by cooler dust emission, the peak of which occurs within the SWS spectral range but longward of  $\sim 20 \mu\text{m}$ . Most sources in this group are PNe, AGB stars, and transition objects, although many are young stellar objects (YSOs).
5. Very red objects. These objects have rising spectra toward longer wavelengths through at least the end of Band 4. Most sources are star-forming regions or PNe.
6. Continuum-free objects but with emission lines. These sources do not have enough continuum emission to allow an unambiguous placement in another group. Emission lines, typically atomic fine-structure lines, dominate the spectra. Objects in this group include supernova remnants and novae. Because these spectra are often difficult to discern from the class 7 spectra, this group may not contain all possible members observed by *ISO*.
7. Flux-free and/or fatally flawed spectra. This group includes objects with no detected flux or flux levels insufficient for classification. In addition to intrinsically faint objects,

this group contains observations with incorrect coordinates, observations intentionally offset from sources (off-positions), and flagged observations. Spectra with enough flux to allow classification appear in the appropriate group whenever possible despite flags or off-target coordinates.

### 3.2. Level 2 Classification

Level 2 classification separates the Level 1 groups into subgroups based on the spectral features superimposed on the overall SED. Each subgroup has a one-, two-, or three-letter designation which succinctly indicates the type of dust and most prominent feature(s), as described below and summarized in Table 2. In addition to the letter designations, one-character suffixes describe any unusual properties of the spectrum (Table 3).

The initial letter of the designation indicates the overall “family” to which an object belongs. The three most important families are “S”, “C”, and “P.” “S” indicates oxygen-rich dust material such as silicate or alumina grains, whereas “C” indicates carbon-rich material. “P” indicates planetary nebulae (PNe), which typically have spectra rich in emission lines.

The second and third letters, if used, indicates the presence of one or more specific spectral features. The letter combinations present in Groups 2–5 are:

**SE**—Silicate or oxygen-rich dust emission feature at  $\sim 10\text{--}12\ \mu\text{m}$ , usually accompanied by a secondary emission feature  $\sim 18\text{--}20\ \mu\text{m}$ .

**SB**—Self-absorbed silicate emission feature at  $10\ \mu\text{m}$ , usually showing emission peaks at 9 and  $11\ \mu\text{m}$ . The secondary emission feature  $\sim 18\text{--}20\ \mu\text{m}$  is common.

**SA**—Silicate absorption feature at  $10\ \mu\text{m}$ . The  $18\text{--}20\ \mu\text{m}$  feature can be in emission or absorption. Features from crystalline silicate emission may also be present at longer wavelengths.

**SC**—Crystalline silicate emission features, especially at  $\sim 33$ , 40, and/or  $43\ \mu\text{m}$ . No significant silicate features apparent  $\sim 10\ \mu\text{m}$ .

**SEC**—Crystalline silicate emission features, especially at  $11\ \mu\text{m}$ , usually at  $\sim 19$ , 23, and  $33\ \mu\text{m}$ , and often at 40 and/or  $43\ \mu\text{m}$ . The presence of crystalline silicates has shifted the emission feature at  $10\ \mu\text{m}$  due to amorphous silicate grains  $\sim 1\ \mu\text{m}$  to the red. The presence of other crystalline features distinguishes this feature from the self-absorbed silicate emission (SB) feature, which also peaks  $\sim 11\ \mu\text{m}$ .

**CE**—Carbon-rich dust emission dominated by the silicon carbide emission feature at  $\sim 11.5\ \mu\text{m}$ .

The shape and wavelength of this feature differs substantially from the SB and SEC features at  $11\ \mu\text{m}$ , and any uncertain cases can be resolved by the presence of a narrow absorption feature at  $13.7\ \mu\text{m}$  (due to  $\text{C}_2\text{H}_2$ ; e.g. Aoki et al. 1999; Cernicharo et al. 1999; Volk et al. 2000).

**CR**—Carbon-rich dust emission showing a reddened continuum (due to a strong contribution from amorphous carbon), the SiC emission feature at  $\sim 11.5\ \mu\text{m}$ , and another emission feature at  $\sim 26\text{--}30\ \mu\text{m}$ .

**CT**—Carbon-rich dust emission characterized by a red continuum and emission features at 8, 11.5, 21,  $26\text{--}30\ \mu\text{m}$ . The “T” stands for the “**T**Wenty-one”  $\mu\text{m}$  emission feature, which is the primary discriminant between CR and CT.

**CN**—Carbon-rich proto-planetary nebulae with  $11.5\ \mu\text{m}$  emission or the  $13.7\ \mu\text{m}$  absorption features, and much redder SEDs as compared to the CRs.

**C/SC**—Carbon-rich features in the blue half of the spectrum, combined with crystalline silicate emission features at 33, 40, and/or  $43\ \mu\text{m}$ .

**C/SE**—Carbon-rich features in the photospheric emission, combined with silicate or oxygen-rich dust emission at  $\sim 10\text{--}12\ \mu\text{m}$ . These are the silicate carbon stars (e.g. Little-Marenin 1986; Lloyd Evans 1990).

**PN**—Prominent emission lines from atomic fine-structure transitions.

**PU**—Similar to PN, but with strong UIR features as well (see below).

**U**—Prominent emission features at 3.3, 6.2,  $\sim 7.7\text{--}7.9$ , 8.6, and  $11.2\ \mu\text{m}$  commonly described as UIR features. They most likely arise from polycyclic aromatic hydrocarbons (PAHs), although this identification remains controversial. Unless specified otherwise, there are no other strong spectral features. Sources with low-contrast UIR emission difficult to detect when examining full-scan spectra may not be classified as “U”. In other words, many sources with fainter UIR features are classified in other groups.

**U/SC**—A combination of UIR emission features in the blue half of the spectrum and crystalline silicate emission features at 33, 40, and/or  $43\ \mu\text{m}$ .

**E**—No discernible spectral structure, except for the presence of atomic emission lines.

**F**—Featureless spectrum (within the signal/noise ratio).

**W**—The continuum emission peaks  $\sim 6\text{--}12\ \mu\text{m}$ , usually with apparent silicate absorption at  $10\ \mu\text{m}$ . The “W” stands for Wolf-Rayet, since these spectra are always produced by Wolf-Rayet stars or R Corona Borealis variables.

**M**—Miscellaneous spectra: most of these objects have distinct features but could not be placed in any of the other existing categories, even with a “p” suffix. Objects that clearly belong in the parent group but are too noisy to classify further into a subgroup also appear here.

Because some spectral characteristics occur across a broad range of temperature, the same Level 2 subgroup description can appear in different Level 1 groups. Table 4 summarizes the occurrence of each Level 2 subgroup within the Level 1 groups.

### 3.3. Group Descriptions and Sample Spectra

Each group of Level 1 spectra separates into several subgroups, often including a subgroup for peculiar or noisy spectra which defied attempts to unambiguously place them elsewhere. The figures illustrate sample spectra for each subgroup. Spectral classifications and source types are taken from the literature or from SIMBAD.

#### 3.3.1. Group 1—*Naked Stars*

The naked stars fall into several easily distinguished subgroups based primarily on the presence or absence of molecular absorption bands. These include ordinary stars (1.N), oxygen-rich stars (1.NO), carbon-rich stars (1.NC), and emission line stars (1.NE). An additional subgroup (1.NM) includes sources whose SEDs are dominated by photospheric emission, but are too noisy or otherwise too peculiar to place with confidence in one of the main subgroups. Figure 1 presents examples of each subgroup.

**1.N** The 1.N stars include the main sequence stars with no molecular bands in their spectrum. A combination of a simple Engelke function (Engelke 1992) and narrow atomic absorption features (primarily hydrogen recombination lines) accurately describes the spectrum. MK classifications of stars in this subgroup range from O9V ( $\zeta$  Oph) to K0Iab ( $\alpha$  UMi).

**1.NO** The 1.NO stars show broad absorption features in their spectra from the CO overtone (maximum absorption  $\sim 2.5 \mu\text{m}$ ), a blend of the SiO overtone ( $4.2 \mu\text{m}$ ) and the CO fundamental ( $4.6 \mu\text{m}$ ), and the SiO fundamental ( $8 \mu\text{m}$ ). Additionally, a complex set of narrow absorption features appears at  $\sim 3\text{--}4 \mu\text{m}$ . Most of these sources are K and M giants and supergiants with C/O ratios less than unity, although there is one F dwarf and 2 S stars.

**1.NC** The 1.NC stars show several molecular absorption bands indicative of a carbon-rich photosphere, including narrow bands at  $\sim 2.5 \mu\text{m}$  (attributed to CO, CN, and  $\text{C}_2$ ), and

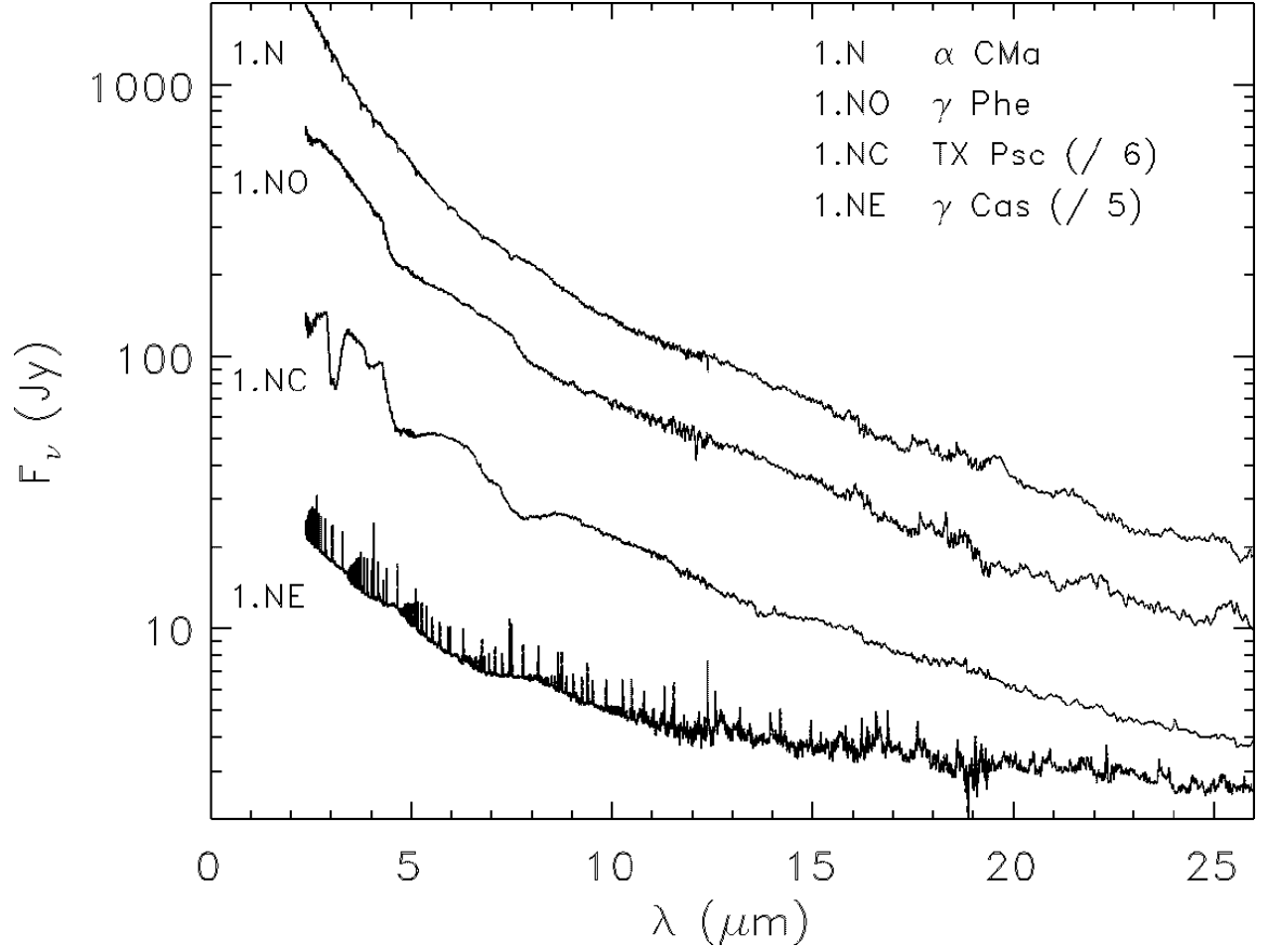


Fig. 1.— Typical spectra from Group 1. Numbers in parentheses after the object name indicate the scaling factor used to make the plots.

3.1  $\mu\text{m}$  (HCN and  $\text{C}_2\text{H}_2$ ) and broad bands at  $\sim 5 \mu\text{m}$  ( $\text{C}_3$ , CO, and CN), 7–8  $\mu\text{m}$  (HCN,  $\text{C}_2\text{H}_2$ , and CS), and 14–15  $\mu\text{m}$  (HCN and  $\text{C}_2\text{H}_2$ ) (e.g. Goebel et al. 1978, 1980; Aoki et al. 1998a, 1999).

**1.NE** The 1.NE stars are emission line stars. Numerous hydrogen recombination lines appear in emission. Recombination lines from helium (Hony et al. 2000) or fine-structure lines from, for example, [Fe II] and [Ni II] (Lamers et al. 1996) may also be present. In some sources, Balmer-like jumps for the infrared series, such as the Humphreys jump  $6-\infty$  near 3.4  $\mu\text{m}$ , produce discontinuities in the continuum (Hony et al. 2000).

Heras et al. (2001) have classified 1.N and 1.NO sources in more detail, reaching Level 3 for  $\sim 40$  sources. They distinguish sub-classes of stars with (1) only strong H lines, (2) strong CO absorption and no SiO, (3) strong CO and SiO absorption bands; and (4) strong CO and SiO features plus the  $\text{H}_2\text{O}$  bending mode feature. The strength of the molecular features increase with decreasing temperature and, consequently, later MK class. They also find that the strength of the infrared bands are well correlated with each other.

### 3.3.2. Group 2—Stars with Dust

Group 2 includes sources with SEDs dominated by the stellar photosphere but also influenced by dust emission (Fig. 2). The nature of the spectral contribution from the dust in the mid-infrared (typically  $\sim 10\text{--}11 \mu\text{m}$ ) determines the subgroup. The dust properties are usually consistent with the photospheric features in the near-infrared. Most of the sources show oxygen-rich dust emission (SE), and we have separated these spectra into three subgroups based on the shape of the spectral emission feature in the  $10\text{--}12 \mu\text{m}$  region analogous to classes defined by LML and SP.

**2.SEa** These spectra show a broad emission feature peaking  $\sim 12 \mu\text{m}$ . The dust emission is usually weak, so the spectra resemble those in subgroup 1.NO. The LML system classifies these as “broad” spectra, and the SP system classifies them as SE1–3. This broad feature arises from amorphous alumina dust (Onaka et al. 1989; Lorenz-Martins & Pompeia 2000). A weak 20  $\mu\text{m}$  silicate feature is usually present, as well as a complex of absorption bands  $\sim 3 \mu\text{m}$  (from ro-vibrational  $\text{H}_2\text{O}$  transitions and a broad, deep OH transition). Some sources show the well-known 13  $\mu\text{m}$  emission feature, often associated with narrow  $\text{CO}_2$  emission bands at 13.87, 14.97, and 16.28  $\mu\text{m}$  (Justtanont et al. 1998). Roughly 15% of the SEa sources have particularly weak dust emission. Heras et al. (2001) note that one of these, V Nor, has anomalous mid-infrared properties relative to its optical classification, probably the result of an unrecognized thin dust shell.



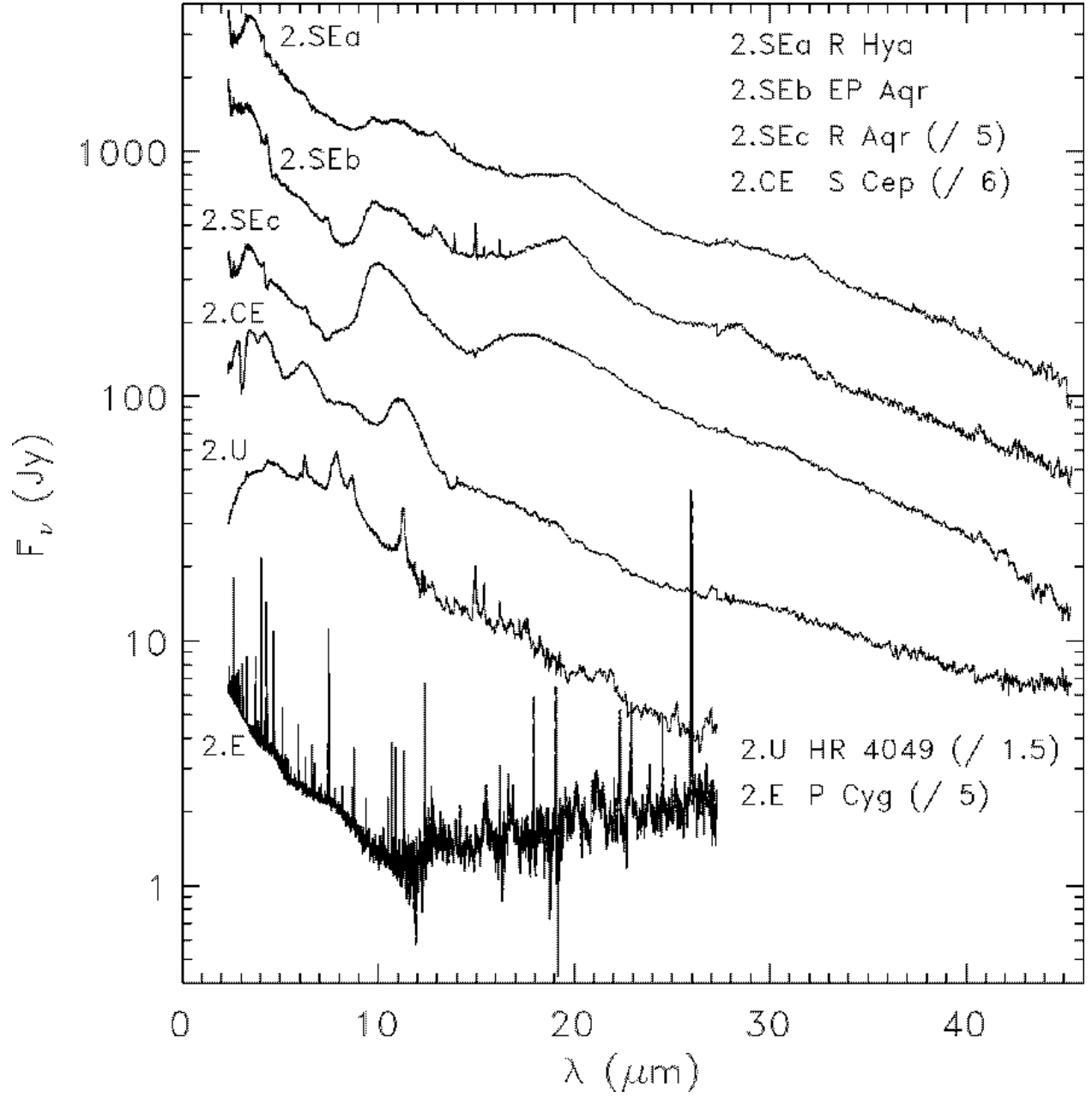


Fig. 2.— Typical spectra in Group 2. The 2.U and 2.E spectra are truncated at 27.5  $\mu\text{m}$  (through Band 3D) due to poor signal-to-noise in Bands 3E and 4.

**2.SEb** The SP system describes these spectra as “structured silicate emission” (SE3–6), while the LML system would classify them as “S”, “3-component”, or “Sil++”. These spectra have 10  $\mu\text{m}$  dust features due to amorphous silicates, but they also show a secondary peak to the emission  $\sim 11 \mu\text{m}$ , and they often have a 13  $\mu\text{m}$  feature as well (with associated  $\text{CO}_2$  bands). The 18–20  $\mu\text{m}$  feature tends to have a moderate strength, and the  $\text{H}_2\text{O}$  feature at 3  $\mu\text{m}$  in 2.SEa and 1.NO sources is also present, although with less influence from OH. The spectral structure at 10 and 11  $\mu\text{m}$  may arise from a mixture of amorphous alumina or silicate grains (Lorenz-Martins & Pompeia 2000) or from optically thick but geometrically thin shells of pure amorphous silicates (where the emission feature has begun to self absorb; Egan & Sloan 2001).

**2.SEc** These sources have strong silicate emission features with peaks at 10 and 18  $\mu\text{m}$ . A few sources also show the 13  $\mu\text{m}$  feature. The LML system classifies these as “Sil” or “Sil+” and the SP system describes them as “classic silicate spectra” with SE indices of 6–8. The photospheric absorption bands shortward of 10  $\mu\text{m}$  are often complex.

**2.CE** These spectra have a strong emission feature at  $\sim 11.5 \mu\text{m}$  due to SiC dust emission. Photospheric features include bands at 2.5 and 3.1  $\mu\text{m}$  attributed to HCN and  $\text{C}_2\text{H}_2$ , and at 4.3–6.0  $\mu\text{m}$  attributed to CO and  $\text{C}_3$  (e.g. Hron et al. 1998; Jørgensen et al. 2000). The complexity of the emission and absorption features shortward of 10  $\mu\text{m}$  makes it difficult to determine the continuum level in this wavelength region.

**2.C/SE** These spectra have carbon-rich photospheric features but the oxygen-rich silicate emission feature at 10–12  $\mu\text{m}$ . Two known silicate carbon stars, V778 Cyg and W Cas, are tentatively joined in this subgroup by RZ Peg.

**2.U** The two sources in this category show stellar photospheres with superimposed UIR emission features. The photospheric spectrum for XX Oph resembles the 1.NO sources. The photosphere for HR 4049, an unusual low-metallicity, high mass-loss, post-AGB star (e.g. van Winckel et al. 1995, and references therein), is unique in the SWS database.

**2.E** These sources show emission lines on a photospheric SED, with possible weak dust emission features in the 12–20  $\mu\text{m}$  range. The exception is WR 147, which may have silicate absorption in its spectrum (Morris et al. 2000).

**2.M** This subgroup includes miscellaneous spectra which contained dust emission but could not be assigned to another subgroup, primarily due to a poor signal/noise ratio in the  $\sim 10$ –12  $\mu\text{m}$  region.

### 3.3.3. Group 3

Emission from warm dust dominates the SEDs of Group 3; this dust emission usually arises from a circumstellar shell. The spectra peak shortward of  $\sim 20 \mu\text{m}$ , usually 10–15  $\mu\text{m}$ , but they show little or no contribution from a stellar photosphere. Like the previous groups, the carbon and oxygen sequences are quite distinct, as Figure 3 illustrates.

**3.SE** These sources show silicate emission at 10  $\mu\text{m}$  superimposed on the thermal continuum from the dust shell. The dust emission features resemble the classic silicate features in subgroup 2.SEc (at 10 and 20  $\mu\text{m}$ ), but with no photospheric emission present due to the optically thicker dust shell. Three sources, all symbiotic novae, show several forbidden emission lines (3.SEe), notably [Ne VI] at 7.65  $\mu\text{m}$ , [Ne V] at 14.32 and 24.32  $\mu\text{m}$ , and [O IV] at 25.89  $\mu\text{m}$ . Three other sources have peculiar spectra (3.SEp) with a weak or missing 20  $\mu\text{m}$  emission feature; two of these are S stars. The more typical 3.SE sources tend to be AGB sources, OH/IR stars, or supergiants, although three of these 14 are pre-main-sequence Ae or Be stars.

**3.SB** These spectra arise from optically thick shells; self absorption of the silicate dust has shifted the 10  $\mu\text{m}$  feature closer to 11  $\mu\text{m}$ . The SEDs peak at  $\sim 18$ –19  $\mu\text{m}$ , and some sources show crystalline silicate features longward of 30  $\mu\text{m}$ . The sources are associated with the AGB or OH/IR stars.

**3.SAe** This unusual subgroup shows a 10  $\mu\text{m}$  absorption feature and bright emission lines from [S IV] at 10.5  $\mu\text{m}$ , [Ne II] at 12.8  $\mu\text{m}$ , [S III] at 15.6  $\mu\text{m}$ , [Fe III] at 22.9  $\mu\text{m}$ , and [S III] at 33.5  $\mu\text{m}$ . The 20  $\mu\text{m}$  silicate emission feature is more rounded than in the SE and SB spectra and appears at a slightly longer wavelength. Both sources are young or pre-main-sequence Be stars.

**3.CE** These spectra resemble the 2.CE subgroup, showing an emission feature  $\sim 11.5 \mu\text{m}$  from SiC, but dust absorption obscures the photospheric absorption features from molecular bands which dominate the near-infrared wavelengths of the 2.CE and 1.NC spectra. Most of the sources show a narrow and often deep C<sub>2</sub>H<sub>2</sub> absorption band at 13.7  $\mu\text{m}$ .

**3.CR** These sources are cooler analogs of the 3.CE sources. The 11.5  $\mu\text{m}$  SiC emission feature still dominates and the C<sub>2</sub>H<sub>2</sub> absorption band at 13.7  $\mu\text{m}$  is still prominent, but other emission features also appear, usually in the 26–30  $\mu\text{m}$  region and sometimes at 8  $\mu\text{m}$ . IRC +10216 is the brightest of these sources; radiative transfer modeling of its spectrum suggests that amorphous carbon dominates the SiC dust component ( $\sim 90$ –95%; e.g. Martin & Rogers 1987; Sloan & Egan 1995). The optical efficiency of amorphous carbon follows a  $\lambda^{-1}$  relation in the mid-infrared, mimicking a blackbody of lower temperature than the actual dust temperature (Martin & Rogers 1987).

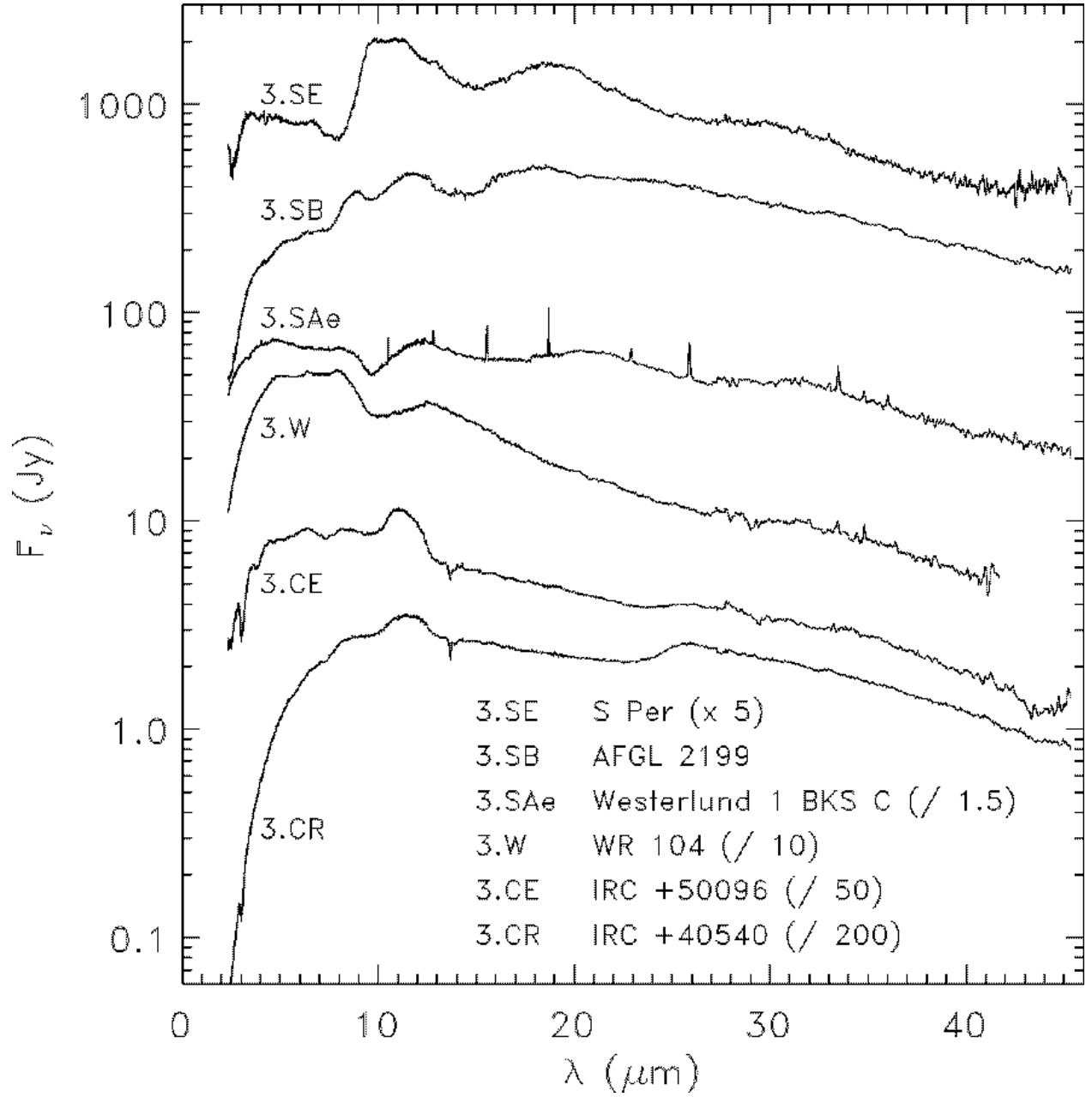


Fig. 3.— Typical spectra in Group 3.

**3.W** The spectra of these sources peak at  $\sim 6\text{--}8\ \mu\text{m}$ . Most show strong silicate absorption features at  $10\ \mu\text{m}$  similar to the 4.SA feature. Except for the  $10\ \mu\text{m}$  feature, the spectra are nearly featureless and have little similarity to sources in any other subgroup. All members are either Wolf-Rayet or R Corona Borealis stars.

#### 3.3.4. Group 4

Dust emission dominates the SEDs of Group 4, and the dust temperature is cooler than in Group 3, with the spectra peaking at wavelengths between  $\sim 20$  and  $\sim 40\ \mu\text{m}$ . The photospheric contribution is generally negligible. Several of the subgroups in Group 4 are analogous to those in Group 3, but with significantly cooler dust. As in the warmer groups, the carbon and oxygen sequences are quite distinct. The carbon-rich spectra continue in relatively tight groups whereas the oxygen-rich dust spectra form a rather heterogeneous group. Finding distinct and self-consistent subgroups for these spectra has proven difficult, and finding subgroups populated by uniform samples has proven impossible. Figure 4 shows sample spectra from Group 4.

**4.SE** These sources show an emission feature from amorphous silicates at  $10\ \mu\text{m}$  superimposed on emission from a cool dust shell. As in subgroup 3.SE, the contrast varies significantly from one source to the next. Most of the SEDs peak around  $20\text{--}25\ \mu\text{m}$ , although in three sources the peak is near  $30\ \mu\text{m}$ . Of all the subgroups in Group 4, this is the most difficult to characterize, due in part to the low signal/noise ratio of many of the spectra. The specific shapes of the SED and the  $10\ \mu\text{m}$  silicate feature differ among the sources. Some spectra, often with bluer SEDs, show forbidden emission lines (the specific transitions vary substantially from source to source). Most 4.SE sources have optical spectral classes of Be, Ae, or Fe, or are described as PNe. While more than half of the sources are post-main-sequence, several are Herbig Ae/Be stars or related pre-main-sequence objects.

**4.SEC** These sources show prominent crystalline silicates in at least two of three positions:  $\sim 11$ ,  $23$ , and  $33\ \mu\text{m}$ . The  $11\ \mu\text{m}$  emission feature may be weak, in which case the usual amorphous feature at  $10\ \mu\text{m}$  appears to be broadened, or it may dominate, producing a strong, sharp peak at  $11\ \mu\text{m}$ . Additional crystalline silicate features may also be present at  $19$  and  $43\ \mu\text{m}$ . Like 4.SE, this subgroup includes a heterogeneous collection of sources, but only three of the 11 objects are clearly identified as pre-main-sequence. The rest tend to be young PNe or proto planetary nebulae (PPNe); the sample also includes one Mira variable and the hypergiant IRC +10420.

**4.SB** The  $10\ \mu\text{m}$  silicate feature is in self-absorption, sometimes strongly, and emission

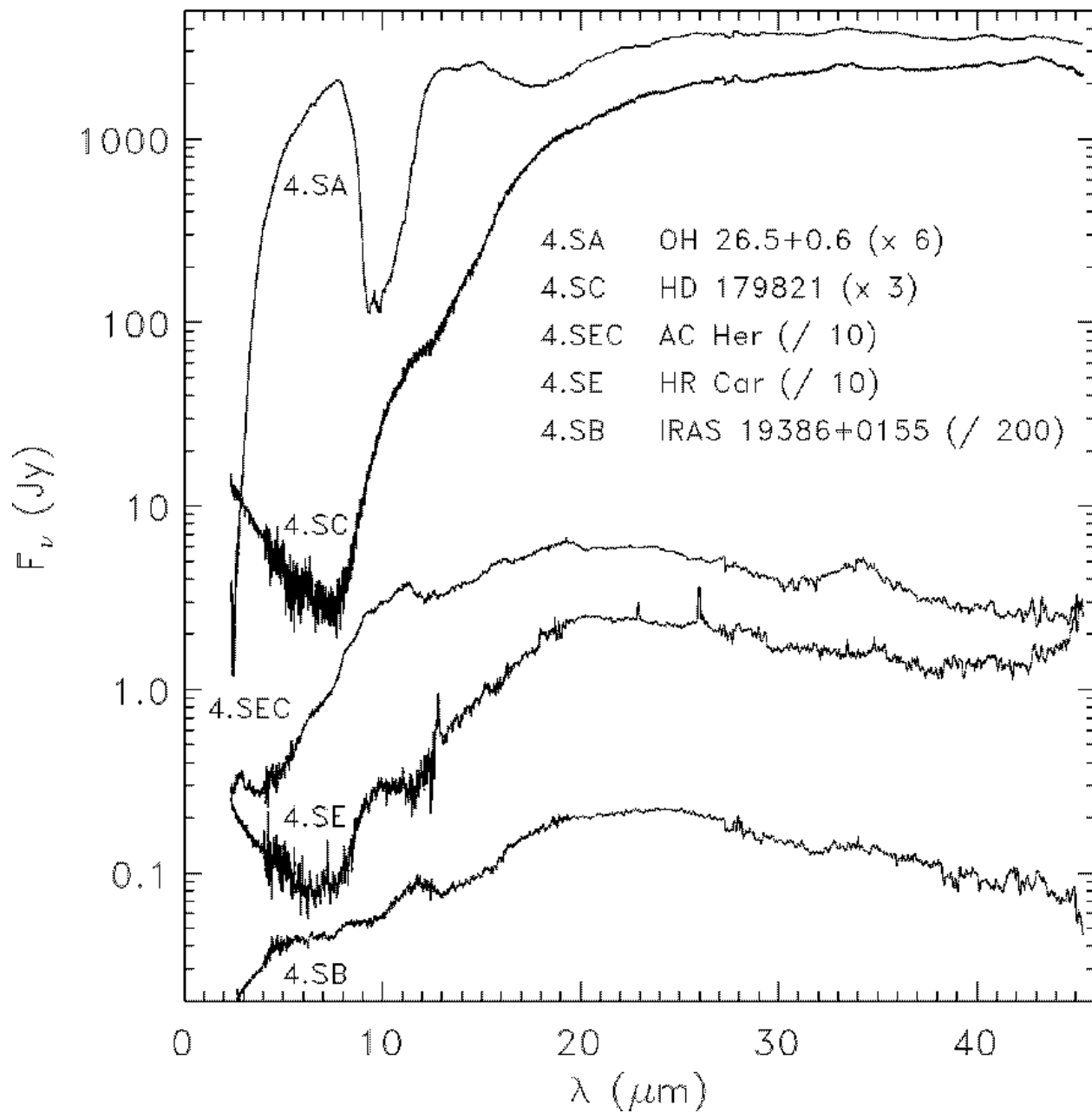


Fig. 4.— Typical spectra for Group 4. (a) oxygen-rich sources, arranged in a possible evolutionary sequence (§4.3.2).

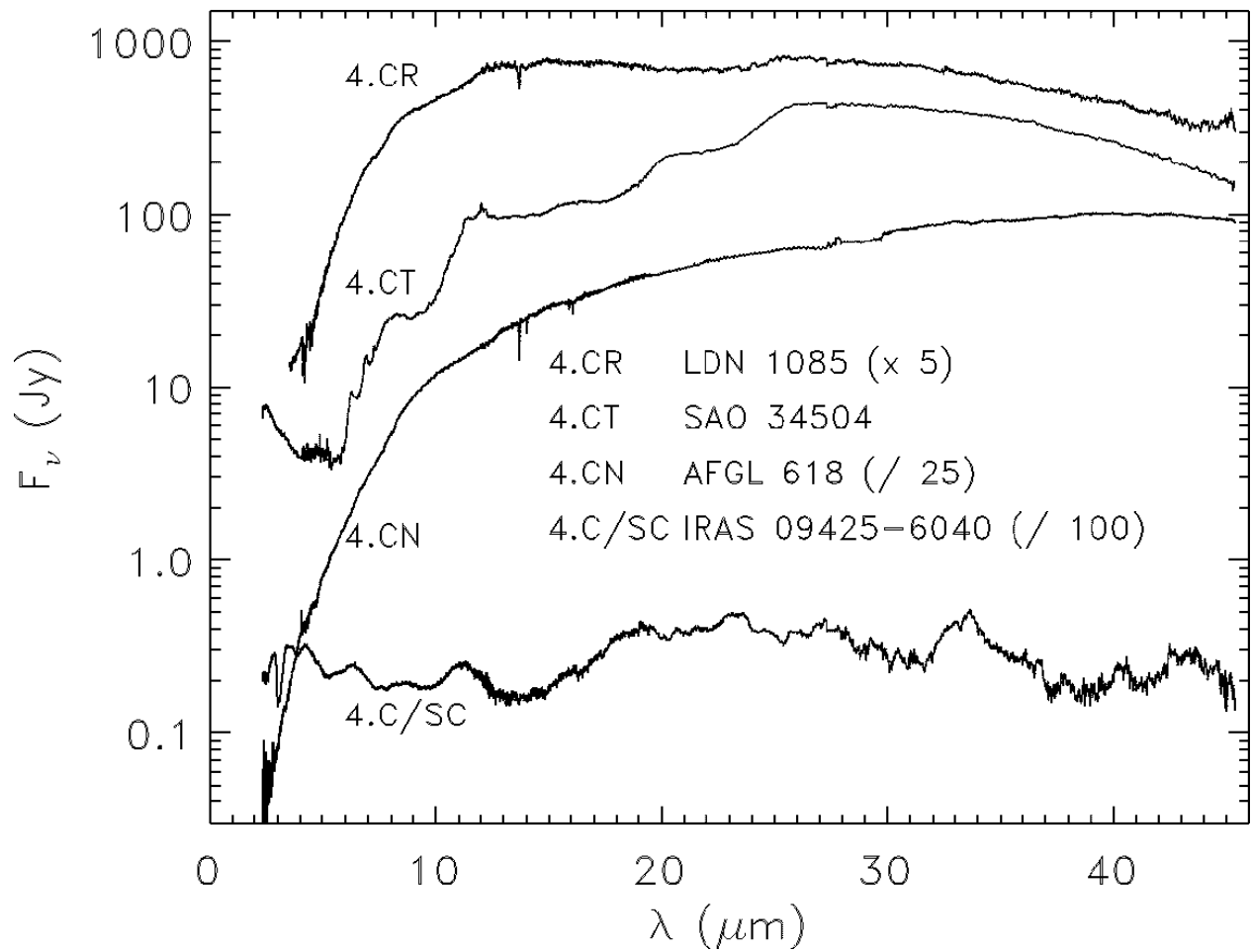


Fig. 4.— Group 4, cont'd. (b) Carbon rich sources. The spectrum for 4.CR is truncated at lower wavelengths due to poor signal-to-noise.

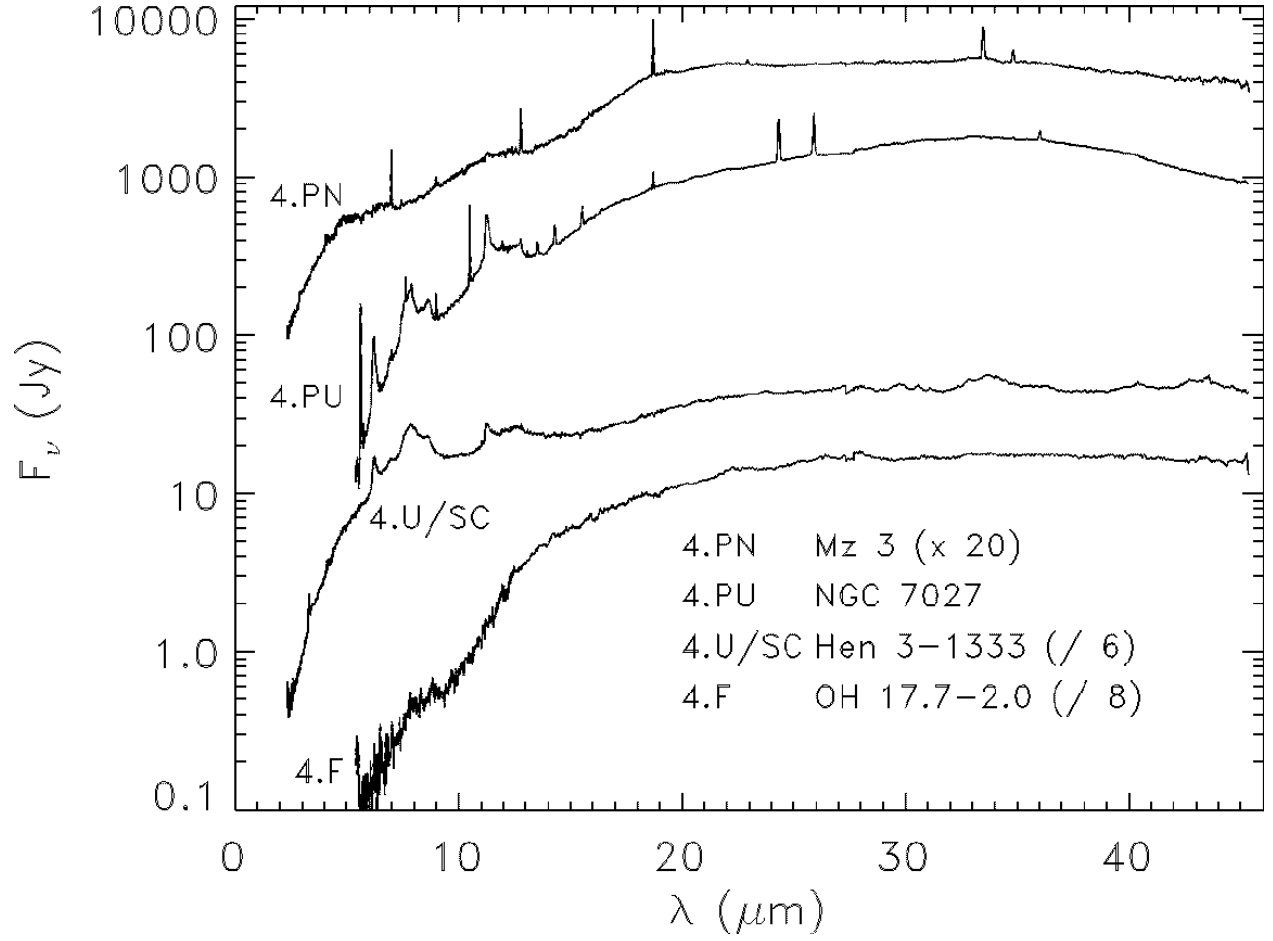


Fig. 4.— Group 4, cont'd. (c) The spectra for 4.PU and 4.F are truncated at lower wavelengths due to poor signal-to-noise.



features from crystalline silicates may be present at 33, 40, and/or 43  $\mu\text{m}$ , though not strongly. The majority of sources are PNe or PPNe, although one may be a pre-main-sequence Ae star, another is a Be variable, and a third is an AGB source.

**4.SA** This subgroup exhibits silicate absorption at 10  $\mu\text{m}$  and sometimes also at 18  $\mu\text{m}$ . Most sources show emission features from crystalline silicates at 33, 40, and 43  $\mu\text{m}$ . Stronger absorption at 10  $\mu\text{m}$  usually occurs with stronger emission from crystalline silicates, especially at 33  $\mu\text{m}$ . The deepest 10  $\mu\text{m}$  absorption features arise from OH/IR stars. Other sources in this subgroup include PPNe and PNe. Two of the three bluest sources are more difficult to characterize and may be pre-main-sequence.

**4.SC** All sources in this subgroup show crystalline silicate emission features at 33 and 43  $\mu\text{m}$ . Many also show crystalline silicate features at 23 and 40  $\mu\text{m}$ . The source types are somewhat heterogeneous, although PPNe and PNe (especially young PNe associated with Be central stars) dominate. Other sources include Wolf Rayet stars, OH/IR stars, and one source identified as a pre-main-sequence G star (DG Tau).

**4.F** The SEDs of sources in this subgroup basically have no features (greater than the noise), with no silicate emission or absorption at 10  $\mu\text{m}$  or any crystalline silicate emission at longer wavelengths. Three sources do show UIR emission, and one has several non-silicate absorption features due to ices. Most sources are PNe or OH/IR stars, except for the source with ice absorption, which is a YSO (R CrA [TS84] IRS 2).

**4.CR** This subgroup continues the carbon-rich dust sequence (2.CE—3.CE—3.CR) to cooler shells. The SEDs peak  $\sim 28$   $\mu\text{m}$ , and are broad and nearly featureless, except for the 26–30  $\mu\text{m}$  emission feature and the  $\text{C}_2\text{H}_2$  absorption feature at 13.7  $\mu\text{m}$ . Extreme carbon stars and carbon-rich PPN candidates dominate the source types.

**4.CT** These sources have SEDs with a step-like appearance produced by emission features on a steadily rising red continuum at 8, 11.5, 21, and 26–30  $\mu\text{m}$ . The 21  $\mu\text{m}$  can be prominent, and the SEDs peak  $\sim 30$   $\mu\text{m}$ . Unlike the other dusty carbon-rich sources, they do not have the  $\text{C}_2\text{H}_2$  absorption feature at 13.7  $\mu\text{m}$ . Sources tend to be F or G supergiants sometimes identified as PPN candidates.

**4.CN** These sources show features such as the  $\text{C}_2\text{H}_2$  13.7  $\mu\text{m}$  absorption or the 11.5  $\mu\text{m}$  emission feature, which indicate they are carbon-rich. The SED peaks  $\sim 40$   $\mu\text{m}$ . All of the sources are identified as PPNe, and this subgroup includes the well-known carbon-rich bipolar nebulae AFGL 618 (the Westbrook Nebula) and AFGL 2688 (the Cygnus Egg). The “N” designation stands for “nebula.”

**4.C/SC** The one source in this subgroup (IRAS 09425–6040) has an unusual spectrum,

showing carbon-rich molecular absorption bands in the near infrared and SiC emission  $\sim 11.5 \mu\text{m}$  as seen in 2.CE spectra as well as strong crystalline silicate emission features at 33, 40, and  $43 \mu\text{m}$ . Molster et al. (2001) suggest that IRAS 09425–6040 may be in transition to a Red Rectangle-like object (see subgroup 4.U/SC below). Normally, a unique spectrum would belong in a miscellaneous subgroup, but the relation of this spectrum to the more numerous U/SC subgroup suggests that more of these sources may be discovered in future observations.

**4.U/SC** The sources in this subgroup combine strong UIR features (at 6.2, 7.7–7.9, 8.6, and  $11.2 \mu\text{m}$ ) and strong crystalline silicate emission features (at 33, 40, and  $43 \mu\text{m}$ ). The  $33 \mu\text{m}$  feature can be quite prominent, and in the bluer sources, can be accompanied by a  $23 \mu\text{m}$  emission feature also due to crystalline silicates. Most spectra show a possible emission feature  $\sim 28.5 \mu\text{m}$  but the poor quality of Band 3E makes this identification problematic. All of the sources are PPN or PN, with the exception of a single Herbig Ae/Be star (HD 100546).

**4.PN** The dominant spectral feature in this subgroup is the presence of strong fine-structure lines superimposed on a SED which peaks in the vicinity of  $30 \mu\text{m}$ . The line-to-continuum ratio can be 5 or greater in some instances. All show, at a minimum, [Ne II] at  $12.8 \mu\text{m}$  and [S III] at  $18.7$  and  $33.5 \mu\text{m}$ . Other common lines include [Ar II] at  $6.99 \mu\text{m}$ , [Ar III] at  $8.99 \mu\text{m}$ , [S IV] at  $10.5 \mu\text{m}$ , [Ne III] at  $15.6$  and  $36.0 \mu\text{m}$ , and [Si II] at  $34.8 \mu\text{m}$ , as well as Br  $\alpha$  and  $\beta$ . Additional detected lines include [Ne V] at  $14.3$  and  $24.3 \mu\text{m}$ , [Ne VI] at  $7.65 \mu\text{m}$ , [Ar V] at  $7.90$  and  $13.1 \mu\text{m}$ , [Ar VI] at  $4.53 \mu\text{m}$ , [O IV] at  $25.9 \mu\text{m}$ , [Mg IV] at  $4.49 \mu\text{m}$ , and [Mg V] at  $5.61$  and  $13.5 \mu\text{m}$ . Some sources also show weak crystalline silicate features, especially at  $33 \mu\text{m}$ . All but one source are planetary nebulae; the exception, IRAS 05341+0852, is a PPN-candidate.

**4.PU** Similar to 4.PN, these sources show strong UIR features in addition to the fine-structure lines. BD +30 3639 shows crystalline silicate emission at  $33 \mu\text{m}$ . Most are planetary nebulae, including one PPN candidate. Three sources with fewer, weaker emission lines than the typical PU spectrum are noted as peculiar with the “p” suffix; otherwise their SEDs and UIR features resemble the other members closely.

**4.M** Each of the four objects in this subgroup is unique.  $\eta$  Car could be described as the prototypically strange spectrum at all wavelengths. Classification of its SWS data is further complicated by the saturation (and automatic flagging) of most of Band 3, the spectral region upon which much of the subgrouping in Group 4 is based. AG Car combines a Group 1 spectrum (1.NE) in the near-infrared with a Group 4 spectrum (possibly 4.PUp) at longer wavelengths. Only a few other objects show this combination of hot photospheric emission with very cool dust. IRAS 21282+5050 has very strong UIR features, most similar to those

in the Red Rectangle (HD 44179, 4.U/SC), but has no crystalline silicate emission and a significantly bluer SED than members of the 4.U/SC subgroup. HD 169142 is somewhat similar to the 4.U/SC or PU groups in terms of its UIR emission and SED, but has no evidence for crystalline silicates or emission lines in its admittedly weak, noisy spectrum.

### 3.3.5. Group 5

Objects in Group 5, whose SEDs are still rising through the end of Band 4, have the coolest dust emission in the database. The subgroups trace the presence of silicate emission or absorption, narrow emission lines, UIR features, and absorption features. Figure 5 shows sample spectra for Group 5.

**5.SE** These sources show broad silicate emission features at  $\lambda \sim 9\text{--}11\ \mu\text{m}$ . One (AB Aur) also shows UIR emission features. All but one are young, Herbig Ae/Be (or Fe) stars. The single evolved source, HD 101584, a PPN-candidate, could be a cooler version of the 4.SE sources or it may actually be a young object misclassified as old.

**5.SA** Sources in this subgroup show a broad silicate absorption feature at  $\lambda \sim 9\text{--}11\ \mu\text{m}$ . Other absorption features often present include bands from  $\text{CO}_2$ , CO, and  $\text{H}_2\text{O}$ . A few also show UIR emission features or weak atomic fine-structure lines ([Ne II], [S III], or [Si II]). Almost all sources are YSOs or in star forming regions. The six (out of 50) which are not YSOs are probably OH/IR stars. Four of the sources in this class with emission lines (5.SAe) are Galactic center objects.

**5.F** These sources show no strong features superimposed on a SED which rises steadily to the red. Some sources in this class may be better placed in other classes, but because the red end of the spectrum is so strong, any structure at  $\lambda \lesssim 15\ \mu\text{m}$  is not visible on the self-scaled plots used for classifying. Three of the sources are evolved; the rest are young.

**5.U** These sources have moderate to strong UIR features but no atomic fine-structure lines. Only one source is considered evolved (Wray 15-543, thought to be a PPN-candidate); the rest are young.

**5.UE** These sources have moderate to strong UIR features and strong atomic fine-structure lines. The majority of the sources are young; a few are thought to be evolved (PNe).

**5.E** These sources have strong atomic fine-structure lines but little or no UIR emission. The composition of this subgroup is similar to 5.UE: mostly pre-main-sequence with a few PNe.

**5.PN** These sources have very strong, numerous atomic fine-structure lines. Crystalline

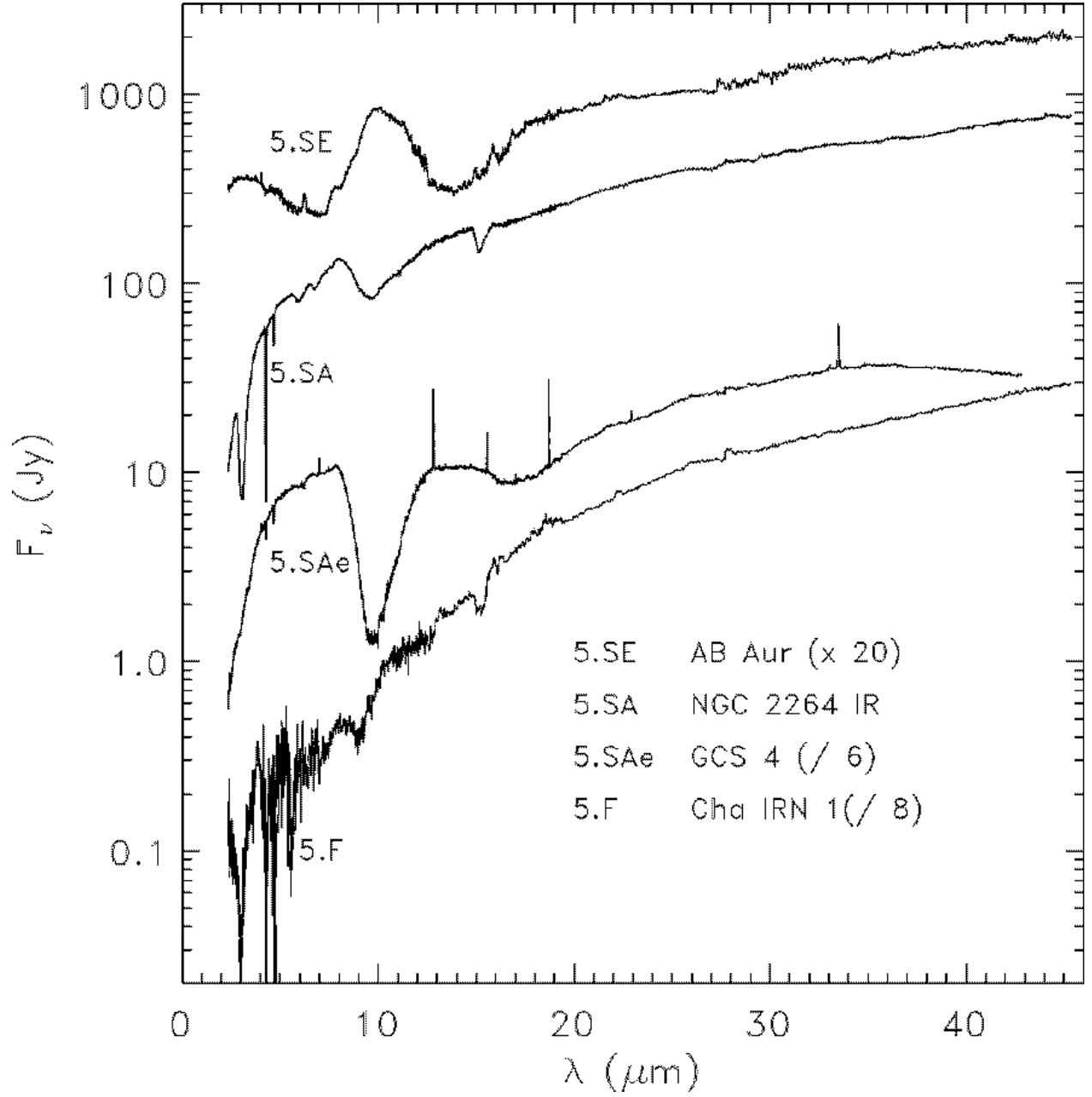


Fig. 5.— (a) Typical spectra in Group 5.

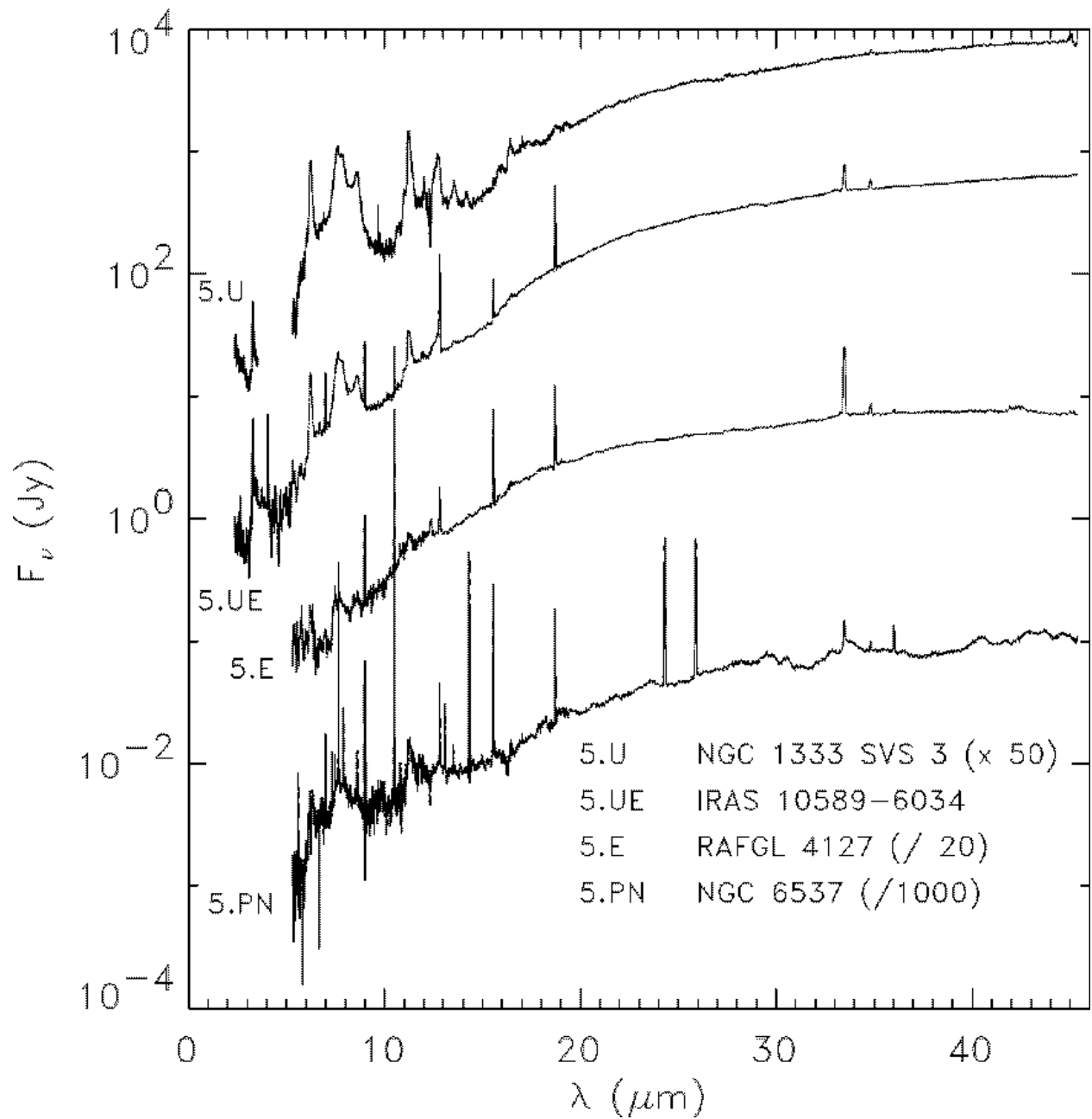


Fig. 5.— Group 5, cont'd. (b) In 5.U, Band 2A is omitted due to poor signal-to-noise. Likewise, the spectra for 5.E and 5.PN are truncated at shorter wavelengths.

silicate emission is often present in the  $\lambda \sim 30\text{--}45 \mu\text{m}$  range, and at least two show UIR emission. All sources are evolved (PNe).

**5.M** The weak signal and poor signal-to-noise ratio of these spectra hide any identifying features which would help to place them in a different subgroup.

## 4. Discussion

### 4.1. Calibration Issues and the Classifications

As mentioned in §2.2, the browse products used to classify most of the spectra did not fully correct for flux discontinuities between bands. The most challenging normalization problems occur between Bands 2C and 3A, at  $\lambda \sim 12 \mu\text{m}$ , and between Bands 3D, 3E, and 4, at  $\lambda \sim 26\text{--}30 \mu\text{m}$ . We discuss them briefly here to the extent that they influence the classification effort.

Spectra in Group 2 are most sensitive to discontinuities and memory effects near  $12 \mu\text{m}$ , because the shape of the emission and absorption features in the  $10\text{--}12 \mu\text{m}$  region serve as the primary features for classification into the subgroups. If the flux discontinuity is simply related to a gain difference between bands, normalization during reprocessing (if needed at all) would simply scale Band 3A to match 2C without changing the basic shape of any features present. If the discontinuity results from memory effects, however, it is more problematic. Even with the *dynadark* correction and normalization some error may remain in the shape of the spectrum. Fortunately, this problem does not compromise the classification of a spectrum as oxygen or carbon-rich, although it might cause a spectrum to be (mis)classified as 2.SEa instead of 2.SEb, for instance.

Normalization of Bands 3D, 3E, and 4 is complicated by a light leak and by the unreliability of 3E. Most spectra show a smooth shape with a roughly constant slope from Band 3D through Band 3E and into Band 4, which allows a straightforward normalization of these bands to each other. However, spectra with structure near  $26 \mu\text{m}$  present more of a problem, since the changing slope of the spectrum makes extrapolation across Band 3E difficult. This problem affects the carbon-rich sources in Groups 3 and 4 most significantly and limits our confidence in the shape of the emission feature in the  $26\text{--}30 \mu\text{m}$  region. In the browse product spectra produced from OLP 7.1, the normalization of the segments makes the  $26\text{--}30 \mu\text{m}$  feature appear narrow and peaked around  $\sim 25\text{--}29 \mu\text{m}$ . Applying our normalization algorithm to data in OLP 10.0 broadens the feature to  $\sim 25\text{--}34 \mu\text{m}$ . The literature tends to refer to this feature as the  $30 \mu\text{m}$  emission feature, possibly attributable to MgS (Goebel & Moseley 1985; Begemann et al. 1994). With the current uncertainties in calibration, we

are unable to definitively address this issue.

To date, no model has been developed to correct the memory effects in Band 4. The entire shape of Band 4 can be compromised, and, in terms of the spectral classification, this influences whether a spectrum is classified in Group 4 or 5. For example, a spectrum could be misclassified, as a 4.PN instead of a 5.PN because the spectrum appears to have turned over in Band 4 when it is actually still climbing. The memory effect in Band 4 can also influence our ability to recognize crystalline silicate features, especially at 40 and 43  $\mu\text{m}$ . These features could be washed out when the two scan directions are combined because of the difference in flux levels between them. As with the other issues raised here, the Band 4 memory effect should have a limited impact on the classifications.

Despite these issues, the basic classification scheme and the grouping of the spectra should prove robust. The movement of a few spectra from CR to CE or from Group 4 to Group 5 will not change the overall nature of the database or the existence of any of the evolutionary patterns discovered therein (§4.3.1–4.3.3).

## 4.2. Comparison With *IRAS* Classifications

Although we are dealing with a non-uniform database (§2.1.2), we can still compare our classifications with the LRS classes (*IRAS* Explanatory Supplement 1988) and the classes of Kwok et al. (1997, hereafter KVB). Only the subset of SWS sources with LRS classifications (379 sources) or KVB (567 sources) classifications can be considered, so the numbers quoted below will not be the same as those given for each subgroup in Table 4. Also, recall that for LRS class  $1n$ ,  $n = 2\beta$  where  $\beta$  is the spectra index:

$$F_\lambda \propto \lambda^{-\beta}. \quad (1)$$

Thus, when  $\beta = 4$ , the spectrum behaves as a pure Rayleigh-Jeans tail and is in LRS class 18. Sources with low-contrast dust mimic lower spectral indices and receive lower LRS characterizations. For example, LML and SP showed that many sources in LRS classes 13–16 show low-contrast alumina-rich dust in their spectra.

#### 4.2.1. Similarities

Group 1, the dust-free stars, corresponds well to the LRS classes 17–19. Of the 60 objects in Group 1 with LRS classifications, 54 are in LRS classes 17–19, with 39 in class 18. Of the 2.SEa sources, with low-contrast dust, 81% of the 53 sources are in LRS classes 13–16, as expected. Similarly, the oxygen-rich dust sequence, described below in §4.3.2, should begin in the  $2n$  range and progress to the  $3n$  range, where  $2n$  corresponds to silicate emission and  $3n$  to silicate absorption. Nearly 90% of the 67 objects in subgroups 2.SEb, 2.SEc, and 3.SE have LRS classes  $2n$ . The sources in 3.SB, the self-absorbed subgroup, are split between  $2n$  and  $3n$ , and 11 of 12 sources in 4.SA are  $3n$  or  $7n$  (recall that  $7n$  is the red counterpart of  $3n$ ). In the carbon-rich sources, 31 of 37 sources in subgroups 2.CE, 3.CE, and 3.CT have LRS= $4n$ , the carbon-rich LRS class. Only about a third (14 of 41) of the PNe subgroups 4.PN, 4.PU, and 5.PN, have LRS classifications, but those that do tend (11 of 14) to be  $9n$ , that is, red objects with emission lines but no detected  $11.3\ \mu\text{m}$  UIR feature. For the young, red sources in Groups 4 and 5, even fewer,  $\sim 25\%$ , have LRS classifications, so small numbers make valid comparisons problematic. Still, most of those with LRS data in our SA or SE subgroups do have silicate absorption or emission LRS classifications.

A comparison of our classifications with those of KVB shows comparable similarities. For example, 37 of the 40 sources with their class C, for carbon-rich, are in one of our carbon-rich subgroups (mostly 2.CE). More than 80% of their A ( $10\ \mu\text{m}$  absorption) sources are in our SA or SB subgroups and more than 90% of their E ( $10\ \mu\text{m}$  emission) sources are in our silicate emission subgroups. Almost 90% of their S (stellar) sources are in Group 1, our naked star category.

#### 4.2.2. Distinctions

While the overall correspondence between our classifications and those from LRS-based schemes is reasonable, there are a number of important differences. For instance, misidentification of UIR features as silicate absorption occurred in the LRS classifications due to the low spectral resolution and bandwidth. This is largely avoided in the SWS database because of the higher spectral resolution and especially the expanded bandwidth. The extended wavelength coverage allows confirmation of suspected  $7\text{--}11\ \mu\text{m}$  UIR features with those at  $6.2$  and  $3.3\ \mu\text{m}$  which were outside the LRS range.

It was mentioned above that most of the 4.SA and 5.SA sources (24 of 27) were in LRS classes corresponding to silicate absorption. However, 17 of those sources were  $3n$ , with ostensibly blue SEDs. Characterizations of  $7n$  would have been more correct, but the short



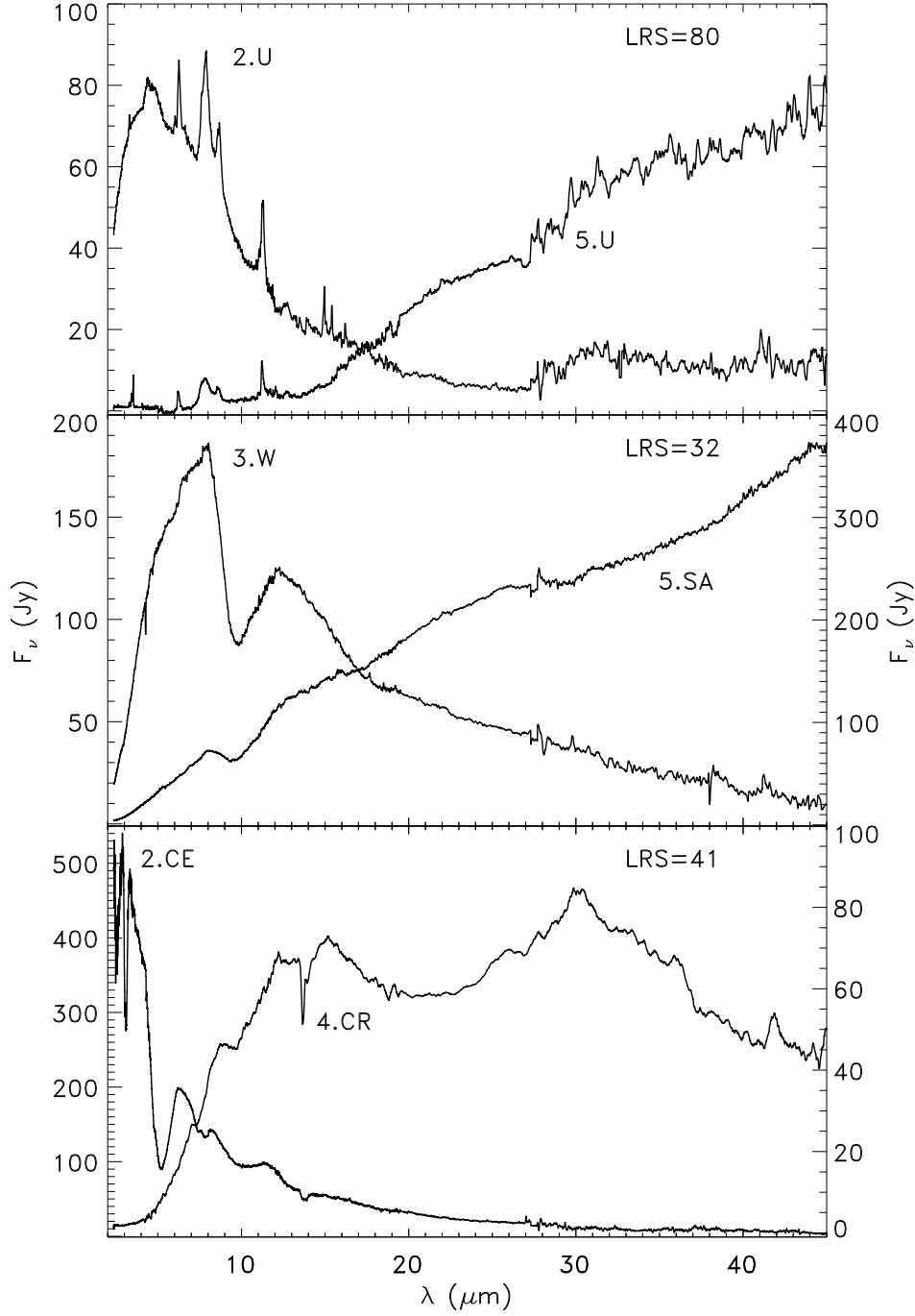


Fig. 6.— Comparison of spectra with the same LRS class but different KSPW classes. Top: LRS=80 (UIR emission): HR 4049 2.U and HD 97048 5.U (smoothed). Middle: LRS=32 (blue SED + silicate absorption): WR 112 3.W and V645 Cyg 5.SA. Bottom: LRS=41 (C-rich): RY Dra 2.CE and IRAS 22303+5950 4.CR.

wavelength cutoff of only  $7\ \mu\text{m}$  presumably prevented an accurate assessment of the overall SED. In the 5.UE group, 25 sources had red LRS characterizations, but less than half (10) were  $8n$ , the UIR+emission line class. Lack of sensitivity of the LRS precluded the detection of UIRs in some sources, while the limited spectral range caused the confusion of UIRs and silicate absorption in others.

Examination of the carbon-rich classes and ostensibly carbon-rich objects further illustrates the limitations of the old LRS classifications when dealing with SWS data. One source, AFGL 2287, was classified as carbon-rich in all three LRS-based schemes but is classified by us as self-absorbed silicate emission (3.SBp). In the limited spectral range of the LRS data, self-absorbed silicates can appear similar to carbon-rich spectra (Walker & Cohen 1988). However, with the SWS, AFGL 2287 can be seen to have none of the other features typical of carbon-rich sources such as the absorption features at  $13.7\ \mu\text{m}$  or  $3\ \mu\text{m}$ . Seven other sources were classified as carbon-rich in the LRS atlas but as oxygen-rich by AutoClass and KVB. With the high-quality data from SWS, we can confirm that they are indeed oxygen-rich<sup>12</sup>.

As an example of a discrepancy in the opposite sense, only one of our 4.CR sources has a carbon-rich LRS class, while most of the rest (8 of 11) are classed as 21–23, low-contrast silicate emission. The AI classifications also mistook most of 4.CR (9 of 10) for oxygen-rich ( $\zeta 4$ ) because of the limited spectral range on which the classifications were based. Of the 31 objects observed with SWS which SIMBAD lists as carbon stars, only two (FI Lyr and CIT 11) are in non-carbon KSPW subgroups; four more are in Group 7 or flagged, so 25 of 27 agree with SIMBAD. The LRS scheme, on the other hand, has only 16 of 24 sources with  $4n$  or  $04$  designations. Again, the superior sensitivity and spectral range of SWS enabled the proper classification of these sources as carbon-rich.

The LRS  $4n$  classes base the second digit on the strength of the  $11.5\ \mu\text{m}$  silicon carbide feature. However, nothing in the LRS classification indicates the shape of the underlying continuum for carbon-rich objects. Thus, sources as dissimilar as RY Dra (2.CE) and IRAS 22303+5950 (4.CR) possess the same LRS classification 41 because both have weak  $11.5\ \mu\text{m}$  features (Fig. 6). LRS class 44 contains both W Ori (2.CE) and IRC +50096 (3.CE) despite their distinctly different underlying SEDs. There simply are *no* appropriate categories in the LRS scheme in which to place *any* of the carbon-rich sources in our Groups 3 and 4 without loss of significant information about the spectra.

Similarly, placing all of our Group 1 naked stars into  $1n$  would also lose important information about the photospheric chemistry (1.NO vs. 1.NC) or the presence of emission

---

<sup>12</sup>They are ST Her (2.SEa), FI Lyr (2.SEa), Z Cas (2.SEap),  $\pi^1$  Gru (2.SEa), AD Per (2.SEa), AFGL 2199 (3.SB), and AFGL 1992 (3.SB).

lines (1.NE). Other KSPW classes with no good LRS counterparts include 2.E, 2.U, 2.C/SE, 4.SC, 4.U/SC, 4.SEC, and 6.

Other LRS classes also mis-matched sources, as Figure 6 shows. These disparate sources were placed in the same LRS classes because of the limited spectral range of the LRS and small number of features considered in that classification scheme. Table 5 compares the KSPW classes to the LRS classes. Column 2 lists the KSPW classes that are well-matched to an LRS class as defined in the *IRAS* Explanatory Supplement (1988), for example 1.N and the  $1n$  class. Column 3 lists our groups that could be placed in an LRS class, but only with information lost, such as 2.C/SE in  $2n$  or 4.U/SC in  $8n$ . The last column lists the other KSPW groups in which the LRS classes actually appear but are not well-suited to each other. Application of the LRS scheme to classify the SWS database would have essentially ignored the additional information gained from the larger bandwidth, higher spectral resolution, and greater sensitivity of SWS.

### 4.3. Clarifying Evolutionary Patterns

#### 4.3.1. The CO Paradigm

The search for patterns and relations among the infrared spectral classifications identified here must first consider the observed dichotomy between carbon-rich and oxygen-rich dust chemistry. In evolved stars, the chemistry of the dust depends on the C/O ratio of the material ejected from the envelope. The formation of CO molecules will exhaust the less abundant of carbon or oxygen, leaving the other element available to form molecules which serve as seeds for dust formation. This CO paradigm works admirably well. In only a few cases does the chemistry of the stellar photosphere differ from that of the dust, and most of these cases probably arise within binary systems. For example, the silicate carbon stars (2.C/SE) show carbon-rich photospheric features and oxygen-rich dust. In these sources, the dust emission may arise from a disk around an unseen companion which trapped mass lost from the primary before it evolved into a carbon star (see Yamamura et al. 2000, for a recent study of the SWS spectrum of V778 Cyg and a discussion of competing models).

Circumstellar dust shells form in relatively pure environments, but interstellar dust represents a mixture of material ejected by many generations of evolved stars with a wide variety of progenitor masses. Since oxygen-rich dust shells outnumber carbon-rich dust shells, oxygen-rich dust dominates in the interstellar medium. This means that an oxygen-rich dust spectrum can arise in either a pre-main-sequence or a post-main-sequence environment, but carbon-rich spectra will only appear in post-main-sequence objects.

#### 4.3.2. *Oxygen-Rich Dust Emission*

The oxygen-rich post-main-sequence objects can be organized along the sequence from AGB source  $\rightarrow$  OH/IR source  $\rightarrow$  PPN  $\rightarrow$  PN. This sequence assumes that as the average oxygen-rich star evolves up the AGB, its mass-loss rate increases, eventually enshrouding it so deeply within its circumstellar dust shell that it disappears completely from the optical sky. This first stage of development is well-documented. Jones et al. (1990), in a study of variable AGB sources identified by the Air Force Geophysics Laboratory (AFGL) infrared sky survey (Price & Murdock 1983), showed that as Miras evolve to OH/IR stars, the period of variability and mass-loss rate steadily increase as the infrared colors progressively redden. They showed photometrically that this evolution transformed the silicate emission feature at  $10\ \mu\text{m}$  to a deep absorption feature. Lloyd Evans (1990) illustrates this change spectroscopically with LRS data in his Figure 3.

Examining the composition of each subgroup (in terms of the fraction represented by AGB sources, OH/IR stars, PPNe, and PNe) helps to organize the spectral subgroups defined in our classification system into an evolutionary sequence. In some cases, the composition of a subgroup is obvious; in others the small sample sizes and the inherent selection effects of the SWS database limit the usefulness of this method.

The initial steps are relatively straightforward to interpret. A star on the early AGB will appear as a naked star with absorption bands from CO and SiO (1.NO). Reinterpreting Figure 8 of Sloan & Price (1995) in terms of the subgroups defined here, the shift from 1.NO to 2.SE occurs between (time-averaged) spectral types of M4 and M5. This marks the onset of significant mass loss and dust formation, but the detailed evolution through the various classes of silicate emission (broad, structured, and classic) is more difficult to trace. Sloan & Price (1995, 1998) found few correlations between spectral type, variability class, and the shape of the silicate dust spectrum. They suggested that the formation of multiple shells might cloud the picture, and that the shape of the spectrum might depend on photospheric C/O ratio, which would imply that dredge-ups of processed material from the stellar interior might determine the shape of the infrared dust features. Detailed analysis of the shape of the silicate feature and related features, such as the CO<sub>2</sub> lines and the 13 and  $19.5\ \mu\text{m}$  bumps, in the 2.SE subgroups may shed further light on this subject (Sloan et al. 2002).

As the dust contribution grows to dominate the stellar spectrum, the spectrum will shift from Group 2 to Group 3 (3.SE). It will then develop into a 3.SB spectrum as the optical depth of the silicate dust increases and drives the  $10\ \mu\text{m}$  feature into self-absorption. The 3.SE sources are a mixture of M stars on the AGB, M supergiants, and optically enshrouded OH/IR stars. The 3.SB sources are more evolved, with later spectral types and longer periods of variability. All of the sources in 3.SE were initially discovered in infrared surveys,

and all show OH masers. The lack of a single source with a 2.SB spectrum suggests that the transition to self-absorption occurs in Group 3.

Evolution continues from 3.SB to 4.SA, where the silicate feature goes into full absorption and the SED becomes redder. The sources in this group are associated with OH/IR stars, many of them Mira variables, and PNe. The transition to SA does not occur within Group 3, because all of the 3.SA spectra are associated with pre-main-sequence sources. It also does not appear to occur frequently within Group 4, as most of the 4.SB sources appear to be much more evolved PNe. Rather, the transition from SB to SA appears to coincide with the transition from Group 3 to Group 4.

The stages following 4.SA are much less clear. Ultimately, the high mass-loss rates associated with the end of the AGB-OH/IR phase will strip the envelope from the core, producing a PPN. As the remnant shell expands and thins, revealing the ionized central regions, the source becomes a PN. How does this process manifest itself into the subgroups not yet included in the sequence: 4.SB, 4.SE, 4.SEC, and 4.SC? All four subgroups show roughly the same percentage of clearly identified PNe (58-60% of the sample, excluding high-mass objects and pre-main-sequence objects), but only 4.SC and 4.SEC include any sources identified as OH/IR stars or still on the AGB. Because of this, we suspect that 4.SC and 4.SEC precede 4.SE and 4.SB on a typical evolutionary path.

Waters et al. (1996) first identified crystalline species of silicates in the spectra of circumstellar dust shells associated with evolved stars using data from the SWS. They noted that the crystalline features do not appear until the color temperature of the shell has decreased to  $\sim 300$  K. Further study of SWS data by Sylvester et al. (1999) relates the presence of crystalline features with the optical depth at  $10\ \mu\text{m}$ . They suggest that crystalline silicates do not appear until the mass-loss rate has crossed a certain threshold. Thus as mass-loss rate increases, absorption strength at  $10\ \mu\text{m}$  grows stronger, and color temperature reddens, a typical source will evolve to SA and then to SC.

Most of the sources in subgroups 4.SC, 4.SEC, 4.SB, and 4.SE appear in the upper middle of the HR diagram (spectral class B, A, F, and G, usually with emission lines, luminosity class I-II). Whatever their precise order, most or all of the post-main-sequence sources with these classes of spectra are obviously in transition from the AGB or red supergiant phase to later stages of evolution. It is likely that the difficulty in ordering these subgroups results from the wide range of stellar masses which can produce oxygen-rich dust shells (from less than  $1\ M_{\odot}$  to beyond  $50\ M_{\odot}$ ). The more massive stars do not follow the standard evolutionary scenario; instead they evolve onto the super-AGB (e.g. Garcia-Berro & Iben 1994). Initial masses  $\geq 11\ M_{\odot}$  produce final core masses beyond the Chandrasekhar limit and become supernovae. Masses  $\gtrsim 50\ M_{\odot}$  are associated with the luminous blue variables

(e.g. Humphreys & Davidson 1994), some of which are in the SWS sample. With all of these sources producing oxygen-rich dust shells, perhaps it is not a surprise that the redder spectra cannot be ordered into a smooth sequence.

Another complication is the mixture of young and old sources in Groups 3 and 4 (in contrast to the oxygen-rich spectra in Groups 1 and 2 (1.NO and 2.SE), most of which are evolved sources). In subgroup 4.SE, 9 of 24 sources are clearly pre-main-sequence; all are Herbig Ae/Be stars except for one source classified as F0e. This represents the majority of the young sources in the sample, but three more Herbig Ae/Be stars appear in subgroup 3.SE (out of 21), both 3.SA spectra are pre-main-sequence Be stars, subgroups 4.SEC and 4.SB each contain two pre-main-sequence sources (out of 10 and 7 respectively), and one of the 14 4.SC sources is young (a T Tauri star). Three of the four young sources in subgroups 4.SEC and 4.SB are Herbig Ae/Be stars; the other source is an Ae star.

It is unfortunate that young and old sources appearing in the same part of the HR diagram, luminous Be, Ae, Fe, and G stars, exhibit similar infrared spectral characteristics. Determining whether these sources were evolving *to* or *from* the main sequence has been a long-standing problem in astronomy. Walker et al. (1989) showed that some types of young and old stars could be separated into different zones using *IRAS* color-color diagrams. As Figures 4 and 5 show, the SWS spectra extend sufficiently beyond 20  $\mu\text{m}$  for the shape of the continuum to be defined, thus showing the underlying dust temperature. The shape of the dust continuum from  $\sim 20$  to  $\sim 40$   $\mu\text{m}$  might be one way of separating the young and old objects. Potentially, the more detailed Level 3 classification will address this issue.

#### 4.3.3. The Carbon-Rich Dust Sequence

While oxygen-rich dust can occur in both evolved stars and environments associated with star formation, carbon-rich dust only occurs in the vicinity of carbon stars or in planetary nebulae which have presumably evolved from carbon stars. Furthermore, the range of stellar masses which evolve to carbon stars is limited to  $\gtrsim 2 M_{\odot}$  and less than several  $M_{\odot}$  (cf. Wallerstein & Knapp 1998, and references therein). Perhaps for these reasons, the carbon-rich spectral classes defined here fall into a reasonably ordered evolutionary sequence: 1.NC  $\rightarrow$  2.CE  $\rightarrow$  3.CE  $\rightarrow$  3.CR  $\rightarrow$  4.CR  $\rightarrow$  4.CN.

As the mass-loss rate from a naked star with a carbon-rich photosphere (1.NC) grows, its infrared spectrum develops a strong emission feature at  $\sim 11.5$   $\mu\text{m}$  from SiC, producing a 2.CE spectrum. Further increases in mass-loss rate lead to a cooler, optically thicker shell which enshrouds the central star. The spectrum is then classified as 3.CE. It next evolves to

3.CR as the emitting layer of the dust shell cools and amorphous carbon begins to dominate the spectrum. Further thickening of the dust shell shifts the spectrum to 4.CR. The next stage is less certain because the relation of 4.CT to the sequence is not clear. Perhaps spectra evolve from 4.CR to 4.CN (i.e. to carbon-rich PPNe), and only some unusual circumstances lead to the development of a 4.CT spectrum. Possibly, all carbon-rich sources pass briefly through this stage. However, the latter possibility seems unlikely given the difficulty of fitting the 4.CT spectra into the rest of the carbon sequence.

## 5. Summary

We examined and categorized the entire *ISO*-SWS database of 1248 SWS01 full-grating spectra. A comprehensive spectral classification system was developed according to the shape of the SED, that is, the temperature of the strongest emitter. Groups were further subdivided based on spectral features such as silicate emission, ice absorption, or fine-structure lines. Most sources which had LRS-based classifications are in similar categories based on their SWS spectra. Where discrepancies occur, e.g. in carbon- vs. oxygen-rich or red vs. blue SEDs, the SWS classification should take precedence because of the larger bandpass, higher resolution (spectral and angular), and greater sensitivity of SWS. As the Level 3 effort progresses, some shifting of individual sources may occur, but the overall classification system should be robust.

KEK would like to thank the National Research Council for support via a Research Associateship through the Air Force Office of Scientific Research. This work was supported in part by a NASA grant for the analysis of *ISO* dedicated time observations. SDP acknowledges the efforts of Thijs de Graauw in conducting this experiment. As the SWS Principal Investigator, his advocacy for the STARTYPE and follow-on related experiments were critical in obtaining the spectra of sources in the “missing” classes. SDP also thanks Thijs de Graauw, Harm Habing and Martin Kessler for contributing a portion of their allocated observing time to this experiment. Timo Prusti helped considerably by providing the dedicated and open time SWS01 observing lists that allowed us to efficiently retarget the STARTYPE sources. Russ Shipman provided helpful insight into the calibration of the SWS Interactive Analysis software and provided an early version of OLP 10.0. This research has made use of NASA’s Astrophysics Data System Abstract Service, SIMBAD, and the on-line Dictionary of Nomenclature of Celestial Objects of the CDS.

## A. The Classifications

Table 6 contains the Group and Subgroup classification for each source. Sources are ordered by increasing right ascension. Columns 1 and 2 contain the source identification and TDT number of the observation; the observed RA and Dec (J2000) are given in columns 3 and 4. The classification is in column 5, and comments found in the table notes are in column 6. The coordinates are as given by the observer and represent the nominal telescope pointing. They can differ by up to several arcseconds with respect to the nominal coordinates of a given object.

The comments can contain important information regarding the reliability of the spectra and their classifications. The most important two comments are “F” and “W.” “F” indicates that a quality flag was attached to the data, either telemetry, pointing, or unknown. Of the 34 flagged observations, 19 could be classified whereas the rest are in Group 7, and are probably irrecoverable. Sources with “W” in the comment column were observed at the wrong coordinates. Two of these were classified based on the detected flux, although a well centered observation might produce a different classification. Note that an observation does not get a “W” if the observer simply mislabelled the object.

### A.1. Source Names

Given the heterogeneity of the source names in the IDA, not to mention the inaccuracy or non-standard nature of some names (e.g. GL989 [sic] for AFGL 899), the source identification is not necessarily that given by the original observer. Coordinates for each observation were submitted to SIMBAD for a list of all objects within 30″. Although this process is subject to the errors known to be in SIMBAD, it succeeded in identifying most “Off” or “Reference” positions, as well as those sources with incorrect coordinates (e.g., the observer submitted B1950 instead of J2000 coordinates).

Generally, we preferred older catalog names over newer designations. For example, we used the Greek+constellation designation over a variable star name, HR over HD, and HD over SAO. Similarly, for nebulae, the Messier number takes precedence over NGC or IC names. However, there are exceptions. If a newer name contains useful information, it might be used instead of an older one. For instance, WR (Wolf-Rayet stars) and MWC (emission line stars) numbers are used instead of HD numbers as appropriate. Another exception to the age preference are Flamsteed numbers, which were generally avoided unless the source is commonly referenced in the literature by that name (5 sources). When in doubt as to what to call a source, we tried to follow the most common usage in the literature as a guide.



A number of observations have no apparent counterpart in the SIMBAD database. In these cases (37), the names given by the observer are used, and their origin is indicated by a notation (“Propn”) in the Comments column of the Table. Objects in the Galactic center have “GC” prepended to their designations. An example of both these situations is GC SE\_NTF\_Xng, where the observer called this position SE\_NTF\_Xng, presumably a non-thermal filament crossing in the southeast; adding the “GC” indicates it is a Galactic center object.

There are also observations of the same source at different positions. These objects were typically either calibration sources such as  $\gamma$  Dra and  $\alpha$  Boo, or extended objects such as Cas A or M 17. A nominal (0,0) position was chosen for each source. The offsets for a particular observation are then included in the name. For example,  $\alpha$  Boo  $-0.39, +3.4$  is  $(\Delta\alpha, \Delta\delta) = (-0^{\circ}39, +3''.4)$  from  $\alpha$  Boo. Nineteen objects and 91 observations have this type of name, and are noted with “Offset” in the comment column.

## REFERENCES

- Aoki, W., Tsuji, T., & Ohnaka, K. 1998, *A&A*, 333, L19
- Aoki, W., Tsuji, T., & Ohnaka, K. 1999, *A&A*, 350, 945
- Begemann, B., Dorschner, J., Henning, T., Mutschke, H., & Thamm, E. 1994, *ApJ*, 423, L71
- Cannon, A. J., & Pickering, E. C. 1918, *Annals of the Harvard College Observatory*, 91, 1
- Cernicharo, J., Yamamura, I., González-Alfonso, E., de Jong, T., Heras, A., Escribano, R., & Ortigoso, J. 1999, *ApJ*, 526, L41
- Cheeseman, P., Stutz, J., Self, M., Taylor, W., Goebel, J., Volk, K., & Walker, H. 1989 “Automatic Classification of Spectra from the Infrared Astronomical Satellite” (NASA RP-1217) (Washington: GPO)
- Cohen, M., Walker, R., Wainscoat, R., Volk, K., Walker, H., & Schwartz, D. 1990, (NASA-CR-177526), NASA
- Creech-Eakman, M. J., Stencel, R. E., Williams, W. J., & Klebe, D. I. 1997, *ApJ*, 825, 831
- de Graauw, T. et al. 1996, *A&A*, 315, L49
- Egan, M. P., & Sloan, G. C. 2001, *ApJ*, 558, 165
- Engelke, C. W. 1992, *AJ*, 104, 1248
- Fouks, B. I. 2001, in *The Calibration Legacy of ISO*, ed. L. Metcalfe & M. F. Kessler (ESA: SP-481), in press
- Fouks, B. I., & Schubert, J. 1995, *SPIE*, 2475, 487
- Garcia-Berro, E., & Iben, I. 1994, *ApJ*, 434, 306
- Goebel, J. H., Bregman, J. D., Goorvitch, D., Strecker, D. W., Puetter, R. C., Russell, R. W., Soifer, B. T., Willner, S. P., Forrest, W. J., Houck, J. R., & McCarthy, J. F. 1980, *ApJ*, 235, 104
- Goebel, J. H., Bregman, J. D., Strecker, D. W., Witteborn, F. C., & Erickson, E. F. 1978, *ApJ*, L129
- Goebel, J. H., & Moseley, S. H. 1985, *ApJ*, 290, L35

- Goebel, J., Volk, K., Walker, H., Gerbault, F., Cheeseman, P., Self, M., Stutz, J., & Taylor, W. 1989, *A&A*, 222, L5
- Hearnshaw, J. B. 1986, *The Analysis of Starlight: One Hundred and Fifty Years of Astronomical Spectroscopy* (Cambridge: Cambridge University Press)
- Heras, A. M., Shipman, R. F., Price, S. D., de Graauw, Th., Walker, H. J., Jourdain de Muizon, M., Kessler, M. F., Prusti, T., Decin, L., Vandenbussche, B., & Waters, L. B. F. M. 2001, *A&A*, in preparation
- Hony, S., Waters, L. B. F. M., Zaal, P. A., de Koter, A., Marlborough, J. M., Millar, C. E., Trams, N. R., Morris, P. W., & de Graauw, T. 2000, *A&A*, 355, 187
- Hron, H., Loidl, R., Jørgensen, U. G., Aringer, B., & Kerschbaum, F. 1998, *A&A*, 335, L69
- Humphreys, R. M., & Davidson, K. 1994, *PASP*, 106, 1025
- IRAS Catalogs & Atlases, Vol. I: Explanatory Supplement* 1988 (Washington: NASA)
- IRAS Science Team* 1986, *A&AS*, 65, 607
- Jones, T. J., Bryja, C. O., Gehrz, R. D., Harrison, T. E., Johnson, J. J., Klebe, D. I., & Lawrence, G. F. 1990, *ApJS*, 74, 785
- Jørgensen, U. G., Hron, J., & Loidl, R. 2000, *A&A*, 356, 253
- Justtanont, K., Feuchtgruber, H., de Jong, T., Cami, J., Waters, L. B. F. M., Yamamura, I., & Onaka, T. 1998, *A&A*, 330, L17
- Kessler, M. F. et al. 1996, *A&A*, 315, L27
- Kester, D., Fouks, B., & Lahuis, F. 2001, in *The Calibration Legacy of ISO*, ed. L. Metcalfe & M. F. Kessler (ESA: SP-481), in press
- Kraemer, K. E., Sloan, G. C., & Price, S. D. 2001, in *The Calibration Legacy of ISO*, ed. L. Metcalfe & M. F. Kessler (ESA: SP-481), in press
- Kwok, S., Volk, K., & Bidelman, W. P. 1997, *ApJS*, 112, 557 (KVB)
- Lamers et al. 1996, *A&A*, 315, L27
- Leech et al. 2001, *The ISO Handbook, Vol. VI: SWS—the Short Wavelength Spectrometer*
- Little-Marenin, I. R. 1986, *ApJ*, 307, L15

- Little-Marenin, I. R., & Little, S. J. 1988, *ApJ*, 333, 305 (LML)
- Little-Marenin, I. R., & Little, S. J. 1990, *AJ*, 99, 1173 (LML)
- Little-Marenin, I. R., & Price, S. D. 1986, in *Summer School on Interstellar Processes*, ed. D. J. Hollenbach & H. A. Thronson (NASA Technical Memorandum 88342), 137
- Little-Marenin, I. R., Ramsey, M. E., Stephenson, C. B., Little, S. J., & Price, S. D. 1987, *AJ*, 93, 663
- Lloyd Evans, T. 1990, *MNRAS*, 243, 336
- Lockyer, J. N. 1887, *Proc. R. Soc.*, 43, 117
- Lockyer, J. N. 1888, *Proc. R. Soc.*, 44, 1
- Lorenz-Martins, S., & Pompeia, L. 2000, *MNRAS*, 315, 856
- Martin, P. G., & Rogers, C. 1987, *ApJ*, 322, 374
- Molster, F. J., Yamamura, I., Waters, L. B. F. M., Nyman, L.-Å., Käufl, H.-U., de Jong, T., & Loup, C. 2001, *A&A*, 366, 923
- Monnier, J. D., Geballe, T. R., & Danchi, W. C. 1998, *ApJ*, 502, 833
- Morgan, W. W. 1938, *ApJ*, 87, 460
- Morgan, W. W., Keenan, P. C., & Kellman, E. 1943, *An Atlas of Stellar Spectra, with an Outline of Spectral Classification* (Chicago, IL: University of Chicago Press)
- Morris, P. W., van der Hucht, K. A., Crowther, P. A., Hillier, D. J., Dessart, L., Williams, P. M., & Willis, A. J. 2000, *A&A*, 353, 624
- Onaka, T., de Jong, T., & Willems, F. J. 1989, *A&A*, 218, 169
- Payne, C. H., & Williams, E. T. R. 1929, *MNRAS*, 89, 526
- Payne, C. H. 1932, *MNRAS*, 92, 368
- Pickering, E. C., 1890, *Annals of the Harvard College Observatory*, 17, 1
- Price, S.D., & Murdock, T.L. 1983, *The Revised AFGL Infrared Sky Survey Catalog*, Document AFGL-TR-83-0161, Air Force Geophysics Laboratory
- Rutherford, L. M. 1863, *American Journal of Science and Arts*, 35, 71

- Secchi, A. 1866, *Comptes Rendus*, 63, 364
- Secchi, A. 1868, *Comptes Rendus*, 67, 373
- Shipman, R. F., et al. 2001, in *The Calibration Legacy of ISO*, ed. L. Metcalfe & M. F. Kessler, (ESA: SP-481), in press
- Sloan, G. C., & Egan, M. P. 1995, *ApJ*, 444, 452
- Sloan, G. C., Goebel, J. H., Kraemer, K. E., & Price, S. D. 2002, *BAAS*
- Sloan, G. C., Kraemer, K. E., & Price, S. D. 2001, in *The Calibration Legacy of ISO*, ed. L. Metcalfe & M. F. Kessler (ESA: SP-481), in press
- Sloan, G. C., LeVan, P. D., & Little-Marenin, I. R. 1996, *ApJ*, 463, 310
- Sloan, G. C., & Price, S. D. 1995, *ApJ*, 451, 758 (SP)
- Sloan, G. C., & Price, S. D. 1998, *ApJS*, 119, 141 (SP)
- Sylvester, R. J., Kemper, F., Barlow, M. J., de Jong, T., Waters, L. B. F. M., Tielens, A. G. G. M., & Omont, A. 1999, *A&A*, 352, 587
- Tananbaum, H. 1999, *IAU Circ.*, 7246
- van Winckel, H., Waelkens, C., & Waters, L. B. F. M. 1995, *A&A*, 293, L25
- Vogel, H. C. 1874, *Astronomische Nachrichten*, 84, 113
- Vogel, H. C., & Wilsing, J. 1899, *Pub. Astrophys. Obs. Potsdam*, 12, 1
- Volk, K., Kwok, S., Stencel, R. E., & Brugel, E. 1991, *ApJS*, 77, 607
- Volk, K., Xiong, G.-Z., & Kwok, S. 2000, *ApJ*, 530, 408
- Wainscoat, R. J., Cohen, M., Volk, K., Walker, H. J., & Schwartz, D. E. 1992, *ApJS*, 83, 111
- Walker, H. J., & Cohen, M. 1988, *AJ*, 95, 1801
- Walker, H. J., Cohen, M., Volk, K., Wainscoat, R. J., & Schwartz, D. E. 1989, *AJ*, 98, 2163
- Wallerstein, G., & Knapp, G. R. 1998, *ARA&A*, 36, 369
- Waters, L. B. F. M., et al. 1996, *A&A*, 315, L361

Yamamura, I., Dominik, C., de Jong, T., Waters, L. B. F. M., & Molster, F.J. 2000, A&A, 363, 629.

Table 1. *IRAS* Population Coverage

Class	Subclass									
	0	1	2	3	4	5	6	7	8	9
LRS Atlas Classifications										
0	0,1/1	6,21/313	3,3/4	0,1/1	1,5/12	8,6/32				
1	1,1/2	0,1/1	2,4/20	3,15/116	7,34/324	19,22/480	22,20/390	11,16/349	40,21/460	7,4/96
2		9,10/43	16,23/151	9,13/137	10,16/155	5,14/163	9,17/175	8,14/197	8,14/210	12,27/499
3		9,10/46	5,11/49	1,4/30	0,6/22	2,4/19	0,3/9	1,1/8	4,3/8	6,4/39
4		6,6/26	15,16/152	6,13/133	9,10/113	5,6/64	1,2/21	1,2/15	0,1/3	1,2/11
5	6,11/51	2,3/4	0,2/4	1,4/4						
6			2,1/2	0,0/3	1,1/6	0,0/3	1,1/4	1,1/7	0,0/3	9,16/50
7		1,4/7	4,4/9	3,2/9	3,2/7	2,1/8	3,2/5	1,0/3	0,0/1	4,4/18
8	9,18/42	12,9/23	3,2/3			1,1/1				
9		9,12/24	3,3/5		3,2/6	6,7/13	1,1/1			
AutoClass Classifications										
$\alpha$	14,18/155	0,2/39	1,2/23	0,0/27	2,4/60	4,10/91	1,5/83			
$\beta$ 0-9	11,23/224	10,17/171	3,8/144	0,1/51	0,5/102	0,1/36	1,1/40	1,1/58	12,14/172	0,3/89
$\beta$ 10-13	0,0/31	9,10/126	0,0/7	0,0/12						
$\gamma$	42,49/102	23,22/55								
$\delta$	44,27/256	14,7/236	2,10/65	0,2/78	0,5/42	2,2/130	0,2/80	0,3/48	6,7/137	
$\epsilon$	6,2/16	6,20/138	5,7/83	0,1/3						
$\zeta$	17,38/98	1,3/45	4,4/28	17,16/63	19,25/121					

Table 1—Continued

Class	Subclass									
	0	1	2	3	4	5	6	7	8	9
$\eta$	0,9/62	2,3/43								
$\theta$	0,4/15									
$\lambda$ 0-9	0,0/1	0,1/22	0,0/5	0,0/3	0,0/3		1,1/45	6,5/124		0,0/1
10-19	0,1/32	0,1/26	4,9/58	0,0/1	0,0/1	0,0/1	1,1/30	0,0/7	1,2/77	1,0/4
20-29	11,23/121	1,7/107	0,1/5		0,8/120	12,18/179	0,0/5	2,3/81	10,8/103	0,1/11
30-35	33,36/273	0,1/37	0,0/4	0,0/5	16,23/139	0,0/5				

Note. — In each class, the numbers given  $a, b/c$  are  $a$  the number of sources actually observed,  $b$  the number selected for observation by STARTYPE, and  $c$  the total number in the subclass.



Table 2. Level 2 Classification Definitions

Class	Description
SE	Silicate (or oxygen-rich) dust <b>E</b> mission (10–12 and 18–20 $\mu\text{m}$ )
SB	Silicate emission in self-a <b>B</b> sorption (10 $\mu\text{m}$ )
SA	Silicate <b>A</b> bsorption (10–12 $\mu\text{m}$ )
SC	Silicate emission from <b>C</b> rystalline grains (33, 40, 43 $\mu\text{m}$ )
SEC	Silicate <b>E</b> mission from <b>C</b> rystalline grains (11, 19, 23, 33 $\mu\text{m}$ )
CE	<b>C</b> arbon-rich dust <b>E</b> mission, primarily from SiC (11.5 $\mu\text{m}$ )
CR	<b>C</b> arbon-rich dust emission in a <b>R</b> eddened shell (with features at 11.5 and 26 $\mu\text{m}$ , often 13.7 $\mu\text{m}$ absorption)
CT	8, 11.5, <b>21</b> , 26 $\mu\text{m}$ , no 13.7 absorption
CN	<b>C</b> arbon-rich <b>N</b> ebulae
C/SE	<b>C</b> arbon-rich, plus <b>S</b> ilicate emission (10–12 $\mu\text{m}$ )
C/SC	<b>C</b> arbon-rich, plus <b>c</b> rystalline <b>s</b> ilicate emission
U/SC	<b>C</b> rystalline <b>s</b> ilicate and <b>U</b> IR emission features
U	Prominent <b>U</b> IR emission features
PN	Many prominent atomic fine-structure lines typical of <b>P</b> lanetary <b>N</b> ebulae
PU	As PN, but with strong <b>U</b> IR emission
W	Emission peaks 6–8 $\mu\text{m}$
F	Basically <b>F</b> eatureless
E	Strong <b>E</b> mission lines
M	<b>M</b> iscellaneous

Table 3. Level 2 Suffixes

Suffix	Description
e	Emission lines (e.g. H-recombination, atomic fine-structure, etc.)
u	UIR features present, but not dominant feature
p	Fits in given category, but is peculiar
:, ::	Uncertain (either noisy or odd)

Table 4. Level 1-2 Cross-References and Statistics

LEVEL 2	LEVEL 1						
	Group 1	Group 2	Group 3	Group 4	Group 5	Group 6	Group 7
N	49/59						
NO	49/90						
NC	4/7						
SE		a: 59/72 <sup>a</sup> b: 26/43 c: 42/53	21/27	25/27	7/7		
SB		...	9/12	7/8	...		
SA		...	2/3	25/30	50/63		
SC		...	...	14/19	...		
SEC		...	...	10/13	...		
CE		29/53	6/6	...	...		
CR		...	9/9	12/14	...		
CT		...	...	9/12	...		
CN		...	...	5/5	...		
C/SE		3/3	...	...	...		
C/SC		...	...	1/2	...		
U/SC		...	...	9/14	...		
U		2/3	...	...	19/26		
PN		...	...	24/35	6/6		
PU		...	...	11/16	...		
W		...	13/15	...	...		
UE		...	...	...	89/96		
E	7/9	3/4	...	...	18/18		
F		...	...	15/16	18/19		
M	11/13	6/6	...	4/8	10/10		
Total:	120/178	170/237	60/72	171/219	217/245	100/113	82+/184

Note. — The format of the entries is Sources/Spectra. “Spectra” refers to the total number of observations in a particular category. “Sources” refers to the number of spatially distinct objects, although this can be debatable in cases of extended, complex sources. For example, the 16 observations of Cas A are counted as one source. Group 7 Sources include only those that are not offs (31), flagged (13), or at the wrong coordinates (28).

<sup>a</sup>Subroup 2.SE is divided into parts a, b, and c (see text).

Table 5. KSPW vs. LRS Classifications

LRS	OK	Information Lost	KSPW	Mismatch
“Blue”				
1 <i>n</i> Featureless	1.N	1.NC, 1.NO (1.NE)	2.CE, 2.M, 2.SEa, 2.SEb, 3.CR, 3.SA, 3.W, 4.CR, 4.SB, 4.U/SC, 6	
2 <i>n</i> 10 $\mu$ m Emission	2.SEa, 2.SEb, 2.SEc, 3.SB, 3.SE	2.C/SE	1.N, 2.CE, 4.CR, 4.SE, 4.SEC	
3 <i>n</i> 10 $\mu$ m Absorption	2.M, 3.SB, 3.W (3.SA)		1.NC, 2.SEb, 4.SA, 4.SB, 4.SC, 5.SA, 5.U, 6	
4 <i>n</i> Carbon-rich	2.CE	3.CE, 3.CR, 4.CR (4.CN, 4.CT, 4.C/SC)	2.SEa, 3.SB, 4.SB	
“Red”				
5 <i>n</i> Featureless	4.F (5.F)	(4.SC)	2.SEa, 3.CR, 4.C/SC, 4.SB, 5.SA, 5.UE	
6 <i>n</i> 10 $\mu$ m Em.	3.SE, 4.SE, 5.SE (4.SB)	4.SEC	2.SEc, 4.CN, 4.SC	
7 <i>n</i> 10 $\mu$ m Abs.	4.SA, 5.SA (3.SA, 4.SB)	4.U/SC	4.F, 4.CN, 4.CT, 4.SC, 5.U, 5.UE	
8 <i>n</i> UIR + lines	4.M, 4.PU, 5.U, 5.UE	2.U, 4.PN		
9 <i>n</i> lines only	4.PN, 5.E, 5.PN	4.PU, 4.SEC, 5.F, 5.SA, 5.UE		

Note. — KSPW classes in parentheses could reasonably have appeared in a given LRS class but did not.

Table 6. Source Classification

Name	TDT	RA (J2000)	Dec (J2000)	Group	Comments
W Cet	37802225	00 <sup>h</sup> 02 <sup>m</sup> 07 <sup>s</sup> .70	−14°40′35″.9	2.SEa:	
SV And	42801007	00 04 20.00	+40 06 37.2	2.SEa:	
SV And	80800708	00 04 20.00	+40 06 37.2	2.SEa	
CIT 1	78201008	00 06 52.30	+43 04 36.0	7	W
HR 10	37802001	00 07 18.20	−17 23 13.2	1.NM:	
$\beta$ Cas	28501420	00 09 10.47	+59 08 59.8	1.N	
V633 Cas	43501514	00 11 26.60	+58 50 04.0	5.SE	W
NGC 40	44401917	00 13 00.91	+72 31 20.0	4.PN	
NGC 40	30003803	00 13 01.10	+72 31 19.1	4.PN	
HR 48	55502138	00 14 38.40	−18 55 58.4	1.NO	
S Scl	73500129	00 15 22.18	−32 02 43.4	2.SEb	
S Scl	37102018	00 15 22.19	−32 02 44.0	2.SEb	
IRAS 00127+5437	39902101	00 15 24.13	+54 54 15.4	4.SE::	
VX And	42801502	00 19 54.10	+44 42 35.0	2.CE	
T Cet	55502308	00 21 46.03	−20 03 30.8	2.SEa	
T Cet	37801819	00 21 46.58	−20 03 28.0	2.SEa	F
RAFGL 5017	54900858	00 21 48.00	−40 17 13.0	4.SEC:	
T Cas	40201208	00 23 14.25	+55 47 33.7	2.SEa	
IRAS 00210+6221	40401901	00 23 51.20	+62 38 07.0	4.CR	
IRAS 00211+6549	44402001	00 23 58.00	+66 06 03.2	5.F:	
R And	40201723	00 24 02.00	+38 34 37.0	2.SEc	
47 Tuc	74803701	00 24 05.10	−72 04 50.5	7	R
Off- $\beta$ Hyi	17900204	00 25 42.85	−77 15 17.2	7	
$\beta$ Hyi	85000604	00 25 44.09	−77 15 16.6	1.N	
Off- $\beta$ Hyi	9200604	00 25 47.34	−77 15 17.3	7	F
$\kappa$ Phe	23200502	00 26 12.16	−43 40 49.1	1.NM:	
VX Cas	42701004	00 31 20.00	+62 00 00.0	7	W
RNO 1B	28500902	00 36 46.26	+63 28 54.4	5.F	
M 31	40001501	00 42 46.01	+41 16 11.9	7	G
WR 1	42500402	00 43 28.40	+64 45 44.5	7	
Off-WR1	42500403	00 43 28.40	+64 47 44.5	7e:	
EG And	57702107	00 44 37.00	+40 40 46.3	1.NO	

Table 6—Continued

Name	TDT	RA (J2000)	Dec (J2000)	Group	Comments
NGC 261	66300214	00 46 32.16	−73 06 03.5	7	G
RW And	42301901	00 47 18.20	+32 40 58.8	7	R:
NGC 253	24701422	00 47 33.20	−25 17 17.2	5.UE	G
[RLB93] SMC-B2	11701107	00 48 07.80	−73 15 14.0	7	G
[RLB93] SMC-B2	54701810	00 48 07.80	−73 15 14.0	7	G
$\delta$ Psc	39502401	00 48 40.88	+07 35 06.2	1.NO	
IRAS 00477−7343	36000902	00 49 30.77	−73 26 50.2	7	G
VY Cas	78201606	00 51 26.11	+62 55 14.0	2.SEb	
VY Cas	41602501	00 51 26.11	+62 55 14.9	2.SEb	
S 184 −14.13, −2 39.8	40201616	00 52 09.78	+56 31 05.8	6	Offset
S 184	40201615	00 52 23.91	+56 33 45.6	5.F	(0,0)
S 184 +25.44, +3 52.6	40201614	00 52 49.35	+56 37 38.2	6	Offset
IRAS 00521−7054	17101907	00 53 56.30	−70 38 07.0	7	G
IRAS 00521−7054	17102008	00 53 56.30	−70 38 07.0	7	G
S 184 +1 50.79, −22.8	40201617	00 54 14.70	+56 33 22.8	7	Offset, R:
W Cas	42301226	00 54 53.83	+58 33 49.8	2.C/SE	
$\gamma$ Cas	24801102	00 56 42.39	+60 43 00.0	1.NE	
[GHJ82] SMC N76B K2	36001101	01 03 07.89	−72 06 27.6	7	G
IRAS 01005+7910	68600302	01 04 45.70	+79 26 47.0	4.PUp:	
Nova Cas 1995	77700106	01 05 05.39	+54 00 40.4	6:	
Nova Cas 1995	24800901	01 05 05.40	+54 00 40.5	6:	
Nova Cas 1995	59502003	01 05 05.40	+54 00 40.5	6	
Nova Cas 1995	64500309	01 05 05.40	+54 00 40.5	6	
Nova Cas 1995	83701909	01 05 05.40	+54 00 40.5	6	
Nova Cas 1995	28301904	01 05 05.41	+54 00 40.8	6	
Nova Cas 1995	65400106	01 05 05.43	+54 00 40.4	6	
IRAS 01039−7305	17101710	01 05 31.50	−72 49 56.0	7	G
IRAS 01039−7305	17101809	01 05 31.50	−72 49 56.0	7	G
CIT 3	39502217	01 06 25.96	+12 35 53.1	3.SB	
CIT 3	76101413	01 06 26.00	+12 35 53.0	3.SB	
IRAS 01045+6505	85303602	01 07 50.67	+65 21 21.7	5.UE	
$\beta$ And	79501002	01 09 43.77	+35 37 15.2	1.NO	

Table 6—Continued

Name	TDT	RA (J2000)	Dec (J2000)	Group	Comments
$\beta$ And	42301404	01 09 43.86	+35 37 14.3	1.NO	
$\beta$ And	44004605	01 09 43.86	+35 37 14.3	1.NO	
HV Cas	43502472	01 11 03.10	+53 43 34.0	7	
HV Cas	62902503	01 11 03.50	+53 43 40.3	2.CE	
HR 365	41602312	01 16 11.90	+71 44 38.7	1.NO	
AFGL 190	68800128	01 17 51.60	+67 13 53.6	4.CR	
S Cas	41602133	01 19 42.03	+72 36 41.0	3.SEp	
Fairall 9	17902439	01 23 45.71	−58 48 20.5	7	G
LHA 115-N 88	66300110	01 24 08.11	−73 09 03.1	5.M:	G
R Scl	37801443	01 26 58.05	−32 32 34.2	2.CE	
R Scl	56900115	01 26 58.09	−32 32 34.9	2.CE	
R Scl	24701012	01 26 58.10	−32 32 34.9	2.CE	
R Scl	37801213	01 26 58.10	−32 32 34.9	2.CE	
R Scl	39901911	01 26 58.10	−32 32 34.9	2.CE	
R Scl	41401514	01 26 58.10	−32 32 34.9	2.CE	
$\gamma$ Phe	54901434	01 28 21.90	−43 19 05.2	1.NO	
CE And	80104817	01 29 33.20	+46 39 33.0	2.SEc	
AFGL 230 −0.6, −6.3	44301870	01 33 50.60	+62 26 47.0	4.SA	Offset
AFGL 230	78800604	01 33 51.20	+62 26 53.3	4.SA	(0,0)
$\alpha$ Eri	17902503	01 37 42.86	−57 14 12.1	1.N	
HR 483	42301707	01 41 46.98	+42 36 48.9	1.N:	
NGC 660	63300301	01 43 02.30	+13 38 45.0	5.UE	G
RMC 50	11501805	01 44 03.98	−74 40 49.6	7	G
IRAS 01420+6401	61301076	01 45 39.58	+64 16 02.1	5.M:	
SV Psc	80501620	01 46 35.30	+19 05 04.0	2.SEb	
WX Cas	43306112	01 54 04.20	+61 06 32.0	1.NO:	
V471 Per	28501652	01 58 49.70	+52 53 48.5	6	
XX Per	61702401	02 03 08.77	+54 53 56.8	7	W
$\gamma^1$ And	43502924	02 03 53.99	+42 19 47.2	1.NO	
3C 58	84901201	02 05 38.20	+64 49 45.0	7	
$\alpha$ Ari	45002411	02 07 10.26	+23 27 45.4	1.NO:	
WR 34	45701204	02 10 15.70	+56 33 32.7	2.SEa	

Table 6—Continued

Name	TDT	RA (J2000)	Dec (J2000)	Group	Comments
V Ari	80700751	02 15 00.10	+12 14 23.1	1.NM::	
O Cet	45101201	02 19 20.78	−02 58 36.2	2.SEC	
HD 14242	61301202	02 20 22.44	+59 40 17.6	2.SECa:	
AD Per	45501603	02 20 29.00	+56 59 35.2	2.SECa:	
AD Per	78800921	02 20 29.00	+56 59 35.2	2.SECap	
FZ Per	43306302	02 20 59.65	+57 09 29.9	2.SECa:	
HD 14404	45501704	02 21 42.43	+57 51 46.2	2.SECap:	
SU Per	43306303	02 22 06.93	+56 36 15.1	2.SEC	
RS Per	45501805	02 22 24.26	+57 06 34.4	2.SEC	
S Per	43306550	02 22 51.70	+58 35 14.1	3.SE	
HD 14580	42701401	02 23 23.96	+57 12 41.9	1.NO:	
HD 14826	61601203	02 25 20.80	+57 26 15.0	2.SECa:	
W 3 IRS 5	42701302	02 25 40.54	+62 05 51.3	5.SA	
W 3 IRS 2	64600609	02 25 44.59	+62 06 11.2	5.UE	F
W 3 IRS 2	78800709	02 25 44.59	+62 06 11.2	5.UE	
IRAS Z02229+6208	44804704	02 26 41.80	+62 21 22.0	4.CT	
Off-IRAS02229+6208	44804703	02 26 59.00	+62 22 22.0	7	
RR Per	61702702	02 28 29.42	+51 16 18.6	2.SECa	
R For	82001817	02 29 15.30	−26 05 56.2	2.CE	
R For	55702018	02 29 15.30	−48 05 56.0	7	W
$\alpha$ UMi	36802830	02 31 47.94	+89 15 50.7	1.N	
$\alpha$ UMi	8000130	02 31 50.08	+89 15 50.8	1.N	F
AFGL 341	80002450	02 33 00.16	+58 02 05.0	3.CR	
IRC −30023	44202463	02 37 23.60	−26 58 39.0	2.SEC	
YZ Per	47301604	02 38 25.33	+57 02 46.2	2.SEC	
IRAS 02383+6241	83901404	02 42 19.82	+62 53 51.8	5.M:	
NGC 1068	28502026	02 42 40.80	−00 00 47.3	5.SAe	G
$\theta$ Per	64900206	02 44 11.92	+49 13 42.7	1.N:	
W Hor	72200302	02 44 14.62	−54 18 03.6	2.SEb	
W Hor	17902728	02 44 14.70	−54 18 04.0	2.SEb	
W Hor	75600502	02 44 14.70	−54 18 04.0	2.SEb	
IRAS 02408+5458	80002504	02 44 25.19	+55 11 15.4	4.CR	

Table 6—Continued

Name	TDT	RA (J2000)	Dec (J2000)	Group	Comments
RAFGL 5081	68300101	02 48 41.61	+69 35 31.8	4.SE::	
W Per	63702662	02 50 37.90	+56 59 00.7	2.SEc	
RZ Ari	46601705	02 55 48.50	+18 19 53.1	1.NO	
HR 877	64900829	02 57 04.60	+04 30 03.6	1.NO	
AFGL 4029	86300968	03 01 31.29	+60 29 13.5	5.U	
$\alpha$ Cet	79702803	03 02 16.80	+04 05 23.2	1.NO	
$\alpha$ Cet	80600924	03 02 16.80	+04 05 23.2	1.NO	
$\rho$ Per	79501105	03 05 10.60	+38 50 25.2	1.NO	
AFGL 437	86300810	03 07 23.68	+58 30 50.6	5.U	
IRAS 03035+5819	63702553	03 07 24.18	+58 30 46.5	5.UEp	
BD+59 594	62301808	03 07 40.01	+60 29 20.9	2.SEa:	
HD 19557	64601230	03 11 25.32	+57 54 11.8	1.NC	
HD 19557	64601301	03 11 25.32	+57 54 11.8	2.SEb	F
IRAS 03093+4313	61601503	03 12 43.17	+43 24 48.7	3.SEp::	
IRAS 03201+5459	62301505	03 23 59.40	+55 10 14.2	3.W:	
IRC +50096	81002351	03 26 29.80	+47 31 47.1	3.CE	
AFGL 490	64001804	03 27 38.71	+58 47 01.1	5.SA	
[SVS76] NGC 1333 13	65201959	03 29 03.74	+31 16 02.7	5.SA	
[SVS76] NGC 1333 3	65902719	03 29 10.37	+31 21 58.3	5.U	
[SVS76] NGC 1333 3	65201807	03 29 10.40	+31 21 51.0	5.U	
IRAS 03313+6058	62301907	03 35 31.50	+61 08 51.0	4.CR	
NGC 1386	79901510	03 36 46.16	−35 59 57.2	7	G
SBSG 0335−052	66500410	03 37 44.00	−05 02 39.0	7	G
SBSG 0335−052	66500511	03 37 44.00	−05 02 39.0	7	G
U Cam	64001445	03 41 48.16	+62 38 55.2	2.CE	
$\delta$ Eri	66301815	03 43 14.82	−09 45 49.7	1.N	
VDB 19 −1.20, +13.0	65201413	03 44 32.90	+32 10 00.0	6	Offset
VDB 19	65201414	03 44 34.10	+32 09 47.0	5.F:	(0,0)
VDB 19 +1.00, −15.0	65201412	03 44 35.10	+32 09 32.0	5.F:	Offset
Off-VDB19	65201411	03 45 34.10	+31 54 47.0	7	
WX Cam	81002721	03 49 03.80	+53 10 59.9	1.NO	
IRAS 04025+5313	68100312	04 06 25.51	+53 21 50.0	6	



Table 6—Continued

Name	TDT	RA (J2000)	Dec (J2000)	Group	Comments
Elias 3-1	67301306	04 18 40.68	+28 19 16.0	4.SBu	
RY Tau	81002824	04 21 57.30	+29 26 37.1	7	W
T Tau	68000503	04 21 59.17	+19 32 06.5	5.SA	
M 4-18	83801755	04 25 50.80	+60 07 12.0	7u:	R
DG Tau	67301204	04 27 04.65	+26 06 16.5	4.SC:	
RV Cam	86202101	04 30 41.70	+57 24 41.8	2.SEb	
RV Cam	83801807	04 30 41.80	+57 24 42.0	2.SEb	
L1551 IRS 5	66001999	04 31 34.08	+18 08 05.1	5.SAe	
HL Tau	68101016	04 31 38.40	+18 13 58.8	5.SA:	
$\alpha$ Tau	63602102	04 35 55.19	+16 30 33.9	1.NO	
R Dor	58900918	04 36 45.72	−62 04 38.0	2.SEa	
AFGL 618	68800561	04 42 53.30	+36 06 53.0	4.CN	
RV Tau	68401252	04 44 01.90	+26 10 45.7	7	W
WOH G 64	56701336	04 55 09.80	−68 20 36.5	5.SA:	G
AB Aur	68001206	04 55 45.69	+30 33 06.0	5.SEu	
RMC 66	14800102	04 56 47.47	−69 50 26.2	7	G
MWC 480	83501201	04 58 46.10	+29 50 37.5	4.SE::	
TX Cam	69501070	05 00 50.39	+56 10 52.6	2.SEc	
IRAS 04579+4703	86201902	05 01 39.70	+47 07 23.2	5.SA	
$\epsilon$ Aur	64500811	05 01 58.10	+43 49 23.8	1.N	
RMC 71	14800210	05 02 07.62	−71 20 13.6	7	G,R
W Ori	85801604	05 05 23.70	+01 10 39.2	2.CE	
TRM 4	26601601	05 11 11.00	−67 52 12.0	7	G
TRM 4	61802102	05 11 11.00	−67 52 12.0	7	G
IRC +50137	86201803	05 11 19.45	+52 52 33.7	3.SB	
HD 33793	72200805	05 11 39.20	−45 00 55.3	7	R:
HD 33793	75601205	05 11 39.34	−45 00 55.6	7	F
$\beta$ Ori	83301505	05 14 32.30	−08 12 06.0	1.N	
HD 34282	83301240	05 16 00.46	−09 48 34.2	7	
$\alpha$ Aur	83801504	05 16 41.38	+46 59 53.8	7	W
HD 34700	66302638	05 19 41.39	+05 38 43.0	5.M:	
IRAS 05167+3858	64501216	05 20 11.04	+39 01 19.7	7	R:

Table 6—Continued

Name	TDT	RA (J2000)	Dec (J2000)	Group	Comments
HD 35187	69501139	05 24 01.18	+24 57 36.4	3.SE::	
IRAS 05221+4139	64501104	05 25 39.77	+41 41 50.3	5.U:	
Nova LMC 1995	57801111	05 26 50.30	−70 01 23.8	7	G
IC 418	82901301	05 27 28.31	−12 41 48.2	4.PN	
IRAS 05294−7104	19001011	05 28 48.70	−71 02 31.0	7	G
IRAS 05298−6957	29801904	05 29 23.06	−69 55 12.5	7	G
TRM 60	62401512	05 32 51.60	−67 06 51.0	7	G
TRM 60	16401105	05 32 51.60	−67 06 53.0	7	G
IRAS 05346−6949	74300825	05 34 13.68	−69 47 29.5	7	G
M 1 −2.64, −15.2	82401714	05 34 29.33	+22 00 36.9	6	Offset <sup>a</sup>
M 1 −0.01, +2 12.6	82602113	05 34 31.96	+22 02 04.7	6	Offset
M 1 +1.66, +0.5	82602219	05 34 33.63	+22 00 52.6	6	Offset
M 1 +2.24, −57.6	82401612	05 34 34.21	+21 59 54.5	6	Offset
Orion Pk1	68701515	05 35 13.67	−05 22 08.5	5.E	Propn
Orion IRc2	68901006	05 35 14.46	−05 22 29.8	5.SAe	Propn
Orion Pk2	83301701	05 35 15.80	−05 22 40.7	5.E	Propn
Orion Bar d8	69501409	05 35 18.22	−05 24 39.9	5.UE	Propn
Orion Bar Brga	69502108	05 35 19.31	−05 24 59.9	5.UE	Propn
Orion Bar d5	69502207	05 35 19.81	−05 25 10.0	5.UE	F,Propn
Orion Bar d5	83101507	05 35 19.81	−05 25 10.0	5.UE	Propn
Orion Bar H2 1	69501806	05 35 20.31	−05 25 20.0	5.UE	Propn
Orion Bar d2	69502005	05 35 21.40	−05 25 40.1	5.UE	Propn
SN 1987 A	81102402	05 35 28.05	−69 16 11.7	7	G
IRAS 05338−0624	70001308	05 36 18.99	−06 22 13.3	5.M:	
IRAS 05341+0852	69702604	05 36 55.00	+08 54 09.0	4.PN	
IRAS 05389−6922	74901823	05 38 33.44	−69 20 34.2	3.SE:	G
30 Dor	17100512	05 38 46.00	−69 05 07.9	5.E	G, (0,0)
30 Dor +8.18, −7.4	62804321	05 38 54.18	−69 05 15.3	5.E	Offset, G
IRC −10095	86801101	05 39 42.60	−08 09 07.9	2.CE	
LHA 120-N 160A IR	62401303	05 39 43.73	−69 38 30.4	5.UE	G, (0,0)
LHA 120-N 160A IR +2.39, −6.2	62804104	05 39 46.12	−69 38 36.6	5.UE	G, Offset
RAFGL 5163	69703802	05 40 27.90	−07 27 29.4	5.SA	

Table 6—Continued

Name	TDT	RA (J2000)	Dec (J2000)	Group	Comments
HR 1939	86603434	05 40 42.00	+31 55 15.0	2.SEa	
Off-NGC2023	65602310	05 40 52.70	−02 15 59.0	7	
NGC 2023	65602309	05 41 38.30	−02 16 32.6	5.U	
TU Tau	85403210	05 45 13.70	+24 25 12.2	2.CE	
FU Ori	87601701	05 45 22.50	+09 04 12.0	7	H
HH111VLA-J	84902106	05 49 46.29	+02 48 38.4	6:	Propn
BC Tau	69901113	05 53 43.70	+24 14 45.0	5.SA	
IRAS 05544−6456	73102513	05 54 38.74	−64 56 19.2	2.SEb:	G
$\alpha$ Ori	69201980	05 55 10.39	+07 24 25.5	2.SEc	
IRC +40149	87102906	05 59 24.80	+38 26 22.0	7	W
$\iota$ Aur	83802031	05 59 56.80	+45 56 12.0	1.NO	
Mon R2 IRS 2	71102004	06 07 45.80	−06 22 50.0	5.UE	
Mon R2 IRS 3	71101712	06 07 47.76	−06 22 56.8	5.SA	
GGD 12	70901305	06 10 50.18	−06 12 01.0	5.UE	
IC 443 −26.80, −27 20.3	83501603	06 17 07.60	+22 25 34.6	6	Offset
IC 443	70001401	06 17 34.40	+22 52 54.9	6	(0,0)
DO 12103	84901804	06 18 44.84	+15 16 43.4	5.E	
HD 44179	70201801	06 19 58.20	−10 38 15.2	4.U/SC	
IRC +00102	87201709	06 21 51.30	−03 51 42.0	7	W
$\beta$ CMa	72301501	06 22 41.90	−17 57 21.5	1.N	
$\alpha$ Car	72902207	06 23 57.09	−52 41 44.5	1.N	
IRC −10122	86706617	06 25 01.60	−09 07 16.0	2.CE	
BL Ori	87702501	06 25 28.20	+14 43 19.0	7	F
AFGL 940	87102602	06 26 37.30	+09 02 16.0	3.CE	
HD 45677	71101992	06 28 17.46	−13 03 10.4	3.SE	
RR Pic	60901001	06 35 36.10	−62 38 23.1	6:	
NGC 2264 IR	71602619	06 41 10.06	+09 29 35.8	5.SA	
$\alpha$ CMa	86801303	06 45 08.97	−16 42 55.9	1.N	
$\alpha$ CMa	68901202	06 45 08.99	−16 42 55.3	1.N	
WR 6	72401201	06 54 13.02	−23 55 42.2	1.NE:	
IRAS 07027−7934	14101101	06 59 26.11	−79 38 48.1	4.U/SC	
IRAS 07027−7934	73501035	06 59 26.29	−79 38 48.0	4.U/SC	

Table 6—Continued

Name	TDT	RA (J2000)	Dec (J2000)	Group	Comments
IRAS 06582+1507	71002102	07 01 08.40	+15 03 40.0	4.CR	
Z CMa	72201607	07 03 43.18	−11 33 06.7	5.SA	
NGC 2346	71602537	07 09 22.50	−00 48 22.4	6	
HD 56126	72201901	07 16 10.17	+09 59 47.4	4.CT	
VY CMa	73103039	07 22 58.20	−25 46 02.7	3.SB:	
NGC 2440	72501762	07 41 55.40	−18 12 31.4	4.PN	
HD 65750	72802231	07 56 50.80	−59 07 32.2	2.SEap	
$\gamma$ Vel	18000101	08 09 32.06	−47 20 11.9	1.NE	
IRAS 09425−6040	8400628	09 44 01.81	−60 54 23.2	4.C/SC	F
IRAS 09425−6040	25400160	09 44 01.87	−60 54 23.0	4.C/SC	
IRC +10216	19700159	09 47 57.37	+13 16 43.8	3.CR	
M 82	11600319	09 55 50.70	+69 40 44.4	5.UE	G
IRAS 09563−5743	17100205	09 58 02.67	−57 57 51.8	5.UE	
MWC 198	7901027	10 04 30.34	−58 39 50.9	5.SE	
S Car	7900620	10 09 22.47	−61 32 58.3	2.M	
CPD−57 2874	8401219	10 15 22.70	−57 51 44.9	3.Wp:	
HR 4049	4000458	10 18 07.60	−28 59 31.3	2.U	
HR 4049	17100101	10 18 07.62	−28 59 31.4	2.U	
Wray 15-543	8400730	10 19 32.61	−60 13 28.9	5.U:	
Roberts 22	8401033	10 21 33.97	−58 05 37.6	4.SC	
Roberts 22	25400259	10 21 33.97	−58 05 37.6	4.U/SC	
$\mu$ UMa	16000806	10 22 19.67	+41 29 57.9	1.NO	
HR Car	8400808	10 22 53.89	−59 37 28.0	4.SEep	
HR Car	24900215	10 22 53.89	−59 37 28.0	4.SEep	
AFGL 4106	10401225	10 23 19.55	−59 32 05.8	4.SCp	
AFGL 4106	24900158	10 23 19.55	−59 32 05.8	4.SCp	
AFGL 4106	6000280	10 23 19.65	−59 32 05.8	4.SCp	
HD 90586	25400410	10 26 15.71	−53 53 29.9	2.SEc	
Car_POL1	26800192	10 42 37.46	−59 31 29.0	5.U:	Propn
Off- $\theta$ Car	25900906	10 42 57.34	−64 26 39.9	7	
$\theta$ Car	25900905	10 42 57.44	−64 23 39.9	1.N:	
Car_POL2	26800193	10 42 58.39	−59 32 54.3	5.UE	Propn

Table 6—Continued

Name	TDT	RA (J2000)	Dec (J2000)	Group	Comments
Car_POL3	26800194	10 43 19.21	−59 34 19.3	5.UE	Propn
Trumpler14	25000467	10 43 23.96	−59 34 28.4	5.UE	Propn
Car_POL4	26800195	10 43 40.14	−59 35 44.2	5.E	Propn
RT Car	25901312	10 44 47.23	−59 24 48.0	2.SEc	
$\eta$ Car	7100250	10 45 03.60	−59 41 04.3	4.M:e	
$\eta$ Car	23701861	10 45 03.60	−59 41 04.3	4.M:e	
GG Car	24900846	10 55 58.89	−60 23 32.2	2.M:	
AG Car	4000652	10 56 11.60	−60 27 13.4	4.Me	
AG Car	22400153	10 56 11.63	−60 27 13.4	4.Me	
GJ 406	17400603	10 56 29.94	+07 01 01.4	7	W
HD 308122	26700202	10 58 15.30	−62 52 01.3	2.SEa	
IRAS 10589−6034	26800760	11 00 59.79	−60 50 27.1	5.UE	
HD 95881	10400818	11 01 57.78	−71 30 51.5	6:	
$\alpha$ UMa	14300723	11 03 43.76	+61 45 03.4	1.N	
HD 97048	14101343	11 08 04.61	−77 39 16.9	5.U	
HD 97048	61801318	11 08 04.61	−77 39 16.9	5.U	
Cha IRN	7200459	11 08 37.49	−77 43 53.6	5.F	
MR 35	7900723	11 08 39.88	−60 42 46.2	4.SC	
NGC 3603	27200587	11 15 07.12	−61 15 33.0	5.E	
RAFGL 4127	26200509	11 16 33.80	−61 29 59.4	5.E	
HD 98434	7901133	11 18 43.67	−58 11 11.1	1.NO	
HD 98800	24001208	11 22 05.34	−24 46 39.5	2.M:	
HD 100453	26000230	11 33 05.68	−54 19 29.0	4.F:u	
HD 100546	27601036	11 33 25.28	−70 11 42.3	4.U/SC	
HD 100546	7200660	11 33 25.52	−70 11 41.8	4.U/SC	
HD 100764	24001729	11 35 42.71	−14 35 35.6	7	R:
HD 101584	7901402	11 40 58.80	−55 34 27.3	5.SE	
$\beta$ Leo	4001710	11 49 03.28	+14 34 19.9	1.N	
$\beta$ Leo	18900244	11 49 03.72	+14 34 19.8	1.N	
NGC 3918	7901201	11 50 18.91	−57 10 51.1	4.PN	F
NGC 3918	29900201	11 50 18.91	−57 10 51.1	4.PN	
HD 104237	23300524	12 00 05.11	−78 11 33.7	4.SE:	

Table 6—Continued

Name	TDT	RA (J2000)	Dec (J2000)	Group	Comments
HD 104237	10400424	12 00 05.98	−78 11 33.7	4.SE:	F
$\delta$ Cen	7200272	12 08 21.51	−50 43 20.7	1.NE	
$\delta$ Cen	7200351	12 08 21.51	−50 43 20.7	1.NE	
Wray 16-106	25901414	12 09 01.16	−63 15 54.7	5.UE	
IRAS 12073−6233	25901572	12 10 00.33	−62 49 56.5	5.UE	
Nova Cru 1995	58400304	12 10 30.60	−61 45 18.0	7	W
Nova Cru 1995	61801207	12 10 30.60	−61 45 18.0	7	W
Nova Cru 1995	30800308	12 10 31.40	−61 45 09.6	7	W
NGC 4151	17201135	12 10 32.60	+39 24 21.0	7	G
CD−53 4543	60700604	12 20 15.04	−53 55 31.4	4.SE:	
SX Cen	26801606	12 21 12.60	−49 12 40.5	7	R
BI Cru	25901615	12 23 26.36	−62 38 16.6	3.CR::	
SS Vir	21100138	12 25 14.40	+00 46 10.2	2.CE	
$\gamma$ Cru	25806177	12 31 09.89	−57 06 46.6	1.NO	
$\gamma$ Cru	60900804	12 31 09.89	−57 06 46.9	1.NO <sub>p</sub>	
$\gamma$ Cru	7901307	12 31 09.89	−57 06 47.0	1.NO	
$\eta$ Crv	24002304	12 32 04.30	−16 11 45.7	1.NO::	
IC 3568	71200614	12 33 06.61	+82 33 49.7	6	
IC 3568	21304923	12 33 06.73	+82 33 49.8	6	
NGC 4507	26000708	12 35 37.01	−39 54 31.1	7	G
IRAS 12331−6134	29900470	12 36 01.90	−61 51 03.9	5.UE	
Y UMa	60200502	12 40 21.20	+55 50 47.4	2.SE <sub>a</sub>	
IRAS 12405−6238	29400410	12 43 31.93	−62 55 11.4	5.UE	
Y CVn	16000926	12 45 07.80	+45 26 24.9	2.CE	
RU Vir	24601053	12 47 18.43	+04 08 41.9	2.CE	
SS73 38	60700908	12 51 26.30	−64 59 59.0	2.CE:	
HH 54 IRS	23300112	12 53 15.92	−77 07 02.0	5.SA	
TU CVn	16001527	12 54 56.49	+47 11 48.2	1.NO	
HH 52	9200725	12 55 07.52	−76 57 50.2	6:	
HH 53A	9200727	12 55 15.87	−76 57 27.1	6:	
$\delta$ Vir	24201225	12 55 36.31	+03 23 50.9	1.NO	
HH 54B	9200828	12 55 50.85	−76 56 18.6	6:	

Table 6—Continued

Name	TDT	RA (J2000)	Dec (J2000)	Group	Comments
RY Dra	54300203	12 56 25.70	+65 59 39.0	2.CE	
TT CVn	22101143	12 59 22.73	+37 49 04.5	7	R
RT Vir	24700319	13 02 37.78	+05 11 09.2	2.SEa	
NGC 4945	26801809	13 05 26.16	−49 28 15.5	5.UE	G
DL Cha	62804032	13 06 08.50	−77 06 28.0	2.SEa	
Wray 16-125	60701101	13 09 36.26	−61 19 34.4	4.SBe	
WR 48a	7902703	13 12 39.32	−62 42 55.5	3.W	
Off- $\alpha$ Vir	25302015	13 25 11.53	−11 06 40.8	7	
$\alpha$ Vir	25302001	13 25 11.55	−11 09 40.8	1.N	
Off- $\alpha$ Vir	25302002	13 25 11.57	−11 12 40.8	7	
$\alpha$ Vir	8201001	13 25 11.66	−11 09 40.6	1.N	
HR 5072	39600606	13 28 25.85	+13 46 45.3	1.N:	
R Hya	8200502	13 29 42.87	−23 16 52.7	2.SEa	
M 51 CCM72	20201816	13 29 44.30	+47 10 23.8	7	G
M 51 CCM10	60400709	13 29 59.90	+47 13 59.0	7	G
M 51 CCM10	61400401	13 29 59.90	+47 13 59.0	7	G
S Vir	25302224	13 33 00.05	−07 11 41.3	2.SEa	
NGC 5189	31800125	13 33 33.42	−65 58 34.9	6	
M 83 RK137	25600907	13 36 01.39	−29 51 28.3	5.E:	G,propn
M 83 RK213	25601501	13 36 52.57	−29 51 47.6	7	F,G,propn
M 83 RK213	44900501	13 36 52.57	−29 51 47.6	7	G,propn
M 83 RK110	25601404	13 37 04.69	−29 51 00.2	7	F,G,propn
M 83 RK110	44900404	13 37 04.69	−29 51 00.2	7	G,propn
HD 118685	13201304	13 41 13.60	−71 52 06.0	1.NO	
AFGL 4176	11701311	13 43 02.10	−62 08 52.0	5.SAe	
IRAS 13416–6243	62803904	13 45 07.61	−62 58 19.0	4.CN:u	
IRAS 13428–6232	60600505	13 46 20.82	−62 48 01.7	4.Fu	
$\tau$ Boo	39400205	13 47 15.80	+17 27 24.3	1.N:	
$\eta$ UMa	17200523	13 47 32.30	+49 18 48.0	1.NM::	
W Hya	8902004	13 49 02.07	−28 22 02.8	2.SEa	
W Hya	41800303	13 49 02.07	−28 22 02.8	2.SEa	
HR 5192	8101808	13 49 26.69	−34 27 01.8	1.NO	

Table 6—Continued

Name	TDT	RA (J2000)	Dec (J2000)	Group	Comments
NGC 5315	43600267	13 53 57.84	−66 30 51.8	4.PN	
NGC 5315	7902104	13 53 57.85	−66 30 51.8	4.PN	
IRAS 13517−6515	44500145	13 55 30.87	−65 30 37.1	3.SE	
$\theta$ Aps	7901809	14 05 19.93	−76 47 47.9	2.SEb	
$\theta$ Cen	43600940	14 06 41.13	−36 22 10.5	1.N	
HD 123337	43400235	14 09 49.50	−68 11 19.0	2.SEb	
HR 5301	8200810	14 10 50.50	−16 18 08.0	1.NO	
Hen 2-104	60701604	14 11 52.00	−51 26 23.0	6:	
Circinus	7902231	14 13 09.70	−65 20 21.5	5.UE	G
Hen 2-106	60702103	14 14 09.00	−63 25 45.0	3.SE	
HD 124237	27602306	14 14 33.69	−61 47 55.5	6	
$\alpha$ Boo −0.50, +3.0	24403270	14 15 39.47	+19 11 06.6	1.NO	Offset
$\alpha$ Boo −0.40, +2.2	24403169	14 15 39.57	+19 11 05.8	1.NO	Offset
$\alpha$ Boo −0.39, +3.4	64100101	14 15 39.58	+19 11 07.0	1.NO	Offset
$\alpha$ Boo −0.31, +1.5	24403068	14 15 39.66	+19 11 05.1	1.NO	Offset
$\alpha$ Boo −0.20, −7.4	24403472	14 15 39.77	+19 10 56.2	1.NO	Offset
$\alpha$ Boo −0.10, +0.8	24402967	14 15 39.87	+19 11 04.4	1.NO	Offset
$\alpha$ Boo −0.05, −1.1	45200101	14 15 39.92	+19 11 02.5	1.NO	Offset
$\alpha$ Boo −0.04, −0.9	41200801	14 15 39.93	+19 11 02.7	7	Offset
$\alpha$ Boo −0.01, −0.2	27503811	14 15 39.96	+19 11 03.4	1.NO	
$\alpha$ Boo	24402866	14 15 39.97	+19 11 03.6	1.NO	(0,0)
$\alpha$ Boo +0.01, −7.2	64100104	14 15 39.98	+19 10 56.4	1.NO	Offset
$\alpha$ Boo +0.03, +0.9	7100434	14 15 40.00	+19 11 04.5	1.NO	Offset
$\alpha$ Boo +0.04, +1.0	5601291	14 15 40.01	+19 11 04.6	1.NO	Offset
$\alpha$ Boo +0.10, −0.7	24402765	14 15 40.07	+19 11 02.9	1.NO	Offset
$\alpha$ Boo +0.20, +7.4	24403371	14 15 40.17	+19 11 11.0	1.NO	Offset
$\alpha$ Boo +0.21, +12.6	64100103	14 15 40.18	+19 11 16.2	1.NO	Offset
$\alpha$ Boo +0.30, −1.5	24402664	14 15 40.27	+19 11 02.1	1.NO	Offset
$\alpha$ Boo +0.40, −2.2	24402563	14 15 40.37	+19 11 01.4	1.NO	Offset
$\alpha$ Boo +0.50, −3.0	24402462	14 15 40.47	+19 11 00.6	1.NO	Offset
$\alpha$ Boo +0.61, +2.0	64100102	14 15 40.58	+19 11 05.6	1.NO	Offset
$\lambda$ Boo	35101303	14 16 23.06	+46 05 17.5	1.N:	



Table 6—Continued

Name	TDT	RA (J2000)	Dec (J2000)	Group	Comments
R Cen	7903010	14 16 34.30	−59 54 46.9	2.SEap	
IC 4406	43600728	14 22 26.48	−44 09 05.9	6	
RX Boo	8201905	14 24 11.63	+25 42 13.8	2.SEa	
Off-V854Cen	29701411	14 34 49.21	−39 28 19.6	7	
V854 Cen	29701401	14 34 49.31	−39 33 19.6	3.W	
CPD−64 2939	60600607	14 37 09.80	−64 48 03.0	4.SC	
RV Boo	8202437	14 39 15.89	+32 32 22.3	2.SEa	F
RV Boo	39401737	14 39 15.90	+32 32 22.3	2.SEa	
$\alpha$ Cen	7902909	14 39 33.70	−60 50 10.1	7	F, W:
$\alpha$ Cen	29400809	14 39 37.65	−60 50 09.7	1.N	
$\alpha$ Cen	60702006	14 39 37.89	−60 50 04.0	1.N	
Mrk 477	19501504	14 40 38.09	+53 30 15.8	7	G
CS 2178	43600471	14 41 02.50	−62 45 54.0	2.CE	
RW Boo	42800541	14 41 13.41	+31 34 19.9	2.SEb	
$\beta$ UMi	7903403	14 50 42.23	+74 09 20.0	1.NO	
$\beta$ UMi	5601993	14 50 42.33	+74 09 19.8	7	F
$\beta$ UMi	18205639	14 50 42.33	+74 09 19.8	1.NO	
GJ 567	28101410	14 53 23.90	+19 09 09.5	1.N:	
Hen 2-113	7903307	14 59 53.49	−54 18 07.7	4.U/SC	
Hen 2-113	43400768	14 59 53.49	−54 18 07.7	4.U/SC	
IRAS 14559−6228	43400328	14 59 59.30	−62 40 44.0	2.M	
AFGL 4972	30601632	15 00 36.61	−58 58 15.8	5.Fe	
IRAS 15100−5613	29101114	15 13 50.21	−56 24 45.9	5.UE	
HD 135344	10401575	15 15 48.36	−37 09 16.3	7	
$\beta$ Lib	8201127	15 17 00.30	−09 22 59.0	1.NM:	
IRAS 15154−5258	27301017	15 19 08.60	−53 09 52.2	4.F::	
Pe 2-8	48800628	15 23 42.86	−57 09 23.3	4.SECe	
RS Lib	8200606	15 24 20.19	−22 54 40.6	2.SEa:	
WR 70	43400604	15 29 44.76	−58 34 50.9	3.W	
Off-HD139614	45800682	15 30 44.92	−42 30 27.4	7	O:
Hen 2-131	67404126	15 37 11.69	−71 54 53.2	4.PN	
Hen 2-131	7902010	15 37 11.69	−71 54 54.3	4.PN	

Table 6—Continued

Name	TDT	RA (J2000)	Dec (J2000)	Group	Comments
HD 139614	29701542	15 40 46.33	−42 29 52.6	4.SE:	
HD 139614	10402442	15 40 48.16	−42 29 52.4	7	F
IRAS 15384−5348	29900661	15 42 17.16	−53 58 31.5	5.UE	
IRAS 15408−5356	12302133	15 44 42.75	−54 05 55.	5.UE	
R CrB	29602404	15 48 34.21	+28 09 22.3	3.W	
R CrB	8202304	15 48 34.33	+28 09 22.3	7	F
R CrB	79200268	15 48 34.40	+28 09 23.8	3.W	
IRAS 15452−5459	45900615	15 49 10.79	−55 08 50.7	4.SAe	
V CrB	42200213	15 49 31.39	+39 34 18.0	2.CE	
V CrB	42300201	15 49 31.39	+39 34 18.0	2.CE	
V CrB	47600302	15 49 31.39	+39 34 18.0	2.CE	
V CrB	57401003	15 49 31.39	+39 34 18.0	2.CE	
V CrB	67600104	15 49 31.40	+39 34 18.0	2.CE	
V CrB	11105149	15 49 31.42	+39 34 18.0	2.CE	
HD 141569	62802937	15 49 57.60	−03 55 16.3	6	
ST Her	41901305	15 50 46.60	+48 28 58.7	2.SEa	
HD 330036	30601107	15 51 16.30	−48 45 01.0	4.U/SC:	
RCW 97	11702216	15 53 05.90	−54 35 21.1	5.UE	
IRAS 15502−5302	27301117	15 54 05.99	−53 11 36.4	5.UE	
MWC 238	32400106	15 56 01.26	−66 09 09.1	4.SC:	
HH 55	29101008	15 56 36.69	−37 50 52.1	6:	
HD 142666	44901283	15 56 40.06	−22 01 39.2	4.SE::	
HD 142666	10402952	15 56 40.07	−22 01 40.9	4.SE:	
HD 142527	10402046	15 56 42.10	−42 19 23.8	5.SE	
RU Lup	29101012	15 56 42.26	−37 49 15.7	7	
HD 143006	62803223	15 58 36.77	−22 57 14.9	6:	
IRAS 15553−5230	43600603	15 59 11.30	−52 38 40.3	4.SA:	
Hen 2-142	30601207	15 59 57.70	−55 55 33.0	4.PU:	
IRAS 15567−5236	29402535	16 00 32.86	−52 44 45.3	5.SAeu	
X Her	8001921	16 02 39.78	+47 14 21.7	2.SEb	
HD 144432	45000284	16 06 58.04	−27 43 08.4	4.SE:	
CPD−52 9243	27300921	16 07 00.87	−53 03 43.7	7	

Table 6—Continued

Name	TDT	RA (J2000)	Dec (J2000)	Group	Comments
Off-HR5999	28901607	16 08 30.29	−39 06 19.0	7	
HR 5999	28901506	16 08 34.30	−39 06 19.0	2.SEb:	
V Nor	45901136	16 10 01.80	−49 14 12.3	2.SEa	
IRAS 16076−5134	29402436	16 11 26.62	−51 41 56.6	5.E	
Lo 14	81600133	16 11 45.50	−51 17 56.9	2.SEc	
NGC 6072	29701632	16 12 58.79	−36 13 38.6	6	
$\delta$ Oph	8201231	16 14 20.60	−03 41 40.0	1.NO	
Wray 17-74	29402233	16 16 39.28	−51 16 58.3	5.UE	
Mz 3	27300834	16 17 13.57	−51 59 06.1	4.PN	
RCW 103	8101310	16 17 34.80	−51 06 13.0	6:	G
HR 6076	8501401	16 19 07.84	−20 13 03.8	1.N:	
SIGMA_SCO_FIL	11801514	16 19 51.50	−25 34 45.0	7	Propn, R:
HD 147104	8501105	16 20 30.79	−20 06 51.3	7	R
IRAS 16172−5028	12302238	16 21 00.43	−50 35 21.1	5.UE	
G333.13−0.43	11701221	16 21 02.70	−50 35 59.0	5.UE	
$\sigma$ Sco	11801612	16 21 09.80	−25 35 31.0	7	R:
$\eta$ Dra	8000921	16 23 59.47	+61 30 51.6	1.N	
RHO_OPH_WEST	12202004	16 24 51.60	−24 35 22.0	7	Propn,R:
SAO 243756	29401311	16 25 02.50	−60 03 32.0	4.F::	
U Her	43402028	16 25 47.70	+18 53 33.0	2.SEc	
Off-DoAr21	11800206	16 25 51.95	−24 23 36.2	7u:	
DoAr 21	11800205	16 26 02.96	−24 23 35.5	5.U:	
RHO_OPH_CENTER	11802102	16 26 11.70	−24 35 20.0	5.U	Propn
Off-ROX16	64101913	16 26 46.23	−24 10 57.6	7	
ROX 16	64101912	16 26 46.25	−24 11 57.6	7	
WL 22	31201201	16 26 59.16	−24 34 57.8	5.U	
WL 16	48400535	16 27 02.01	−24 37 25.6	5.U	
Elias 2-29	26700814	16 27 09.32	−24 37 21.1	5.SA	
Off-Wray15-1484	29901002	16 27 14.90	−48 38 45.0	7	
Wray 15-1484	29901001	16 27 14.90	−48 39 26.7	3.CR::	
WL 5	45902801	16 27 17.94	−24 28 51.5	6:	
ZZ Her	80000104	16 28 38.52	+41 52 53.9	2.SEa	

Table 6—Continued

Name	TDT	RA (J2000)	Dec (J2000)	Group	Comments
ZZ Her	42401416	16 28 38.58	+41 52 53.7	2.SEa	
ZZ Her	11103947	16 28 38.62	+41 52 53.7	2.SEa	
Off-V853Oph	29201506	16 28 45.27	−24 26 16.7	7	
V853 Oph	29201505	16 28 45.31	−24 28 16.7	7	
$\alpha$ Sco	8200369	16 29 24.42	−26 25 54.1	2.SEc	
Off-ROX42	29501310	16 31 06.65	−24 34 01.2	7	
ROX 42	29501309	16 31 15.46	−24 34 00.6	7	R:
NGC 6153	8402713	16 31 30.88	−40 15 22.4	4.PN	
NGC 6153	45901470	16 31 30.88	−40 15 22.4	4.PN	
IRAS 16279−4757	64402513	16 31 38.30	−48 04 06.4	4.U/SC	
HH 57 IRS	28900125	16 32 32.06	−44 55 28.6	5.SA	
$\tau$ Sco	64701504	16 35 52.90	−28 12 56.4	1.N:	
H Sco	84700107	16 36 22.52	−35 15 19.0	1.NO	
$\zeta$ Oph	62803102	16 37 09.50	−10 34 01.7	1.N:	
$\zeta$ Oph	12200516	16 37 22.00	−10 31 19.0	7	F,W
IRAS 16342−3814	45801328	16 37 39.97	−38 20 14.3	5.F	
IRAS 16350−4754	45901249	16 38 48.10	−48 00 10.0	3.SE	
HD 150193	8200444	16 40 17.91	−23 53 45.2	3.SE	
IRAS 16374−4701	12302539	16 41 07.76	−47 07 32.7	5.UE	
M 13	77602302	16 41 41.39	+36 27 36.9	7	
AX Sco	12101602	16 41 49.69	−27 06 18.3	2.SEa	
NGC 6210	30400331	16 44 29.40	+23 47 48.0	4.PN	
Wray 17-76	29302010	16 44 49.10	−28 04 05.0	4.F	
Wray 17-76	67501241	16 44 49.10	−28 04 05.0	4.F	
Wray 17-76	30600401	16 44 58.20	−28 03 59.0	7	W
Cl* Westerlund 1 BKS C	81400201	16 47 04.10	−45 50 31.5	3.SAe:	
Cl* Westerlund 1 BKS C	29900802	16 47 04.81	−45 50 33.1	3.SAe	
WR 78	45800705	16 52 19.17	−41 51 16.2	1.NE:	
$\zeta$ Sco	28900543	16 53 59.63	−42 21 43.2	1.NMp	
Off-AK Sco	28902102	16 54 44.72	−36 51 17.6	7	
AK Sco	28902101	16 54 44.78	−36 53 17.6	6	
CD−42 11721	28900461	16 59 05.82	−42 42 14.8	5.UE	

Table 6—Continued

Name	TDT	RA (J2000)	Dec (J2000)	Group	Comments
CD–42 11721	64701904	16 59 06.80	–42 42 08.0	5.UE	
CD–42 11721	8402527	16 59 06.82	–42 42 07.6	5.UE	
SS 293	45800441	17 03 09.67	–47 00 27.9	4.CT	
IRAS 17004–4119	28901123	17 03 55.90	–41 24 02.2	4.SA	
IRAS 17010–3840	45901669	17 04 28.30	–38 44 23.0	4.SA	
MWC 247	8402942	17 04 36.23	–33 59 18.9	4.SE:e	
M 2-9	31800537	17 05 37.79	–10 08 32.4	4.SAe	
Hen 3-1333	13602083	17 09 00.90	–56 54 47.2	4.U/SC	
Hen 3-1333	27301339	17 09 00.91	–56 54 48.1	4.U/SC	
C* 2398	46200878	17 09 05.59	–43 46 25.0	2.CE:	
IRAS 17059–4132	13502641	17 09 31.25	–41 35 55.5	5.UE	
Hen 3-1347	46000943	17 10 24.19	–18 49 00.5	4.PN::	
IRAS 17074–4549	87200109	17 11 06.62	–45 52 59.5	5.UEp	
IRAS 17074–4549	13601925	17 11 12.66	–45 52 15.6	7	W
AH Sco	8403013	17 11 17.02	–32 19 30.9	2.SEc	
NGC 6302	9400716	17 13 44.21	–37 06 06.2	5.PNup	
$\alpha$ Her	28101115	17 14 39.20	+14 23 21.8	1.NOp	
V438 Oph	11601203	17 14 39.79	+11 04 10.4	2.SEa	
V438 Oph	81001108	17 14 39.80	+11 04 10.0	2.SEa	
Wray 15-1654	45900849	17 16 21.13	–59 29 23.2	4.PN:	
RAFGL 6815	28902214	17 18 19.80	–32 27 23.0	4.SA	
WR 86	49401315	17 18 23.00	–34 24 30.8	7	R:
Off-NGC6334	64702216	17 19 19.76	–35 03 04.1	7	
IRAS 17160–3707	32400821	17 19 26.10	–37 10 53.8	5.UE	
NGC 6334V	64702301	17 19 57.36	–35 57 52.5	5.F	
NGC 6334A	64801905	17 20 19.29	–35 54 54.9	5.UE	
C* 2429	46200776	17 20 46.20	–40 23 18.1	2.CE	
NGC 6334I	13502736	17 20 53.00	–35 47 02.4	5.SAe	
NGC 6334I	9401025	17 20 53.38	–35 47 01.4	5.SAeu	
H 1-9	9500544	17 21 31.81	–30 20 48.3	4.SEE:	
IRAS 17195–2710	47601204	17 22 43.40	–27 13 37.0	4.SA	
NGC 6357I	32702329	17 24 40.30	–34 10 21.0	5.E	Propn

Table 6—Continued

Name	TDT	RA (J2000)	Dec (J2000)	Group	Comments
IRAS 17221–3619	33100380	17 25 31.67	–36 21 53.5	5.UE	
NGC6357IIIb	32700430	17 25 34.90	–34 22 37.0	5.UE	Propn
H 1-12	14100205	17 26 24.00	–35 01 51.0	5.PN:	
$\sigma$ Oph	10200835	17 26 30.80	+04 08 25.0	1.NO	
H 1-13	48401422	17 28 27.10	–35 07 42.7	4.PN	
NGC 6369	45601901	17 29 20.80	–23 45 32.0	4.PU	
$\beta$ Dra	8001631	17 30 25.99	+52 18 05.0	1.N	
RAFGL 5347	32200877	17 31 17.97	–33 52 49.3	5.UE	
51 Oph	10703103	17 31 24.97	–23 57 45.5	2.SEc::	
IRC +20326	81601210	17 31 54.90	+17 45 20.0	3.CR	
Off- $\lambda$ Sco	49101004	17 33 21.45	–37 06 14.6	7	
$\lambda$ Sco	49101016	17 33 36.46	–37 06 13.5	1.N	
Off- $\lambda$ Sco	49101017	17 33 51.46	–37 06 12.4	7	
CD–49 11554	10300636	17 35 02.41	–49 26 22.3	4.CT	
Nova Oph 1994	45801902	17 35 44.60	–19 19 34.0	6:	
IRAS 17319–6234	13602128	17 36 38.43	–62 35 55.2	4.SA	
TY Dra	74102309	17 36 59.99	+57 44 25.0	2.SEc	
TY Dra	46600803	17 37 00.00	+57 44 25.8	2.SEc	
IRAS 17347–3139	32701619	17 38 00.32	–31 41 01.1	4.Fu	
IRAS 17347–3139	87000939	17 38 00.62	–31 40 54.2	5.UE	
V492 Sco	32702415	17 38 45.58	–34 57 20.0	2.SEb	
AFGL 1992	28700701	17 39 15.50	–30 14 24.0	4.SB	
AFGL 1992	48601302	17 39 15.50	–30 14 24.0	4.SB	
WR 98a	9401206	17 41 12.87	–30 32 29.1	3.W	
IRC –30316	82700405	17 42 35.00	–30 05 39.1	3.SE	
GCM –0.96 +0.13	31301102	17 42 48.27	–29 41 09.1	6	
XX Oph	46000601	17 43 56.43	–06 16 08.0	2.U	
RAFGL 5379	32200779	17 44 22.53	–31 55 43.4	4.SA	
RAFGL 5379	13601695	17 44 23.53	–31 55 44.3	4.SA	
RAFGL 5379	84300128	17 44 23.88	–31 55 39.4	4.SA	
RAFGL 5379	9402123	17 44 25.23	–31 55 39.2	4.SA	
GC Sgr C	84100301	17 44 35.64	–29 27 29.3	5.UE	

Table 6—Continued

Name	TDT	RA (J2000)	Dec (J2000)	Group	Comments
HD 161796	7100579	17 44 55.50	+50 02 39.8	4.SC	
HD 161796	34209765	17 44 55.50	+50 02 39.8	4.SC	
SZ Sgr	86400616	17 44 56.50	−18 39 27.0	2.CE	
IRAS 17418−2713	13600731	17 44 59.23	−27 14 40.4	4.F:	
IRAS 17418−2713	85000523	17 45 06.70	−27 14 39.0	7	W
Hen 3-1475	48700267	17 45 14.10	−17 56 46.9	5.F:	
GC Ring SW	9401905	17 45 38.60	−29 01 05.7	5.UE	Propn
GC SgrA*	13600935	17 45 39.97	−29 00 22.6	5.SAe	
GC SgrA*	9401801	17 45 40.00	−29 00 28.6	5.SAe	
GC Ring NE	9500203	17 45 41.80	−28 59 50.5	5.UE	Propn
MWC 270	46900969	17 45 57.71	−30 12 00.4	4.SEC:e	
GCM +0.24 +0.02	32601124	17 46 07.94	−28 43 21.5	5.E	
GC SSW	46301403	17 46 11.03	−28 54 36.3	5.UE	Propn
GC G0.18−2	67700503	17 46 14.16	−28 47 47.1	5.UE	Propn
GCS 3 I	28701246	17 46 14.80	−28 49 34.0	5.SAe	
GC Pistol Star	84101302	17 46 15.21	−28 50 04.0	5.E	
GCS 4	29702147	17 46 15.71	−28 49 47.0	5.SAe	
Off-GC	46300902	17 46 25.52	−28 54 06.3	5.UE	
GC SSE	49800804	17 46 31.36	−28 55 48.8	5.UE	Propn
GC SE_NTF_Xng	46300901	17 46 43.79	−28 52 53.9	5.E	Propn
RAFGL 5385	33102402	17 47 13.20	−24 12 47.5	4.CT:	
IRAS 17443−2949	13601533	17 47 35.29	−29 51 02.2	4.SA	
GCM +0.76 −0.05	31301509	17 47 36.84	−28 18 31.0	6:	
Hb 5	49400104	17 47 56.02	−29 59 39.3	4.PU	
HD 316285	30101147	17 48 14.00	−28 00 53.0	2.E	
GC Sgr D	28701327	17 48 41.52	−28 01 38.3	5.UE	
NGC 6445	48700507	17 49 14.41	−20 00 23.5	6	
H 1-36	32400609	17 49 48.20	−37 01 27.0	4.SEE	
RS Oph	31101275	17 50 13.20	−06 42 28.5	7	R:
M 3-44	9500646	17 51 18.88	−30 23 54.0	4.SC:	
V4334 Sgr	51501501	17 52 32.70	−17 41 08.0	6:	
AFGL 2019	84900929	17 53 18.80	−26 56 37.0	3.SB	

Table 6—Continued

Name	TDT	RA (J2000)	Dec (J2000)	Group	Comments
$\xi$ Dra	31404910	17 53 31.66	+56 52 21.3	1.NO:	
$\xi$ Dra	6800697	17 53 31.67	+56 52 21.3	1.NO:	
Nova Sco 1997	64701801	17 54 11.20	−30 02 53.3	7	
Nova Sco 1997	67700102	17 54 11.21	−30 02 53.3	6	
IRAS 17516−2525	46401343	17 54 43.49	−25 26 29.8	4.SAp	
89 Her	8202007	17 55 25.20	+26 02 58.1	3.SEp	
89 Her	51800719	17 55 25.20	+26 03 00.0	3.SEp	
H 1-40	9500348	17 55 36.06	−30 33 32.3	4.SE:e	
MWC 275	32901191	17 56 21.35	−21 57 19.5	4.SEu:	
T Dra	54600104	17 56 23.27	+58 13 06.1	2.CE	
T Dra	43700103	17 56 23.27	+58 13 06.6	2.CE	
T Dra	38303014	17 56 23.29	+58 13 05.6	2.CE	
T Dra	11101727	17 56 23.29	+58 13 06.4	2.CE	
T Dra	24800101	17 56 23.30	+58 13 06.4	2.CE	
T Dra	34601702	17 56 23.30	+58 13 06.4	2.CE	
T Dra	42902712	17 56 23.30	+58 13 06.4	2.CE	
T Dra	64500205	17 56 23.30	+58 13 06.4	2.CE	
$\gamma$ Dra −0.60, +0.0	12601519	17 56 35.81	+51 29 20.3	1.NO	Offset
$\gamma$ Dra −0.30, +0.0	12601418	17 56 36.11	+51 29 20.3	1.NO	Offset
$\gamma$ Dra	81100302	17 56 36.40	+51 29 20.2	1.NO	
$\gamma$ Dra	2402105	17 56 36.40	+51 29 20.3	1.NO	
$\gamma$ Dra	37704637	17 56 36.40	+51 29 20.3	1.NO	
$\gamma$ Dra	49603004	17 56 36.40	+51 29 20.3	1.NO	
$\gamma$ Dra +0.00, −3.0	12601721	17 56 36.41	+51 29 17.3	1.NO	Offset
$\gamma$ Dra	2401579	17 56 36.41	+51 29 20.3	1.NO	(0,0)
$\gamma$ Dra	4002405	17 56 36.41	+51 29 20.3	1.NO	
$\gamma$ Dra	12601315	17 56 36.41	+51 29 20.3	1.NO	
$\gamma$ Dra +0.00, +3.0	12601620	17 56 36.41	+51 29 23.3	1.NO	Offset
$\gamma$ Dra +0.30, +0.0	12601216	17 56 36.71	+51 29 20.3	1.NO	Offset
RAFGL 5416	12102004	17 56 36.90	−30 30 47.0	4.CR	
$\gamma$ Dra +0.60, +0.0	12601117	17 56 37.01	+51 29 20.3	1.NO	Offset
OP Her	77800625	17 56 48.60	+45 21 03.1	1.NO	



Table 6—Continued

Name	TDT	RA (J2000)	Dec (J2000)	Group	Comments
AU Her	45401501	17 57 19.50	+29 46 32.0	2.SEc	
GJ 699	33200302	17 57 48.67	+04 41 02.8	1.NMp	?
AI Sco	31801403	17 58 11.38	−33 49 12.1	7	W
NGC 6543	2400910	17 58 33.39	+66 37 59.5	4.PN	
NGC 6543	2400714	17 58 33.40	+66 37 59.5	4.PN	
NGC 6543	2400807	17 58 33.40	+66 37 59.5	4.PN	
NGC 6543	2800908	17 58 33.40	+66 37 59.5	4.PN	
NGC 6543	3201202	17 58 33.40	+66 37 59.5	4.PN	
W28 A2	9901027	18 00 30.37	−24 04 02.5	5.F	
W28 A2	12500843	18 00 32.07	−24 04 03.4	5.UE	
WR 104	9901207	18 02 04.06	−23 37 41.6	3.W	
IRAS 17591−2228	51500580	18 02 13.15	−22 27 59.3	5.UE	
HH 399 +0.00, +20.0	49301902	18 02 28.70	−23 03 31.8	6u:	Offset
HH 399	47700503	18 02 28.70	−23 03 51.8	5.UE:	(0,0)
HH 399 +0.00, −20.0	49302109	18 02 28.70	−23 04 11.8	5.UE:	Offset
M 8 E	47700328	18 04 52.70	−24 26 36.4	5.SA	
NGC 6537	70300475	18 05 13.14	−19 50 34.5	5.PNup	
NGC 6537	47000722	18 05 13.33	−19 50 13.6	5.PN:	
IRAS 18032−2032	51500478	18 06 13.93	−20 31 43.7	5.UE	
WR 110	49300513	18 07 56.70	−19 23 58.0	7	R:
VX Sgr	9900171	18 08 04.00	−22 13 26.8	3.SE	
IRAS 18062+2410	46000275	18 08 20.15	+24 10 43.9	4.SE:	
AX Sgr	51502010	18 08 26.44	−18 33 08.8	2.SEc	F
SGR1806−20	49301104	18 08 40.28	−20 24 41.1	6:	Propn
HD 165774	14100603	18 09 17.20	−36 57 58.0	1.NO:	
M 1-42	70302306	18 11 04.60	−28 59 00.5	6	
IRAS 18095+2704	31101819	18 11 30.60	+27 05 16.0	4.SEC	
NGC 6572	31901125	18 12 07.41	+06 51 24.7	4.PN	
IRAS 18110−1854	14801636	18 14 00.86	−18 53 20.2	5.UE	
AS 296	47201603	18 14 06.40	−00 18 59.0	7	W
V4046 Sgr	47101803	18 14 10.42	−32 47 32.2	6	
Off-V4046Sgr	47101804	18 14 10.47	−32 49 32.2	7e:	

Table 6—Continued

Name	TDT	RA (J2000)	Dec (J2000)	Group	Comments
AFGL 2094	14801733	18 14 35.22	−16 45 20.6	5.UE	
W 33A	32900920	18 14 39.44	−17 52 01.4	5.SA	
IRAS 18123+0511	83401008	18 14 49.40	+05 12 56.0	6	
IRAS 18119−1342	70301713	18 14 50.30	−13 41 05.6	1.NO:	
MWC 288	47101511	18 16 12.20	−30 52 07.0	4.SEue	
WR 112	10201908	18 16 33.47	−18 58 41.1	3.W	
OH 12.8−0.9	33101801	18 16 49.10	−18 15 02.0	5.SA	
CN 3-1	47202064	18 17 34.00	+10 09 03.4	4.PN:	
M 2-36	70302403	18 17 41.80	−29 08 19.6	6	
M 16	87700401	18 18 56.60	−13 48 52.5	7	
Off-M16	87700502	18 18 59.90	−13 49 47.6	7	F
HH 80	32901351	18 19 06.03	−20 51 49.1	7	
HH 81	32901361	18 19 06.61	−20 51 06.0	6	
GGD 27 IRS	14900323	18 19 12.03	−20 47 30.6	5.U	
GGD 27 IRS	14802136	18 19 12.04	−20 47 31.0	5.U	
HH 80N	32901364	18 19 19.70	−20 41 35.1	6	
M 17 −8.32, −1 46.8	10201820	18 20 16.51	−16 13 21.7	5.U	Offset <sup>a</sup>
M 17 −6.92, −1 36.7	9901419	18 20 17.91	−16 13 11.6	5.UE	Offset
M 17 −5.52, −1 26.6	9900218	18 20 19.31	−16 13 01.5	5.UE	Offset
M 17 −4.13, −1 16.5	9901417	18 20 20.70	−16 12 51.4	5.UE	Offset
M 17 −2.73, −1 6.4	9900216	18 20 22.10	−16 12 41.3	5.UE	Offset
M 17 −2.73, −1 6.4	32900866	18 20 22.10	−16 12 41.3	5.UE	Offset
M 17 −1.43, −56.3	9901415	18 20 23.40	−16 12 31.2	5.UE	Offset
M 17 −0.04, −46.2	9900214	18 20 24.79	−16 12 21.1	5.UE	Offset
M 17 +1.36, −36.1	9901413	18 20 26.19	−16 12 11.0	5.E	Offset
M 17 +2.75, −26.0	9900212	18 20 27.58	−16 12 00.9	5.E	Offset
M 17 +4.15, −15.9	10201811	18 20 28.98	−16 11 50.8	5.UE	Offset
M 17 +7.94, +9 52.4	9901105	18 20 32.77	−16 01 42.5	5.UE	Offset
Off-M17	9901106	18 20 46.91	−16 03 45.5	5.UE	
χ Dra	56300507	18 21 03.09	+72 43 59.2	1.N:	
MWC 922	70301807	18 21 16.00	−13 01 30.0	4.U/SC	
MWC 922	15301566	18 21 16.14	−13 01 23.3	4.U/SC	

Table 6—Continued

Name	TDT	RA (J2000)	Dec (J2000)	Group	Comments
Nova Sgr 1998	87901801	18 21 40.50	−27 31 38.0	7	
QSO 1821+643	17801806	18 21 57.23	+64 20 36.3	7	G
QSO 1821+643	63501206	18 21 57.23	+64 20 36.3	7	G
AFGL 2136 IRS 1	33000222	18 22 26.22	−13 30 08.3	5.SA	
Nova Sgr 1996	47700201	18 23 42.50	−18 07 15.0	6	
Nova Sgr 1996	51301208	18 23 42.50	−18 07 15.0	6	
ε Sgr	13601739	18 24 10.30	−34 23 05.0	1.NM:	
HD 169142	13601359	18 24 29.87	−29 46 50.3	4.Mu:	
DO 16793	47100261	18 26 05.69	+23 28 46.3	3.CR	
M 2-43	14900804	18 26 40.00	−02 42 57.0	4.PU:	
M 2-43	13401911	18 26 40.00	−02 47 57.0	7	W
MWC 297	70800234	18 27 39.49	−03 49 52.1	5.SA	
OH 21.5+0.5	87200833	18 28 30.90	−09 58 16.0	4.SA	
Cn 1-5	47101650	18 29 11.60	−31 29 59.7	6	
LDN 379 IRS 3	48300731	18 29 24.74	−15 15 48.9	5.E:	
MWC 300	51601005	18 29 25.70	−06 04 37.4	4.SB	
OO Ser	14901407	18 29 49.07	+01 16 19.5	5.SA	
OO Ser	29000211	18 29 49.07	+01 16 19.5	5.SA	
OO Ser	34300317	18 29 49.07	+01 16 19.5	5.SA	
OO Ser	47800222	18 29 49.07	+01 16 19.5	5.SA	
OO Ser	51301128	18 29 49.07	+01 16 19.5	5.SA	
OO Ser	67601733	18 29 49.07	+01 16 19.5	5.SA	
AC Her	10600409	18 30 16.05	+21 51 59.1	4.SEC	
AC Her	52000423	18 30 16.20	+21 52 00.4	4.SEC	
AC Her	10600514	18 30 16.30	+21 52 00.0	4.SEC	
OH 17.7−2.0	51601520	18 30 30.67	−14 28 57.0	4.SA	
OH 17.7−2.0	10802940	18 30 30.67	−14 28 57.1	4.F	
WR 118	10802509	18 31 42.21	−09 59 14.8	3.W	
IRAS 18292−1153	34101206	18 32 04.20	−11 51 25.3	6:	
RAFGL 5502	11401742	18 33 30.36	−05 01 06.7	5.SAu	
RAFGL 7009	15201140	18 34 20.59	−05 59 45.2	5.SA	
RAFGL 7009	47801137	18 34 20.89	−05 59 42.4	5.SA	

Table 6—Continued

Name	TDT	RA (J2000)	Dec (J2000)	Group	Comments
IRAS 18317–0757	47801040	18 34 24.94	–07 54 47.9	5.UE	
AFGL 2199	71200120	18 35 46.80	+05 35 47.0	3.SB	
PK 010–08 1	48300913	18 36 22.80	–23 55 19.3	5.M:	
RT Pav	52300444	18 36 29.70	–69 53 06.0	2.SEb	
$\alpha$ Lyr	17800501	18 36 56.24	+38 47 00.2	1.N	
$\alpha$ Lyr	10601001	18 36 56.66	+38 47 00.1	1.N	F
CZ Ser	83701639	18 37 21.00	–02 39 36.0	6	
OH 26.5+0.6	33000525	18 37 32.49	–05 23 59.3	4.SA	
X Oph	47201847	18 38 21.10	+08 50 02.3	2.SEa	
LOS2	51600816	18 39 15.84	–05 42 40.9	6u:	Propn
LOS2	51600915	18 39 15.84	–05 42 40.9	6u:	Propn
V348 Sgr	48301104	18 40 19.80	–22 54 29.0	3.W:	
V348 Sgr	48301110	18 40 19.80	–22 54 29.0	3.W:	
Off-V348 Sgr	48301114	18 40 19.80	–22 59 29.0	7	
OH 26.2–0.6	86901013	18 41 13.80	–06 15 01.0	4.SA	
IRC +20370	83801219	18 41 53.90	+17 40 33.0	7	W
FI Lyr	82700735	18 42 04.80	+28 57 29.0	2.SEa	
IRC +00365	49901342	18 42 24.68	–02 17 25.2	3.CE	
HR 7023	71101311	18 42 55.10	–19 17 02.9	1.NO	
IRC +10374	87201107	18 43 34.50	+13 57 35.0	7	W
WR 121	13402006	18 44 12.12	–03 47 57.6	7	R:
IRAS 18416–0421	13402168	18 44 15.19	–04 17 56.4	5.UE	
IRAS 18430–0237	30802201	18 45 39.69	–02 34 32.3	2.CE::	
AFGL 2245	15201383	18 46 04.00	–02 39 20.5	5.UE	
IRAS 18441–0134	30801220	18 46 44.29	–01 30 54.6	5.UE	
LOS1_T	52302017	18 46 48.03	–01 32 55.6	6u:	Propn
LOS1_T	52700822	18 46 48.03	–01 32 55.6	6u:	Propn
R Sct	11402015	18 47 29.01	–05 42 19.0	2.SEa:	
RAFGL 5535	30801670	18 48 41.90	–02 50 28.2	4.SA	
AFGL 2256	48300563	18 49 10.35	–06 53 03.4	4.CR	
IRAS 18469–0132	71100888	18 49 32.96	–01 29 03.6	5.UE	
HU 2-1	13400705	18 49 47.60	+20 50 39.3	4.PN	

Table 6—Continued

Name	TDT	RA (J2000)	Dec (J2000)	Group	Comments
S Sct	16401849	18 50 19.93	−07 54 26.4	2.CE	
RAFGL 5536	15201791	18 50 30.80	−00 01 59.4	5.UE	
OH 32.0−0.5	85700231	18 51 26.80	−01 03 49.0	6:	
OH 32.8−0.3	32001560	18 52 22.23	−00 14 10.4	4.SA	
IRAS 18502+0051	15201645	18 52 50.21	+00 55 27.6	5.UE	
NGC 6720	36600207	18 53 35.68	+33 01 40.3	6	
$\delta^2$ Lyr	10200126	18 54 30.25	+36 53 55.1	1.NO	
$\sigma$ Sgr	49700213	18 55 15.79	−26 17 48.1	1.N	
Off- $\sigma$ Sgr	49700214	18 55 15.86	−26 20 48.6	7	
R Lyr	53000214	18 55 19.91	+43 56 41.8	1.NO	
GJ 735	12000774	18 55 27.05	+08 24 12.3	7	R:
BD+00 4054	85700137	18 55 46.60	+00 20 41.0	6:	
PK 039+02 1	49900640	18 56 18.05	+07 07 25.6	4.PU	
OH 35.6−0.3	85700314	18 57 27.30	+02 11 45.0	6:	
AFGL 2287	85600104	18 57 36.50	+03 27 24.0	3.SBp	
EIC 722	47801654	18 58 03.90	+08 15 28.0	3.SE	
OH 39.7+1.5	70900322	18 58 30.30	+06 42 25.9	4.SB	
AFGL 2298	32401203	19 00 10.50	+03 45 48.0	4.PUp:	
TY CrA	34801419	19 01 40.70	−36 52 32.6	5.U	
TY CrA	33400603	19 01 40.71	−36 52 32.5	5.U	
TY CrA	71502003	19 01 40.71	−36 52 32.5	5.U	
R CrA IRS 2	52301201	19 01 41.50	−36 58 28.5	4.F:	
R CrA IRS 1	52301106	19 01 50.70	−36 58 09.9	5.SA	
R CrA	14100458	19 01 53.93	−36 57 09.7	4.SECe	
R CrA	70400558	19 01 53.93	−36 57 09.7	4.SECe	
R CrA	49501016	19 01 55.82	−36 57 01.6	5.F:	W:
T CrA	33402096	19 01 58.84	−36 57 49.4	4.SE:	F
T CrA	68900196	19 01 58.84	−36 57 49.4	5.SE	
OH 37.1−0.8	32301106	19 02 06.20	+03 20 16.0	5.SA:	
OH 37.1−0.8	49901206	19 02 06.20	+03 20 16.0	5.SA:	
NGC 6741	13401806	19 02 37.10	−00 26 58.6	4.PN	
Case 181	87201221	19 03 18.10	+07 30 44.0	3.CE	

Table 6—Continued

Name	TDT	RA (J2000)	Dec (J2000)	Group	Comments
V Aql	16402151	19 04 24.07	−05 41 05.7	2.CE	
Off-NovaAql1995	35000607	19 05 26.60	−01 27 30.0	7	
Nova Aql 1995	52600105	19 05 26.60	−01 42 03.3	6	
Nova Aql 1995	30401501	19 05 26.60	−01 42 03.5	6	
Nova Aql 1995	35000606	19 05 26.60	−01 42 03.5	6	
Nova Aql 1995	48000202	19 05 26.60	−01 42 03.5	6	
Nova Aql 1995	48002314	19 05 26.60	−01 42 03.5	6	
R Aql	12200329	19 06 22.19	+08 13 47.3	2.SEb	
R Aql	53400105	19 06 22.19	+08 13 47.3	2.SEb	
R Aql	47801417	19 06 22.20	+08 13 47.2	2.SEb	
R Aql	67600406	19 06 22.20	+08 13 47.2	2.SEb	
R Aql	32000318	19 06 22.21	+08 13 47.3	2.SEb	
Sgr 1900+14	48903903	19 07 15.20	+09 19 21.3	7	R:
U Tel	52300905	19 08 01.81	−48 54 14.0	2.SEc	
IRAS 19068+0544	47901374	19 09 15.40	+05 49 06.0	3.CE	
U Dra	40001013	19 09 58.30	+67 16 37.0	7	
U Dra	52404014	19 09 58.30	+67 16 37.0	2.M	
U Dra	69500515	19 09 58.30	+67 16 37.0	7	
NGC 6765	73600222	19 11 06.50	+30 32 45.0	6	
MWC 614	32301321	19 11 11.16	+15 47 16.6	4.SECu	
WR 124	72500754	19 11 31.10	+16 51 32.0	6	
$\delta$ Dra	7201132	19 12 33.09	+67 39 41.2	1.N	
$\delta$ Dra	20601232	19 12 33.24	+67 39 41.3	1.N	
S Lyr	52000546	19 13 11.39	+26 00 25.4	2.CE:	
IRAS 19110+1045	49900902	19 13 22.00	+10 50 53.4	5.SA	
HD 179821	11301444	19 13 58.53	+00 07 31.6	4.SC	
HD 179821	52000234	19 13 58.60	+00 07 31.8	4.SC	
IRAS 19120+1103	33701512	19 14 21.70	+11 09 13.6	5.UE	
Granat 1915+105	11301301	19 15 11.52	+10 56 44.9	7	F
Granat 1915+105	47901101	19 15 11.52	+10 56 44.9	6:	
W Aql	16402335	19 15 23.21	−07 02 49.8	3.SEp	
Off-RYSgr	49500513	19 16 08.90	−33 31 20.4	7	

Table 6—Continued

Name	TDT	RA (J2000)	Dec (J2000)	Group	Comments
RY Sgr	49500503	19 16 32.80	−33 31 20.4	3.W	
$\kappa$ Cyg	8001522	19 17 06.22	+53 22 06.0	1.N	
Nova Aql 1919	32002409	19 18 20.50	+01 46 59.4	4.SA	
NGC 6781	47901509	19 18 28.05	+06 32 18.5	6	
HR 7341	6001362	19 18 37.79	+49 34 09.6	7	R
AFGL 2374	35001427	19 21 36.32	+09 27 51.5	3.SB:	
T Sge	73201510	19 21 42.00	+17 40 00.0	2.SEa	
T Sge	12000604	19 21 42.00	+17 40 00.2	2.SEa	
IRAS 19195+1650	52600503	19 21 50.00	+16 56 16.0	4.F:	
NGC 6790	13401107	19 22 57.00	+01 30 46.5	4.SE:e	
IRAS 19207+1410	15001041	19 23 02.45	+14 16 40.6	5.UE	
W 51 IRS2	12801416	19 23 39.90	+14 31 06.1	5.UE	
Vy 2-2	32002528	19 24 21.88	+09 53 54.8	4.SECe	
CH Cyg	54101201	19 24 33.00	+50 14 29.0	2.SEc	
CH Cyg	38301404	19 24 33.10	+50 14 29.6	2.SEc	
WW Vul	17600305	19 25 59.00	+21 12 30.0	4.SE::	
IRC +10420	12801311	19 26 47.99	+11 21 16.8	4.SEC	
AFGL 2392	85800120	19 27 14.40	+07 04 10.0	2.CE	
PK 56+2.1	17600529	19 27 44.00	+21 30 03.4	5.M:	
AFGL 2403	32000603	19 30 29.50	+19 50 42.0	4.SA	
AFGL 2403	50200604	19 30 29.50	+19 50 42.0	4.SA	
$\sigma$ Dra	8000345	19 32 21.33	+69 39 46.8	1.N:	
IRAS 19306+1407	52501428	19 32 55.00	+14 13 40.0	4.SC	
M 1-91	73600323	19 32 57.60	+26 52 44.0	4.SA::	
V1965 Cyg	52601240	19 34 13.09	+28 03 36.5	7	W
BD+30 3639	35501531	19 34 45.17	+30 30 58.7	4.PU	
BD+30 3639	86500540	19 34 45.20	+30 30 58.8	4.PU	
M 1-92	36701903	19 36 18.86	+29 32 50.0	5.SA	
R Cyg	42201625	19 36 49.33	+50 12 00.2	2.SEb	
HH 119A	17800870	19 36 51.47	+07 34 10.2	6	
HH 119B	17800872	19 36 57.17	+07 34 06.6	6	
HH 119C	17800876	19 37 04.77	+07 34 07.1	6:	

Table 6—Continued

Name	TDT	RA (J2000)	Dec (J2000)	Group	Comments
HR 7475	31601515	19 39 25.31	+16 34 15.8	1.NO	
TT Cyg	56100935	19 40 56.96	+32 37 05.9	1.NC	
TT Cyg	73600518	19 40 57.00	+32 37 06.0	1.NC	
IRAS 19386+0155	53400617	19 41 08.30	+02 02 31.0	4.SB	
HM Sge	54700107	19 41 57.06	+16 44 40.0	3.SEe	
HM Sge	31901701	19 41 57.10	+16 44 39.8	3.SEe	
HR 7509	74005215	19 42 04.10	+55 27 47.0	1.NO	
NGC 6826	30201114	19 44 48.18	+50 31 30.9	4.PN	
NGC 6826	27200786	19 44 48.20	+50 31 30.0	4.PN	
S87 IRS1	15000444	19 46 20.09	+24 35 29.4	5.UE	
S87 IRS1	19200933	19 46 20.09	+24 35 29.4	5.UE	
IRAS 19477+2401	52601347	19 47 24.25	+29 28 11.8	4.CN	
ER Cyg	38405519	19 49 13.90	+30 24 17.0	7	W
HD 331319	36100905	19 49 29.44	+31 27 14.0	4.SC	
HD 331319	52000931	19 49 29.60	+31 27 17.3	4.SC	
IRAS 19477+2401	18101405	19 49 54.40	+24 08 48.0	4.F:	
GY Aql	34401040	19 50 07.00	−07 36 54.0	2.SEc	
IRAS 19480+2504	38300108	19 50 07.96	+25 11 55.2	4.F	
NR Vul	53701751	19 50 11.50	+24 55 20.0	2.SEc	
$\chi$ Cyg	15900437	19 50 33.92	+32 54 51.3	2.SEb	
$\alpha$ Aql	18100805	19 50 46.85	+08 52 04.3	1.N	
$\alpha$ Aql	12801105	19 50 47.16	+08 52 04.5	1.N	F
NS Vul	32301516	19 52 29.99	+22 27 14.3	2.SEb	
HD 187885	14400346	19 52 52.59	−17 01 49.6	4.CT	
S Pav	14401702	19 55 13.90	−59 11 44.2	2.SEa	
AFGL 2477	52601705	19 56 47.86	+30 43 58.2	4.CR	
AFGL 2477	56100849	19 56 48.26	+30 43 59.2	4.CR	
V1016 Cyg	35500977	19 57 05.00	+39 49 36.1	3.SEe	
V1016 Cyg	55102706	19 57 05.00	+39 49 36.1	3.SEe	
V1016 Cyg	74601883	19 57 05.00	+39 49 36.1	3.SEe	
RR Aql	53400809	19 57 36.00	−01 53 10.4	2.SEc	
IRAS 19584+2652	52600868	20 00 31.00	+27 00 37.0	3.SBp	



Table 6—Continued

Name	TDT	RA (J2000)	Dec (J2000)	Group	Comments
HD 189711	52600445	20 01 03.79	+09 30 51.9	1.NM::	
AFGL 2494	12702002	20 01 08.50	+30 55 40.0	7	W
Z Cyg	49100106	20 01 27.51	+50 02 31.2	2.SEc	
Z Cyg	26300316	20 01 27.56	+50 02 31.0	2.SEc	
Z Cyg	32601321	20 01 27.56	+50 02 31.0	2.SEc	
Z Cyg	37400126	20 01 27.56	+50 02 31.0	2.SEc	
Z Cyg	43402401	20 01 27.56	+50 02 31.0	2.SEc	
Z Cyg	54600211	20 01 27.56	+50 02 31.0	2.SEc	
Z Cyg	63103501	20 01 27.56	+50 02 31.0	2.SEc	F
NU Pav	12103028	20 01 44.70	−59 22 33.5	1.NO	
K 3-50	14601350	20 01 45.54	+33 32 43.6	5.SAeu	
K 3-50	38402466	20 01 45.70	+33 32 43.3	5.SAeu	
BD−13 5550	33601901	20 01 49.80	−12 41 15.0	4.PN:	
IRAS 20000+3239	18500531	20 01 59.50	+32 47 33.0	4.CT	
V1027 Cyg	52601618	20 02 27.30	+30 04 25.0	2.SEc	
RR Tel	12402160	20 04 18.50	−55 43 33.6	3.SEe	
RR Tel	73402079	20 04 18.50	−55 43 33.6	3.SEe	
RR Tel	54601206	20 04 18.60	−55 43 33.2	3.SEe	
M 3-60	35801319	20 04 22.45	+33 38 59.0	5.UE:	
AA Cyg	36401817	20 04 27.60	+36 48 59.0	2.M	
IRAS20028+3910	13001348	20 04 34.91	+39 18 38.0	4.F:	
AFGL 4259	73600404	20 06 22.89	+27 02 11.2	4.SA	
V1943 Sgr	85700514	20 06 55.20	−27 13 29.0	2.SEa	
IRAS 20050+2720 −6.82, +39.5	38405815	20 06 59.87	+27 29 32.5	6	Offset
IRAS 20050+2720	32301613	20 07 06.69	+27 28 53.0	5.SA	(0,0)
IRAS 20050+2720 +5.21, +0.3	32301718	20 07 11.90	+27 28 53.3	6	Offset
V2234 Sgr	12501616	20 07 40.20	−42 31 34.5	7	W, F
V2234 Sgr	33402216	20 07 40.20	−42 31 34.5	7	W
δ Pav	29902110	20 08 42.94	−66 10 51.8	1.N	
δ Pav	10100310	20 08 43.91	−66 10 51.2	7	F
Off-LOS1	34501821	20 09 48.12	−02 21 07.0	7	
Off-WR134	17601109	20 10 06.20	+36 10 35.7	7	

Table 6—Continued

Name	TDT	RA (J2000)	Dec (J2000)	Group	Comments
WR 134	17601108	20 10 14.20	+36 10 35.7	7	R:
NGC 6884	13901709	20 10 23.70	+46 27 39.4	5.PN:	
IRC −10529	34400878	20 10 26.00	−06 15 46.8	7	W
IRC −10529	17000529	20 10 26.31	−06 16 12.8	4.CR:	W
V584 Aql	73200811	20 10 29.70	−01 37 39.9	2.SEb	
V584 Aql	54200304	20 10 29.70	−01 37 40.2	2.SEb	
R Cap	53701377	20 11 18.80	−14 16 01.9	7	R:
X Pav	14401801	20 11 45.91	−59 56 13.0	2.SEb	
WR 135	36100510	20 11 53.51	+36 11 50.9	7	R:
FG Sge	18101101	20 11 56.08	+20 20 04.1	3.W:	
Off-FGSge	18101102	20 11 56.08	+20 25 03.3	7	
WR 136	38102211	20 12 06.50	+38 21 18.2	1.NE:	
WR 136	38101711	20 12 06.51	+38 21 16.9	1.NE:	
Off-WR136	38101712	20 12 12.21	+38 19 52.0	7e:	
NGC 6886	13400810	20 12 42.80	+19 59 23.0	4.PN:	
Hen 2-459	15101105	20 13 57.80	+29 33 56.0	4.Fe	
R Sge	17600204	20 14 03.71	+16 43 35.2	4.SE::	
IRAS 20126+4104	35500738	20 14 25.97	+41 13 31.6	5.F	
HR 7736	38101302	20 14 31.68	+36 48 22.8	1.N:	
HR 7736	38101406	20 14 31.68	+36 48 22.8	1.N:	
WR 137	35501212	20 14 31.72	+36 39 39.8	7	R:
NGC 6891	37600943	20 15 09.30	+12 42 07.0	4.PN:	
HR 7722	34301309	20 15 17.10	−27 01 58.4	1.N:	
RZ Sgr	14100818	20 15 28.30	−44 24 38.0	2.SEa	
P Cyg	33504020	20 17 47.20	+38 01 58.2	2.E	
P Cyg	3201129	20 17 47.20	+38 01 58.3	2.E	
IC 4997	31901334	20 20 08.70	+16 43 53.3	4.SE:e	
WR 140	35200913	20 20 27.92	+43 51 16.4	1.NE:	
BD+40 4124	35500693	20 20 28.31	+41 21 51.4	5.U	
Lk H $\alpha$ 224	85800502	20 20 29.20	+41 21 27.0	5.F	
Lk H $\alpha$ 225	85800403	20 20 30.40	+41 21 27.0	5.SAe	
$\beta$ Cap	14400108	20 21 00.61	−14 46 53.3	1.N	

Table 6—Continued

Name	TDT	RA (J2000)	Dec (J2000)	Group	Comments
Off-BD+354077	52601908	20 21 12.15	+35 37 10.8	7	
PU Vul	33601674	20 21 13.30	+21 34 18.0	7	W
BD+35 4077	73000622	20 21 14.10	+35 37 16.5	2.SEb	
MWC 1014	13900707	20 21 15.04	+37 24 11.0	7	W
BI Cyg	38101617	20 21 21.75	+36 55 55.4	2.SEc	
BC Cyg	35201201	20 21 38.49	+37 31 58.4	2.SEc <sub>p</sub>	
Off- $\alpha$ Pav	33300703	20 25 38.60	−56 41 06.0	7	
$\alpha$ Pav	33300707	20 25 38.77	−56 44 06.0	1.N	
Off- $\alpha$ Pav	33300708	20 25 38.92	−56 47 06.0	7	
KY Cyg	12700917	20 25 57.30	+38 21 10.6	3.SE	
S106 IRS4	33504295	20 27 26.68	+37 22 47.9	5.UE	
T Mic	14401129	20 27 55.20	−28 15 39.9	2.SEa	
T Mic	87201305	20 27 55.20	−28 15 40.0	2.SEa	
RW Cyg	12701432	20 28 50.60	+39 58 54.0	2.SEc	
OH 75.3−1.8	74500903	20 29 07.93	+35 45 38.8	4.SC:	
AFGL 2591	35700734	20 29 24.65	+40 11 19.1	5.SA	
AFGL 2591	2800433	20 29 24.66	+40 11 18.9	5.SA	
Nova Cyg 1992	34601878	20 30 31.70	+52 37 50.8	6	
HR 7847	14302717	20 30 59.00	+36 56 09.3	1.N:	
CD−33 14985	71901011	20 31 21.08	−32 59 57.6	7	
IRC +40427	53000406	20 31 28.64	+40 38 43.1	2.SEap:	
Cyg OB2 No. 12	33504130	20 32 40.97	+41 14 28.3	1.NMp	
Cyg OB2 No. 12	3602226	20 32 41.00	+41 14 29.3	1.NMp	F
Cyg OB2 No. 12	13901048	20 32 41.07	+41 14 29.8	1.NMp	
MWC 349	18500704	20 32 45.52	+40 39 36.5	3.SAe	
Cyg OB2 No. 9	13901508	20 33 10.73	+41 15 09.0	1.NM:	
V778 Cyg	53200677	20 36 07.24	+60 05 26.3	2.C/SE	
V778 Cyg	4001456	20 36 10.60	+60 05 20.0	7	W
Off-V778Cyg	33900541	20 36 10.67	+60 05 20.5	7	
WR 147	33800415	20 36 43.51	+40 21 08.1	2.E	
DR21 −1 6.17, −31.7	53001684	20 37 54.76	+42 19 10.2	6u:	Offset
DR 21	15200555	20 39 00.93	+42 19 41.9	5.UE	(0,0)

Table 6—Continued

Name	TDT	RA (J2000)	Dec (J2000)	Group	Comments
L1157 −3.77, +2 19.8	28801224	20 39 02.68	+68 04 33.3	7	Offset
L1157	28200221	20 39 06.45	+68 02 13.5	7	(0,0)
DR21 +7.82, +11.5	52201283	20 39 08.75	+42 19 53.4	5.UE	Offset
L1157 +3.64, −59.8	28200427	20 39 10.09	+68 01 13.7	6	Offset
CIT 11	40503119	20 39 36.31	+39 12 08.8	2.SEb	
V Cyg	42100111	20 41 18.20	+48 08 29.0	2.CE	
V Cyg	42300307	20 41 18.20	+48 08 29.0	2.CE	
V Cyg	51401308	20 41 18.20	+48 08 29.0	2.CE	
V Cyg	59501909	20 41 18.20	+48 08 29.0	2.CE	
V Cyg	69500110	20 41 18.22	+48 08 28.8	2.CE	
V Cyg	8001855	20 41 18.28	+48 08 28.9	2.CE	
α Cyg	8002002	20 41 25.81	+45 16 49.3	1.N	
HR Del	37401373	20 42 20.30	+19 09 39.3	6:	
IRAS 20406+2953	18500307	20 42 45.80	+30 04 13.0	4.SA	
Mrk 509	17001027	20 44 09.70	−10 43 24.6	7	G
AU Mic	13501003	20 45 09.50	−31 20 26.3	7	R
PV Cep	14302273	20 45 54.01	+67 57 36.0	5.SA:	
ψ Cap	34301203	20 46 05.71	−25 16 15.3	1.N:	
NML Cyg	5200726	20 46 25.50	+40 06 59.4	3.SB	
NML Cyg	34201224	20 46 25.50	+40 06 59.4	3.SB	
NML Cyg	74103105	20 46 25.50	+40 06 59.4	3.SB	
IRC +00490	51801556	20 46 36.60	−00 54 11.0	2.SEc	
FI Vul	73201716	20 48 51.20	+22 59 38.0	7	F,H
FI Vul	87700716	20 48 51.20	+22 59 38.0	2.SEa	
RX Vul	53502929	20 52 59.80	+23 22 16.3	2.SEa	
UX Cyg	35701412	20 55 05.49	+30 24 52.1	2.SEc	
NGC 7000 −1 42.60, +40 16.3	38301204	20 56 08.98	+44 01 32.9	6	Offset
NGC 7000	38301303	20 57 51.58	+43 21 16.6	6	(0,0)
NGC 7000 +34.69, +59.4	38302802	20 58 26.27	+43 22 16.0	6	Offset
IRAS 20572+4919	40300736	20 58 55.60	+49 31 13.0	4.SE:	
NGC 7000 +1 15.66, −39.4	38302701	20 59 07.24	+43 20 37.2	6	Offset
NGC 7023 −1.49, +0.0	48101804	21 01 30.40	+68 10 22.1	5.U	Offset

Table 6—Continued

Name	TDT	RA (J2000)	Dec (J2000)	Group	Comments
NGC 7023	20700801	21 01 31.89	+68 10 22.1	5.U	(0,0)
NGC 7023 +2.02, +43.9	74602095	21 01 33.91	+68 11 06.0	5.M:	Offset
HD 200775	33901897	21 01 36.77	+68 09 48.7	5.SE	
NGC 7023 +4.91, +1 6.0	20700802	21 01 36.80	+68 11 28.1	6	Offset
Off-AFGL2688	15200813	21 02 14.83	+36 41 52.6	7	
AFGL 2688	35102563	21 02 18.80	+36 41 37.8	4.CN	
NGC 7009	73801242	21 04 10.69	−11 21 49.1	4.PN	
NGC 7009	34400518	21 04 10.79	−11 21 56.6	4.PN	
AFGL 2699	77800722	21 04 14.70	+53 21 03.0	3.CE	
Off-NGC7023	20700803	21 04 37.70	+68 09 10.0	7	
RV Aqr	51801475	21 05 50.30	−00 12 49.0	7	
TW Cyg	38300216	21 05 59.70	+29 24 27.8	2.SEa	
NGC 7027	55800537	21 07 01.63	+42 14 10.3	4.PU	
NGC 7027	23001256	21 07 01.70	+42 14 09.1	4.PU	
NGC 7027	23001357	21 07 01.70	+42 14 09.1	4.PU	
NGC 7027	23001458	21 07 01.70	+42 14 09.1	4.PU	
NGC 7027	2401183	21 07 01.71	+42 14 09.1	4.PU	
T Cep	26300141	21 09 31.69	+68 29 27.8	2.SEa	
T Cep	34601646	21 09 31.70	+68 29 27.0	2.SEa	
T Cep	42602251	21 09 31.70	+68 29 27.0	2.SEa	
T Cep	57501031	21 09 31.70	+68 29 27.0	2.SEa	
T Cep	66101436	21 09 31.70	+68 29 27.0	2.SEa	
T Cep	74602101	21 09 31.70	+68 29 27.0	2.SEa	
T Cep	51401256	21 09 31.71	+68 29 27.0	2.SEa	
T Cep	40800106	21 09 31.82	+68 29 27.4	2.SEa	
IRAS 21080+4758	44500611	21 09 46.40	+48 10 58.5	5.U	
T Ind	13501827	21 20 09.50	−45 01 19.0	7	F
T Ind	37300427	21 20 09.51	−45 01 19.0	1.NC	
T Ind	71800602	21 20 09.51	−45 01 19.0	1.NC	
M 1-78	57702302	21 20 44.80	+51 53 25.5	5.UE	
M 1-78	15901853	21 20 44.85	+51 53 26.6	5.UE	
IRAS 21270+5423	82100309	21 28 41.91	+54 36 51.5	5.E:	

Table 6—Continued

Name	TDT	RA (J2000)	Dec (J2000)	Group	Comments
IRAS 21282+5050	5602477	21 29 58.42	+51 03 59.8	4.Mu	
IRAS 21282+5050	15901777	21 29 58.42	+51 03 59.8	4.Mu	
IRAS 21282+5050	36801940	21 29 58.42	+51 03 59.8	4.Mu	
S 128	47300216	21 32 10.70	+55 52 46.0	5.PN:	
S 128	82301012	21 32 11.40	+55 53 23.9	5.F:	
IC 5117	36701824	21 32 30.83	+44 35 47.3	4.PU	
Hu 1-2	35801255	21 33 08.00	+39 38 01.0	6	
LDN 1085	11101103	21 33 22.30	+56 44 39.8	4.CR	
LDN 1085	54600506	21 33 22.98	+56 44 35.0	4.CR	
S Cep	56200926	21 35 12.79	+78 37 28.2	2.CE	
S Cep	75100424	21 35 12.81	+78 37 28.0	2.CE	
A66 78	73600709	21 35 29.40	+31 41 44.7	5.Fe	
A66 78	18301603	21 35 29.40	+31 41 46.0	5.Fe	
V645 Cyg	26301850	21 39 58.18	+50 14 21.7	5.SA	
IC 1396N	54600353	21 40 42.30	+58 16 09.8	5.F:	
Off-IC1396N	54600354	21 40 54.97	+58 16 26.0	7	
AM Cep	80000938	21 41 31.00	+76 22 42.0	7	W
V460 Cyg	42201734	21 42 01.06	+35 30 36.5	2.CE	
V460 Cyg	74500512	21 42 01.10	+35 30 36.0	2.CE	
DC 240 B25	41300309	21 42 29.54	+57 44 09.9	6	Propn
$\mu$ Cep	8001274	21 43 30.37	+58 46 48.8	2.SEc	
$\mu$ Cep	39802402	21 43 30.40	+58 46 48.0	2.SEc	
$\mu$ Cep	5602852	21 43 30.40	+58 46 48.1	2.SEc	
VDB 145	8302021	21 43 36.73	+48 53 02.7	7	R
DO 40123	42602373	21 44 28.80	+73 38 03.0	2.CE	
IRAS 21434+4936	41600137	21 45 16.23	+49 50 30.9	2.SEb:	
EP Aqr	38600922	21 46 31.89	−02 12 45.9	2.SEb	
EP Aqr	53501243	21 46 31.90	−02 12 45.9	2.SEb	
Elias 1-12	26301354	21 47 20.60	+47 32 04.7	5.M:	
IRAS 21489+5301	15901205	21 50 45.00	+53 15 28.0	3.CR	
S 125 −12.10, +2 6.5	34602403	21 53 32.71	+47 16 18.3	6:	Offset
S 125	34602404	21 53 44.81	+47 14 11.8	6	(0,0)

Table 6—Continued

Name	TDT	RA (J2000)	Dec (J2000)	Group	Comments
S 125 +13.10, −2 7.5	34602405	21 53 57.91	+47 12 04.3	6:	Offset
IRAS 21554+6204	39500195	21 56 58.18	+62 18 43.6	4.SA	
IRAS 22023+5249	41600993	22 04 12.38	+53 04 02.1	4.SC:	
IRAS 22036+5306	39500297	22 05 30.77	+53 21 32.8	5.SA	
HD 235718	36601389	22 05 32.16	+53 22 09.9	7	
SV Peg	74500605	22 05 42.10	+35 20 53.0	2.SEA	
SV Peg	17301206	22 05 42.10	+35 20 54.0	2.SEA	
$\alpha$ Aqr	17300749	22 05 46.90	−00 19 11.0	1.N	
$\alpha$ Aqr	18800749	22 05 46.90	−00 19 11.0	1.N	
RZ Peg	20601527	22 05 52.81	+33 30 27.0	2.C/SE:	
$\lambda$ Gru	53904837	22 06 06.91	−39 32 35.7	1.NO	
DC244 C	41100205	22 11 19.71	+59 21 23.0	7	Proprn, R:
Ced 201	10101909	22 13 24.39	+70 15 05.6	7	R:
$\alpha$ Tuc	86602401	22 18 30.12	−60 15 34.9	1.NO	
S 140 −0.13, +0.5	9101922	22 19 18.17	+63 18 47.6	5.SA	Offset
S 140 −0.13, +0.5	22002135	22 19 18.17	+63 18 47.6	5.SA	Offset
S 140	6401081	22 19 18.30	+63 18 47.1	5.SA	(0,0)
S 140 +0.07, +3.5	17701049	22 19 18.37	+63 18 50.6	5.SA	Offset
OH 104.91 +2.41	28300921	22 19 26.38	+59 51 23.0	4.SA	
S 140 +26.6, +1.3	9101923	22 19 44.90	+63 18 48.4	6	Offset
S 140 +1 20.06, +2.9	9101924	22 20 38.36	+63 18 50.0	7	Offset
S 140 +2 13.42, +4.6	9101925	22 21 31.72	+63 18 51.7	7	Offset
SV Cep	28800703	22 21 33.00	+73 40 24.0	4.SE::	
DZ Aqr	53500647	22 21 41.80	−07 36 30.4	2.SEB	
$\pi^1$ Gru	34402039	22 22 43.81	−45 56 50.4	2.SEA	
RW Cep	57401207	22 23 06.97	+55 57 48.0	2.SEC	
CD Gru	53904667	22 26 10.50	−45 14 13.0	3.SE	
S Lac	18500622	22 29 00.99	+40 18 57.9	2.SEA	
NGC 7293 −28.70, −21.5	74601307	22 29 09.70	−20 49 52.4	6	Offset
HD 235858	36601502	22 29 10.29	+54 51 06.6	4.CT	
HD 235858	26302115	22 29 10.31	+54 51 07.2	4.CT	
NGC 7293	74600408	22 29 38.40	−20 50 13.9	7	(0,0)

Table 6—Continued

Name	TDT	RA (J2000)	Dec (J2000)	Group	Comments
$\alpha$ Lac	41601102	22 31 17.36	+50 16 57.3	1.N:	
IRAS 22303+5950	77900836	22 32 12.80	+60 06 04.0	4.CR	
M 2-53	74501718	22 32 17.60	+56 10 23.1	6	
S 138	17701258	22 32 45.95	+58 28 21.0	5.UE	
S 138	56101082	22 32 45.95	+58 28 22.0	5.UE	
V354 Cep	41300101	22 33 35.70	+58 53 36.3	2.SEc	
SS Peg	53702031	22 33 58.30	+24 33 54.3	2.SEa	
HD 213985	53601009	22 35 27.38	−17 15 26.3	4.SE::	
$\beta$ Gru	53802302	22 42 40.06	−46 53 04.7	1.NO	
$\beta$ Gru	14401412	22 42 40.14	−46 53 05.0	1.NO	
U Lac	41400406	22 47 43.39	+55 09 31.0	2.SEc	
$\epsilon$ Gru	20000101	22 48 33.20	−51 19 00.0	1.N:	
RX Lac	78200427	22 49 56.80	+41 03 04.0	2.SEa	
IRC +60370	42300706	22 50 04.26	+60 17 36.7	7	W
M 2-54	41601295	22 51 38.98	+51 50 41.6	4.SC::	
HR 8714	37401910	22 54 35.60	+16 56 30.0	1.NO	
Cep A IRS 6A	84300404	22 56 18.60	+62 01 59.9	5.F	
Cep B	83901103	22 57 07.20	+62 37 33.1	5.UE	
$\alpha$ PsA	16402602	22 57 38.89	−29 37 19.7	1.N	
AFGL 2999	9604831	22 57 42.06	+58 49 14.2	3.SE	
IRAS 22568+6141	41401197	22 58 51.91	+61 57 44.6	4.F:	
IRAS 22574+6609	39601910	22 59 18.30	+66 25 49.0	4.PUp:	
$\beta$ Peg	20601346	23 03 46.45	+28 04 57.6	1.NO	
$\beta$ Peg	20601613	23 03 46.45	+28 04 57.6	1.NO	
$\beta$ Peg	55100705	23 03 46.46	+28 04 57.7	1.NO	
$\beta$ Peg	5602595	23 03 46.55	+28 04 57.6	1.NO	
NGC 7510	22000961	23 05 10.57	+60 14 40.6	5.UE	
AFGL 3022	77900911	23 05 58.40	+60 14 58.0	2.SEc	
R Peg	41500123	23 06 39.14	+10 32 36.5	2.SEa	
IRAS 23060+0505	18300807	23 08 33.93	+05 21 29.8	7	G
IRAS 23060+0505	18300904	23 08 33.93	+05 21 29.8	7	G
IRAS 23060+0505	37200209	23 08 33.93	+05 21 29.8	7	G



Table 6—Continued

Name	TDT	RA (J2000)	Dec (J2000)	Group	Comments
IRAS 23060+0505	37200308	23 08 33.93	+05 21 29.8	7	G
IRAS 23060+0505	37800211	23 08 33.93	+05 21 29.8	7	G
IRAS 23060+0505	37800710	23 08 33.93	+05 21 29.8	7	G
57 Peg	37600306	23 09 31.50	+08 40 37.0	1.NO	
HR 8832	38500708	23 13 16.21	+57 10 05.3	1.N:	
NGC 7538 IRS1	9102647	23 13 45.27	+61 28 10.0	5.SAeu	
NGC 7538 IRS1	38501842	23 13 45.27	+61 28 10.0	5.SAeu:	
NGC 7538 IRS9	9801532	23 14 01.63	+61 27 20.4	5.SA	
IRAS 23133+6050	22001506	23 15 31.44	+61 07 08.5	5.UE	
IRAS 23151+5912	38501251	23 17 21.44	+59 28 47.1	5.SA	
MWC 1080	28301459	23 17 25.76	+60 50 43.4	5.U	
MWC 1080	26301659	23 17 25.77	+60 50 43.1	5.U	F
NGC 7582	16700767	23 18 23.70	−42 22 13.3	5.M:	G
AFGL 3068	37900867	23 19 12.48	+17 11 33.4	4.CR	
RY And	38202204	23 20 37.00	+39 37 15.0	2.SEa:	
IRAS 23196+1615	41702418	23 22 06.58	+16 31 43.7	6:	
Cas A −8.93, −1 10.8	57302210	23 23 19.01	+58 47 31.6	6	Offset <sup>a</sup>
Cas A −7.44, +47.6	75100641	23 23 20.50	+58 49 30.0	6	Offset
Cas A −7.05, +1 40.3	41801604	23 23 20.89	+58 50 22.7	6	Offset
Cas A −4.03, +1 40.3	41801703	23 23 23.91	+58 50 22.7	6	Offset
Cas A −2.74, +1 42.6	75100643	23 23 25.20	+58 50 25.0	6	Offset
Cas A −2.21, +1 21.3	22000706	23 23 25.73	+58 50 03.7	6	Offset
Cas A −1.20, +1 16.3	57101109	23 23 26.74	+58 49 58.7	6	Offset
Cas A −1.00, +1 40.3	41801802	23 23 26.94	+58 50 22.7	6	Offset
Off-CasA	75100642	23 23 27.50	+58 55 17.0	7	
Cas A −0.18, +4.3	56401807	23 23 27.76	+58 48 46.7	6	Offset
Cas A +0.81, +1 35.4	56401808	23 23 28.75	+58 50 17.8	6	Offset
Cas A +2.01, +2 10.4	22001905	23 23 29.95	+58 50 52.8	7	Offset
Cas A +2.02, +1 40.4	22001801	23 23 29.96	+58 50 22.8	6	Offset
Cas A +7.08, −11.6	41801911	23 23 35.02	+58 48 30.8	6:	Offset
Cas A +10.10, +18.5	41802008	23 23 38.04	+58 49 00.9	6	Offset
Cas A +10.11, −41.5	42300610	23 23 38.05	+58 48 00.9	6	Offset

Table 6—Continued

Name	TDT	RA (J2000)	Dec (J2000)	Group	Comments
Cas A +10.11, -11.5	41802107	23 23 38.05	+58 48 30.9	6	Offset
BU And	38201201	23 23 39.90	+39 43 38.4	2.SEA	
<i>v</i> Peg	21900653	23 25 22.65	+23 24 14.8	1.N:	
NGC 7662	43700427	23 25 53.86	+42 32 05.4	4.PN	
Hb 12	43700330	23 26 14.68	+58 10 54.7	4.SECe	
RU Phe	34401919	23 28 08.30	−47 27 29.3	2.SEc:	
AFGL 3099	78200523	23 28 16.90	+10 54 40.0	3.CR	
IRAS 23262+6401	43305805	23 28 27.70	+64 17 32.9	5.SA	
V582 Cas	38501620	23 30 10.85	+60 16 34.1	2.SEc	
V582 Cas	42300804	23 30 27.33	+57 58 34.5	2.SEc	
IRAS 23304+6147	24800452	23 32 44.94	+62 03 49.5	4.CT	
IRAS 23304+6147	39601867	23 32 44.94	+62 03 49.6	4.CT	
IRAS 23304+6147	8502452	23 32 44.95	+62 03 49.5	4.CT	F
IRAS 23321+6545	25500248	23 34 22.53	+66 01 50.4	4.CN:	
IRC +40540	38201557	23 34 27.86	+43 33 00.4	3.CR	
Nova Cas 1993	24800307	23 41 47.19	+57 31 01.3	6	
R Aqr	18100530	23 43 49.36	−15 17 04.3	2.SEc	
PZ Cas	9502846	23 44 03.30	+61 47 22.3	2.SEc	
PZ Cas	42604702	23 44 03.30	+61 47 22.3	2.SEc	
Z Cas	10101714	23 44 31.49	+56 34 52.6	2.SEap	
TX Psc	75700419	23 46 23.50	+03 29 12.0	1.NC	
TX Psc	55501379	23 46 23.50	+03 29 12.6	1.NC	
HR 9043	40400904	23 53 20.79	−24 13 45.3	7	R
M 2-56	43700232	23 56 36.47	+70 48 13.1	4.SB	
R Cas	24800223	23 58 24.77	+51 23 18.7	2.SEb	
R Cas	26301524	23 58 24.77	+51 23 18.8	2.SEb	F
R Cas	38300825	23 58 24.78	+51 23 18.8	2.SEb	
R Cas	39501330	23 58 24.78	+51 23 18.8	2.SEb	
R Cas	42100215	23 58 24.78	+51 23 18.8	2.SEb	
R Cas	44301926	23 58 24.78	+51 23 18.8	2.SEb	
R Cas	62702122	23 58 24.78	+51 23 18.8	2.SEb	
R Cas	38302016	23 58 24.79	+51 23 19.2	2.SEb	

Table 6—Continued

Name	TDT	RA (J2000)	Dec (J2000)	Group	Comments
------	-----	------------	-------------	-------	----------

Note. — Comments include: F = quality flag such as pointing or telemetry problems; G = extragalactic source; W = wrong coordinates; o: probably an off, but odd in some way; R, R: = possibly a recoverable group 7; H = probably irrecoverable in group 7; Offset = name includes offsets from nominal position indicated by (0,0); Propn = Name from original observer

<sup>a</sup> M 1: (0,0) position is  $\alpha, \delta = 05\ 34\ 31.97, +22\ 00\ 52.1$  (J2000; Han & Tian 1999); M 17: (0,0) position is  $\alpha, \delta = 18\ 20\ 24.83, -16\ 11\ 34.9$  (J2000, Johnson et al. 1998); Cas A: (0,0) position is the Chandra point source  $\alpha, \delta = 23\ 23\ 27.94, +58\ 48\ 42.4$  (J2000; Tananbaum 1999).